

Investigating the dynamics of task-induced modulation and test-retest stability in the triple resting-state networks using functional magnetic resonance imaging

Hasan Mohammad Hasan Sbaihah

Investigating the dynamics of task-induced modulation and test-retest stability in the triple resting-state networks using functional magnetic resonance imaging

Von der Medizinischen Fakultät
der Rheinisch-Westfälischen Technischen Hochschule Aachen
zur Erlangung des akademischen Grades eines Doktors der Theoretischen Medizin
genehmigte Dissertation

vorgelegt von

Hasan Mohammad Hasan Sbaihat

aus

Nazareth

Berichter: Frau Univ.-Prof. Dr. med. Irene Neuner
Herr Univ.-Prof. Dr. rer. nat. Nadim Joni Shah

Tag der mündlichen Prüfung: 12.10.2022

Diese Dissertation ist auf den Internetseiten der Universitätsbibliothek online verfügbar.

D82 (Diss. RWTH Aachen University, 2022)

Hasan Sbaihat, Ravichandran Rajkumar, Shukti Ramkiran, Abed Al-Nasser Assi, N. Jon Shah, Tanja Veselinović, Irene Neuner. Dynamics of task-induced modulation of spontaneous brain activity and functional connectivity in the triple resting-state networks assessed using the visual oddball paradigm. PLoS One. 2021 Nov 4;16(11):e0246709. doi: 10.1371/journal.pone.0246709. PMID: 34735449; PMCID: PMC8568109.

Hasan Sbaihat, Ravichandran Rajkumar, Shukti Ramkiran, Abed Al-Nasser Assi, Jörg Felder, N. Jon Shah, Tanja Veselinović, Irene Neuner. Test-retest stability of spontaneous brain activity and functional connectivity in the core resting-state networks assessed with ultrahigh field 7-Tesla resting-state functional magnetic resonance imaging. Human brain mapping, 2022 January 1-15. DOI: 10.1002/hbm.25771.

This doctoral dissertation is dedicated to my parents Radia and Mohammed Sbaihat, and to my late aunt Nada Sbaihat.

List of publications

Publications of this dissertation:

Hasan Sbaihat, Ravichandran Rajkumar, Shukti Ramkiran, Abed Al-Nasser Assi, N. Jon Shah, Tanja Veselinović, Irene Neuner. Dynamics of task-induced modulation of spontaneous brain activity and functional connectivity in the triple resting-state networks assessed using the visual oddball paradigm. *PLoS One*. 2021 Nov 4;16(11):e0246709. doi: 10.1371/journal.pone.0246709. PMID: 34735449; PMCID: PMC8568109.

Hasan Sbaihat, Ravichandran Rajkumar, Shukti Ramkiran, Abed Al-Nasser Assi, Jörg Felder, N. Jon Shah, Tanja Veselinović, Irene Neuner. Test-retest stability of spontaneous brain activity and functional connectivity in the core resting-state networks assessed with ultrahigh field 7-Tesla resting-state functional magnetic resonance imaging. *Human brain mapping*, 2022 January 1-15. DOI: 10.1002/hbm.25771.

Other publications:

Dilsa Cemre Akkoc Altinok, Ravichandran Rajkumar, Dominik Nießen, **Hasan Sbaihat**, Margo Kersey, N. Jon Shah, Tanja Veselinović, and Irene Neuner. Common neurobiological correlates of resilience and personality traits within the triple resting-state brain networks assessed by 7-Tesla ultra-high field MRI. *Scientific Reports*. 2021 Jun 2;11(1):11564. doi: 10.1038/s41598-021-91056-y. PMID: 34079001; PMCID: PMC8172832.

Cláudia Brambilla, Tanja Veselinovic, Ravichandran Rajkumar, Joerg Mauler, Andreas Matusch, Andrej Ruch, Linda Orth, Shukti Ramkiran, **Hasan Sbaihat**, Nicolas Kaulen, Nibal Khudeish, Christine Wyss, Karsten Heekeren, Wolfram Kawohl, Elena Rota Kops, Lutz Tellmann, Jürgen Scheins, Frank Boers, Bernd Neumaier, Johannes Ermert, Markus Lang, Stefan Stüsgen, Hans Herzog, Karl-Josef Langen, Jon Shah, Christoph Lerche, and Irene Neuner. mGluR5 Binding Changes During a Mismatch Negativity Task in a Multimodal Protocol with [11C]ABP688 PET/MR-EEG. *Translational Psychiatry*. 2022 January 12:6; <https://doi.org/10.1038/s41398-021-01763-3>.

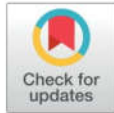
Nicolas Kaulen, Ravichandran Rajkumar, Claudia Régio Brambilla, Jörg Mauler, Shukti Ramkiran, Linda Orth, **Hasan Sbaihat**, Markus Lang, Christine Wyss, Elena Rota Kops, Jürgen Scheins, Bernd Neumaier, Johannes Ermert, Hans R. Herzog, Karl-Josef Langen, Christoph Lerche, N. Jon Shah, Tanja Veselinović, and Irene Neuner. mGluR5 and GABAA Receptor Specific Parametric PET Atlas Construction - PET/MR Data Processing Pipeline, Validation and Application. *Human brain mapping*, 2022 January 1-16. DOI: 10.1002/hbm.25778.

RESEARCH ARTICLE

Dynamics of task-induced modulation of spontaneous brain activity and functional connectivity in the triple resting-state networks assessed using the visual oddball paradigm

Hasan Sbaihat^{1,2,3}, Ravichandran Rajkumar^{1,3,4}, Shukti Ramkiran^{1,3,4}, Abed Al-Nasser Assi², N. Jon Shah^{1,4,5,6}, Tanja Veselinovic^{1,3,6}, Irene Neuner^{1,3,4}*

1 Institute of Neuroscience and Medicine, INM-4, Forschungszentrum Jülich GmbH, Jülich, Germany, **2** Department of Medical Imaging, Arab-American University Palestine, AAUP, Jenin, Palestine, **3** Department of Psychiatry, Psychotherapy and Psychosomatics, RWTH Aachen University, Aachen, Germany, **4** JARA-BRAIN-Translational Medicine, Aachen, Germany, **5** Department of Neurology, RWTH Aachen University, Aachen, Germany, **6** Institute of Neuroscience and Medicine, INM-11, Forschungszentrum Jülich GmbH, Jülich, Germany



OPEN ACCESS

Citation: Sbaihat H, Rajkumar R, Ramkiran S, Assi AA-N, Shah NJ, Veselinovic T, et al. (2021) Dynamics of task-induced modulation of spontaneous brain activity and functional connectivity in the triple resting-state networks assessed using the visual oddball paradigm. *PLoS ONE* 16(11): e0246709. <https://doi.org/10.1371/journal.pone.0246709>

Editor: David V. Smith, Temple University, UNITED STATES

Received: January 22, 2021

Accepted: October 16, 2021

Published: November 4, 2021

Copyright: © 2021 Sbaihat et al. This is an open access article distributed under the terms of the [Creative Commons Attribution License](https://creativecommons.org/licenses/by/4.0/), which permits unrestricted use, distribution, and reproduction in any medium, provided the original author and source are credited.

Data Availability Statement: The data are subject to some legal and ethical restrictions, which are also stated in the informed consent form approved by the Ethics Committee of the Medical Faculty of RWTH Aachen University and signed by each participant. The general rules of the Forschungszentrum Juelich, RWTH Aachen University and the Ethics Committee of the Medical Faculty of RWTH Aachen University provide the following procedure for the sharing of anonymized

* These authors contributed equally to this work.
* i.neuner@fz-juelich.de

Abstract

The default mode network (DMN), the salience network (SN), and the central executive network (CEN) are considered as the core resting-state brain networks (RSN) due to their involvement in a wide range of cognitive tasks. Despite the large body of knowledge related to their regional spontaneous activity (RSA) and functional connectivity (FC) of these networks, less is known about the dynamics of the task-associated modulation on these parameters and the task-induced interaction between these three networks. We have investigated the effects of the visual-oddball paradigm on three fMRI measures (amplitude of low-frequency fluctuations for RSA, regional homogeneity for local FC, and degree centrality for global FC) in these three core RSN. A rest-task-rest paradigm was used and the RSNs were identified using independent component analysis (ICA) on the resting-state data. The observed patterns of change differed noticeably between the networks and were tightly associated with the task-related brain activity and the distinct involvement of the networks in the performance of the single subtasks. Furthermore, the inter-network analysis showed an increased synchronization of CEN with the DMN and the SN immediately after the task, but not between the DMN and SN. Higher pre-task inter-network synchronization between the DMN and the CEN was associated with shorter reaction times and thus better performance. Our results provide some additional insights into the dynamics within and between the triple RSN. Further investigations are required in order to understand better their functional importance and interplay.

MRI data: Data may be shared with interested researchers whose identity and affiliation to a research institution must be ensured and confirmed. It must be made clear that the data will only be used by the interested researchers for research purposes in accordance with the provisions of the Declaration of Helsinki and in accordance with the provisions of the applicable data protection regulations (The General Data Protection Regulation). So, all data used for this publication is available upon request via the following institutional point of contact who can field data inquiries from fellow researchers: Secretary's office of the Institute of Neuroscience and Medicine (INM-4) Forschungszentrum Jülich Secretary: Wilma Fladung building: 15.14, room: 201 phone: +49-2461-61-85575 fax: +49-2461-61-1919 INM4-Sekretariat@fz-juelich.de.

Funding: Hasan Sbaihat received a Ph.D. stipend from the Federal Ministry of Education and Research (BMBF), Germany under the Palestinian German Science Bridge, project number D.B. R01436. The funders have no role in study design, data collection, validation, resources, decision to publish.

Competing interests: The authors have declared that no competing interests exist.

Introduction

Examination of regional spontaneous brain activity (RSA) and functional connectivity (FC) during resting-state (RS) conditions appears to be a promising approach for understanding brain organization at the systems level [1]. Within the several stable RS networks identified up to now, three networks stand out for their importance and synchronized interplay: the default mode network (DMN), the salience network (SN), and the central executive network (CEN). These networks are often jointly referred to as the triple network model [2] and are considered to be the core neurocognitive networks due to their involvement in a wide range of cognitive tasks [1,3,4].

Specifically, the DMN is known to be a task-negative network associated with self-referential thoughts and mind-wandering [5]. It shows decreased activation during tasks in which self-referential and stimulus-independent intellectual activity is not involved [6,7]. Even more, numerous studies have demonstrated that midline DMN regions are among the most efficiently wired brain areas, serving as global hubs that bridge different functional systems across the brain [8,9]. Increased DMN connectivity with regions of other brain networks has been shown to facilitate performance during goal-directed tasks [10]. Thus, DMN is not engaged only under resting-state conditions but also under task performance and post-task processes as well [10–12].

The CEN is a task-positive network, engaged in higher-order cognitive and attention control as well as in working memory, decision making and goal-directed behavior [13–15]. Conversely, the SN is involved in detecting, filtering and integrating relevant internal (e.g., autonomic input) and external (e.g., emotional information) salient stimuli in order to guide behavior [1,16]. Furthermore, it displays a crucial role in the functional and dynamic switching between the DMN and CEN (i.e., between task-based and task-free states) [17,18].

Dynamic interactions between the three networks of the triple network model influence cognition and emotion, affecting performance and impulsivity [19–21]. Moreover, an altered interaction between these networks has been shown in patients with major depressive disorder [22], post-traumatic stress disorder [23], obsessive-compulsive disorder [24], and schizophrenia [25,26]. Altogether, an increasing body of evidence suggests that aberrant function of the triple networks underlies the psychopathology of all major psychiatric disorders [27] and disturbed functional interactions among them may be considered a potential neurophysiological biomarker for different psychopathological phenomena across several neuropsychiatric disorders [28]. It is therefore particularly important to understand the physiological fluctuations in the activity and interactions of these networks in order to be able to differentiate them from pathological conditions.

Continuous fluctuations of the main properties of the networks (as RSA and FC) have been shown during rest and during task-associated activities [29,30]. Much less is known about the extent to which these properties can be influenced by a specific task and to what extent a task-associated activity affects the interaction between the networks.

A simple method to investigate the effects of task-related activation on the RSA is the rest-task-rest paradigm (RTR) [5,31]. To date, a task-induced modulation of the RSA has been observed following cognitive tasks involving working memory, emotion, visual perception, and motor training. However, previous studies have mainly focused on whole-brain [31–35] or on specific brain structures known to be involved in the tasks [36,37]. None of the mentioned studies has specifically addressed the impact of a task on the triple network. Moreover, previous investigations have overall reported changes in static connectivity in different time periods (before and after the task), but the dynamic of the changes during the task performance as well as changes in the relationship between the different networks (particularly in

the triple network, which is the focus of this study) remain poorly understood. Thus, in this study, we have specifically examined the dynamic of the task-induced changes in RSA and FC within the triple network of the RS (DMN, SN and CEN) and the task-induced effects on the interactions between them.

Concretely, this study aims to assess the dynamics of the influence exerted by a well-established task—the visual oddball paradigm (VOP) [38]—on the triple RS networks using a RTR design. The VOP was chosen as it elicits the blood oxygen level dependent (BOLD) response in a large set of distributed networks [39–43]. In particular, the task performance is associated with activation in brain regions linked to the three networks (the SN [44], the dorsolateral prefrontal cortex (CEN) [45,46], and the cingulate and prefrontal cortex (DMN) [47]).

For the identification of the triple network regions, we applied a group independent component analysis (ICA) to the RS data. Several different measures of FC can be calculated from fMRI, each reflecting a different property of the brain networks. For this approach, we chose two such measures, the regional homogeneity (ReHo) [48] and the degree centrality (DC) [49], as these are suitable for investigating the voxel level local and global FC, respectively. Furthermore, the amplitude of low-frequency fluctuations (ALFF) [50], is suitable for depicting the RSA. Combining these measures enables the complementary characterization of changes in activation and communication of specific networks or regions.

We hypothesized that the task-based activity would distinctly affect the RS RSA as well as the local and the global connectivity in the triple network. Due to the central role of the SN during the occurrence of salient stimuli or during the performance of a cognitive task, we also expected internetwork functional connectivity to increase between the SN and the other two networks of the triple network model (DMN, CEN).

Materials and methods

Subjects

21 right-handed healthy subjects (17 males and 4 females) were included in this study (age range between 19 to 40 years; mean: 29 ± 5.6 years). The possible influence of gender was not further investigated in this study due to the large imbalance between the number of men and women and the relatively small sample size. Moreover, a mutual gender effect was not the focus in the study design presented. All subjects were healthy and without a history of neurological or psychiatric disorders. The study was approved by the Ethics Committee of the Medical Faculty of the RWTH Aachen University, Germany. Written informed consent was obtained from all subjects following the recommendations of the Declaration of Helsinki.

Experimental design

To investigate the effects of task-induced brain activity on the post-task resting-state, the experiment followed a rest-task-rest (RTR) design consisting of five different conditions: first RS (R1), active state (the visual oddball paradigm (VOP) comprised of three subtasks: passive (T1), count (T2), and respond (T3)) and the second, post-task RS (R2) (Fig 1).

During the two RS conditions, the subjects were instructed to close their eyes and not to focus on any specific thoughts. All fMRI data were acquired in a single scanning session and instructions were given to the subjects in-between each condition via a microphone. Both RS conditions lasted 6 minutes.

The VOP comprised of three subtasks: passive (T1), count (T2), and respond (T3). Each subtask lasted 10 minutes and 8 seconds. In the task, blue circles were used as targets while yellow circles represented frequent stimuli. Each subtask included 200 trials (160 frequent and 40 target stimuli). The single stimulus was 30 cm in diameter shown on a black background for

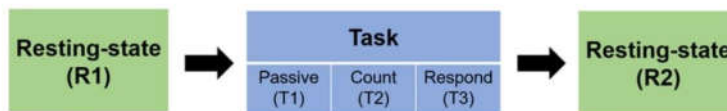


Fig 1. Experimental design of the rest-task-rest paradigm (RTR) which includes two resting-state conditions (pre- and post-task resting-state, R1 and R2) and the task condition composed of three subtasks (passive (T1), count (T2) and response (T3)) of the visual oddball paradigm (VOP).

<https://doi.org/10.1371/journal.pone.0246709.g001>

500 milliseconds with a variable interstimulus interval (ISI) of 500–10,000 milliseconds. The stimulus generator board (ViSaGe MKII, Cambridge Research System Ltd.) was used to generate the stimuli and a thin-film transistor display was used to view the stimuli. The thin-film transistor display was installed behind the scanner and was viewed using a mirror placed on the head coil of the magnetic resonance (MR) scanner. The order of the stimuli during the single subtasks were generated using optseq (<http://surfer.nmr.mgh.harvard.edu/optseq>).

During T1 the subjects were asked to simply keep the stimuli under observation. During T2 they were asked to count the target stimuli (blue circles) and report the number at the end of the run. During T3 they were instructed to press a button (Lumitouch, Photon Control Inc., Burnaby, BC, Canada) using their right index finger as soon as they recognize the target stimuli. Instructions were given before each imaging sequence and the measurement started immediately following the instructions, without any time delay and without a break between the individual sections.

The passive condition was performed in the beginning for all subjects to exclude any bias caused by the previous knowledge about the blue circles as the targets. The order of the count and respond conditions was counterbalanced across subjects. In general, T1 is suitable for capturing effects of pure sensory perception of the stimuli, while T2 includes an additional cognitive process (counting the target stimuli) and T3 also records effects of the motor response.

A part of this data set ($N = 16$), which mainly focused on the analysis of the effects of different response modalities on the fMRI BOLD activation during the visual oddball paradigm, has been published previously [51]. Further details on the paradigm are also available in this publication.

MR data acquisition

MR data were acquired using a 3T scanner (TIM-Trio, Siemens Healthineers, Erlangen, Germany). Sponge pads were used to reduce motion artefacts by limiting the subject's head movement. The fMRI data were acquired using an echo planner imaging (EPI) sequence. The number of volumes were 304 for each task and 180 for each RS condition (repetition time (TR) = 2000 ms, echo time (TE) = 30 ms, flip angle (FA) = 79°, field of view (FOV) = 200 × 200 mm, 64 × 64 matrix, slice thickness = 3 mm, number of slices = 33, and voxel size 3.1 × 3.1 × 4.2 mm).

Structural images were acquired using a magnetization prepared rapid gradient echo (MP-RAGE) sequence (TR = 2250 ms, TE = 3.03 ms, FA = 9°, FOV = 256 × 265 mm, 64 × 64 matrix, 176 slices, voxel size 1 × 1 × 1 mm).

fMRI data analysis

The preprocessing of the RS and task data was performed in three separate procedures—firstly the triple network identification was performed using ICA, secondly the task data was processed using general linear modelling (GLM) and finally fMRI parameters (ReHo, DC and

ALFF) were calculated for all the five conditions. Detailed explanation on each of these procedures is given below.

Triple network identification

The multivariate exploratory linear decomposition into independent components (MELODIC) tool from the FSL software package was used to identify the triple networks (DMN, CEN, and SN) using pre-task RS fMRI data. Subject level RS-fMRI data were pre-processed as follows: the first eight fMRI volume images were removed, followed by slice timing correction, brain extraction (BET) [52], motion correction (MCFLIRT) [53], spatial smoothing FWHM = 5 mm, and high-pass temporal filtering 125s. The functional MRI images were co-registered linearly to high-resolution structural images and nonlinearly to MNI standard space using FLIRT [54]. Group ICA analysis was used to decompose the pre-task RS data into 20 components.

To identify the triple networks, a cross-correlation was performed between the functional brain networks atlas [55] and each of the ICA components. The cross-correlation was performed using the FSLUTILS (<https://fsl.fmrib.ox.ac.uk/fsl/fslwiki/Fslutils>) tool implemented in the FSL software package. ICA components that showed maximum correlation with each of the three networks in the functional brain networks atlas were chosen. The identified brain networks were binarized and used in the subsequent analysis as masks. The binarized masks were corrected for grey matter (GM) by including the voxels which showed more than 50% probability of being GM. The GM correction was performed using a tissue segmented MNI152 ($2 \times 2 \times 2$ mm) template.

Task data. The analysis of the task-related brain activation was performed using FSL software package (FMRIB's Software Library, www.fmrib.ox.ac.uk/fsl). The pre-processing included slice timing correction, brain extraction (using BET) [52], motion correction (MCFLIRT) [53], spatial smoothing using a Gaussian kernel of full width at half maximum (FWHM) of 5 mm, and high pass temporal filtering (100s). A time-series of BOLD signal based on the general linear model for each individual data set was performed using FILM with local autocorrelation correction [56]. The functional images were registered to the high-resolution structural images and subsequently to the Montreal Neurological Institute (MNI) standard space using the FLIRT tool [54]. The first-level analysis was performed with two explanatory variables (EV). The EVs were convolved with a double-gamma hemodynamic response function (HRF). Four contrasts were then created: target stimuli, frequent stimuli, target > frequent, frequent > target.

Group-level mixed-effects analysis was performed for the passive, count and respond sub-tasks to create a mean for each first level contrast using FLAME with spatial normalization to MNI space. Cluster correction for multiple comparison was performed using FEAT with a cluster significance threshold of $Z > 2.3$, $p = 0.01$ [57]. A tripled two-group difference ("triple t-test") was performed to evaluate the additional activation added to the passive condition by the count and respond conditions. The activation pattern regions were defined using Harvard-Oxford Cortical Structural Atlas in FSL software (FMRIB, Oxford, UK).

The reaction time (RT) was calculated as the co-registered time delay between the presentation of the stimulus and the time at which the subject responded to the stimuli by pressing the specified button on the Lumitouch.

fMRI measures calculation

The fMRI measures were computed for both the tasks and RS-fMRI using data processing and analysis for brain imaging (DPABI) [58], and SPM12 (<http://www.fil.ion.ucl.ac.uk/spm/>)

toolboxes built on MATLAB software package version 2017b (The Math Works, Inc., Natick, MA, USA). Pre-processing was performed using the data processing assistant for the RS-fMRI (DPARSF) [59] advanced edition as follows: first eight fMRI volume images of each condition in each subject's dataset were removed, followed by slice timing correction, realignment, nuisance covariates regression (NCR) and temporal filtering between 0.01 and 0.08 Hz. The covariates for NCR included head motion parameter, whole-brain white matter (WM) and cerebrospinal fluid (CSF) mean signals, and the constant, linear and quadratic trends in the BOLD signals. To ensure the quality of the data and minimize the movement artefacts, the subjects head motion parameters was estimated and corrected for fMRI data using Friston 24-parameter model [60]. The model showed for all subjects a head motion ≤ 2 mm in translation or $\leq 2^\circ$ in rotation in any direction. The fMRI measures were calculated for each subject separately in individual brain imaging space. The DC was computed by applying a Pearson correlation coefficient between the time series of a given voxel and all other voxels in the whole brain by thresholding each correlation at ($r > 0.25$, $p \leq 0.001$) [61]. ReHo was calculated by estimating the synchronization or similarity between the time series of a given voxel and 26 nearby neighbor voxels [48] using Kendall's coefficient of concordance (KCC) [62]. The ALFF was calculated within the low-frequency range (0.01–0.1 Hz) [63]. The fMRI measures were normalized using a Z-value standardization procedure by subtracting the mean from each voxel and then dividing the value by the standard deviation of the whole brain. The Z-value standardized measures were spatially normalized to the MNI standard space ($2 \times 2 \times 2$ mm), and, finally, spatial smoothing with FWHM at 4mm^3 was performed.

Further calculated values

The fMRI measures ALFF, ReHo, and DC were extracted from all voxels of the triple network for each condition in all subjects using the binarized triple network masks. The extracted voxel-level values were used to calculate several parameters of interest, relevant for the examination of the task effect on the post task resting-state. These parameters and the exact description of how they were calculated are shown in Table 1.

To compare the dynamics of the three fMRI measures during the different study conditions in the three networks, a three-way repeated measures analysis of variance (rm ANOVA) was carried out in order to investigate the effects of the network (three levels—DMN, CEN and SN), fMRI measure (ALFF, ReHo, DC), condition (R1, T1, T2, T3, R2) as well as the network*measure*condition interaction. Only in case of a statistically significant effect obtained in the global F test and a significant measure*condition interaction in the network, post hoc t

Table 1. Description of parameters used to examine the effect of the task on the fMRI measures in the post-task RS.

| Parameter | Calculation procedure/ meaning |
|--------------------------------|---|
| R1 | Voxel-level fMRI measures during the first (pre-task) resting-state (RS) (baseline) |
| R2 | Voxel-level fMRI measures during the second (post-task) RS. |
| T1, T2, T3 | Voxel-level fMRI measures during the three subtasks of the visual oddball paradigm. |
| RS difference (RSD) | Difference between post- and pre-task RS (R2—R1) in the voxel-level fMRI measures for each subject. |
| Task _(whole) | $\text{Task}_{(whole)} = (T1 + T2 + T3) / 3$ (mean values of the fMRI measures during the three subtasks) |
| Main task _(whole) | $\text{Task}_{(whole)} - R1$ |
| RS similarity (RSS) | Correlation coefficient between R1 and R2 for each subject. |
| Task effect at the group level | Correlation coefficients between the differences (Task _(whole) —R1) and (R2—R1). All correlation coefficients were computed using Pearson's correlation coefficients at a significance level of $p < 0.05$. |

<https://doi.org/10.1371/journal.pone.0246709.t001>

tests were performed for multiple pairwise comparisons. Due to the different number of voxels in the networks and the whole-network based approach in our study, the mean values from the whole network for each of the three parameters were included in this analysis for each subject. The calculations were performed using the software package IBM SPSS Version 25.

The inter-network FC of the three networks were calculated by first extracting the mean of the BOLD signal time series from the binarized mask of each network, followed by the computation of the Pearson's correlation coefficient between each pair of networks. Fisher r to z transformation was performed to improve the normal distribution.

To investigate the relationship between the behavioral data (e.g. reaction time) and the fMRI measures, the correlation coefficients between the RSD and subject's reaction time in the response condition was performed. Further, we investigated the association between the RT and the inter-network connectivity by calculating the correlation coefficients between the RT in the response condition and the inter-network connectivity. Also, to examine the relationship between the functional connectivity measures (ReHo, and DC), the correlation coefficients between the ReHo and the DC were calculated in each condition for each network.

Due to the exploratory approach, no correction for multiple comparisons was performed in this study.

Results

Behavioural data

The mean reaction time of the respond condition was 477 ms (SD = 13).

Imaging data—task data

The task data were initially analyzed and reported following the examination of the first 16 participants [51]. The current analysis includes an enlarged collective of test subjects ($N = 21$) and confirms previously reported findings. In summary, activation in regions associated with a response to visual stimulation (occipital cortex) for both the target and the frequent stimuli was observed during all three subtasks of the visual oddball paradigm. Both, the count and respond conditions differed significantly from the passive condition in a number of brain regions including the pre- and post-central gyri, regions of the parietal cortex and the middle and inferior frontal gyri. Compared to the count condition, the response contrast yielded significant differences in the parietal operculum, inferior parietal lobule, insula, anterior cingulate cortex, and the posterior cingulate cortex (PCC). The BOLD activation in response to target and frequent stimuli in the passive, count and respond condition are shown in the S1 Fig. Further, in the S2 Fig we show the tripled two-group differences for the first level contrast (target > frequent stimuli) which was calculated in a pairwise comparison of the three task conditions.

Imaging data -triple network resting-state data

The triple network was identified using group independent component analysis (Fig 2). Specifically, the DMN included the posterior cingulate cortex (PCC), precuneus, angular gyrus, and medial prefrontal cortex (mPFC); the CEN included the lateral posterior parietal cortex (LPCC) and dorsolateral prefrontal cortex (DLPFC); the SN included the frontal insular cortex (FIC), and anterior cingulate cortex (ACC).

RSA and FC across different study conditions

The fMRI measures showed different values of the RSA and the local and global FC during the different study conditions (rest-task-rest). The mean values and the standard deviations of the

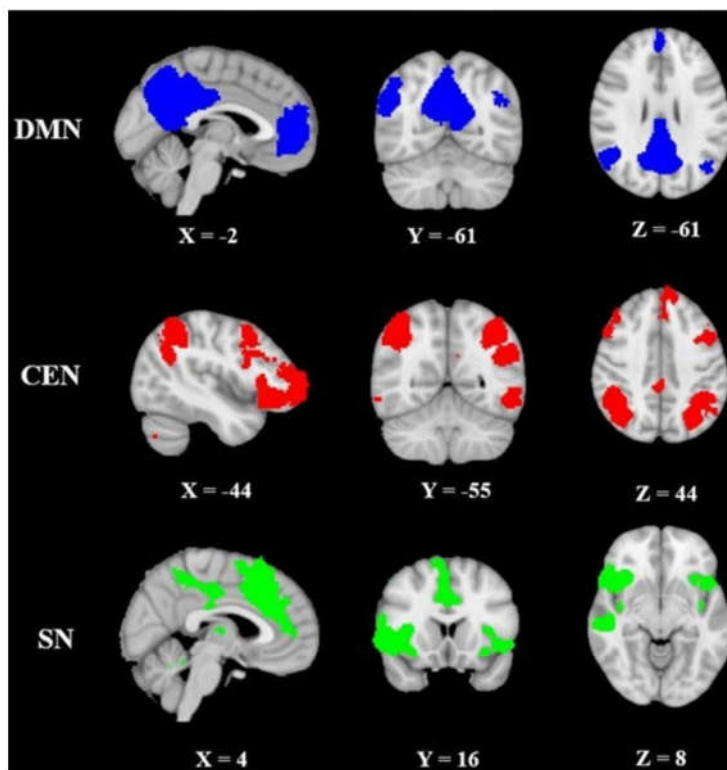


Fig 2. Depiction of the triple networks referred to as the triple network: Default mode network (DMN, blue colour), central executive network (CEN, red colour), and salience network (SN, green colour). The networks were identified by decomposing the pre-task resting-state condition into 20 components from 21 subjects.

<https://doi.org/10.1371/journal.pone.0246709.g002>

fMRI measures during the two RS periods and the three subtasks based on the mean values of each parameter in 21 subjects are shown in Table 2.

ALFF, ReHo and DC values obtained during the two resting states and during the whole task are depicted in Fig 3. The contrast between the two RS conditions (R2 -R1) is shown in the right part of the figure (Fig 3B).

The dynamics of the changes in the individual fMRI parameters during the different phases of the study for the three core RS networks on which the focus of the current study was placed are shown in Fig 4. The three-way repeated measure ANOVA revealed a significant threefold interaction between the factors network, fMRI parameter and condition ($F(5, 255) = 3.55$; $p = 0.005$). Significant two way interactions could be observed for the parameters measured condition within the DMN ($F(2,752) = 4.355$; $p = 0.01$) and for the CEN ($F(4,115) = 2.953$; $p = 0.024$). This interaction was not significant in the SN ($F(4,835) = 0.803$; $p = 0.547$). Thus, post hoc comparisons between the single condition for each fMRI measure were performed only in the DMN and CEN.

Table 2. Mean values and standard deviations (SD) of the three fMRI measures during the two RS periods (R1 and R2) and the three subtasks of the VOP (T1, T2 and T3) obtained from the triple network (default mode network (DMN), salience network (SN), and central executive network (CEN)), based on the mean values of each parameter in 21 subjects.

| Brain network | Task | | | | R2 (mean (SD)) |
|---|----------------|----------------|----------------|----------------|----------------|
| | R1 (mean (SD)) | T1 (mean (SD)) | T2 (mean (SD)) | T3 (mean (SD)) | |
| Amplitude of low frequency fluctuations (ALFF) | | | | | |
| DMN | 0.042 (0.063) | 0.046 (0.064) | 0.044 (0.066) | 0.048 (0.071) | 0.047 (0.074) |
| CEN | -0.022 (0.063) | -0.005 (0.058) | -0.005 (0.069) | -0.004 (0.068) | -0.011 (0.056) |
| SN | -0.012 (0.442) | -0.011 (0.051) | -0.019 (0.058) | -0.009 (0.058) | -0.018 (0.057) |
| Regional homogeneity (ReHo) | | | | | |
| DMN | 0.375 (0.148) | 0.419 (0.164) | 0.373 (0.184) | 0.404 (0.188) | 0.393 (0.147) |
| CEN | 0.265 (0.106) | 0.319 (0.108) | 0.323 (0.097) | 0.334 (0.106) | 0.261 (0.112) |
| SN | 0.147 (0.126) | 0.143 (0.118) | 0.154 (0.111) | 0.169 (0.133) | 0.13 (0.103) |
| Degree centrality (DC) | | | | | |
| DMN | 0.082 (0.099) | 0.182 (0.225) | 0.205 (0.283) | 0.244 (0.308) | 0.121 (0.116) |
| CEN | 0.053 (0.079) | 0.081 (0.159) | 0.147 (0.191) | 0.139 (0.187) | 0.077 (0.116) |
| SN | 0.040 (0.069) | 0.024 (0.107) | 0.044 (0.099) | 0.061 (0.128) | 0.043 (0.051) |

<https://doi.org/10.1371/journal.pone.0246709.t002>

Due to a significant Mauchly-test all reported values were adapted using the Greenhouse-Geisser method [64]. The post-hoc pair-wise comparison between the single values within the networks revealed some significant results as shown in Fig 4.

Concretely, we could not observe significant changes of the ALFF between the five investigated conditions in none of the three investigated core RS networks.

In the DMN the parameter ReHo increased non-significantly in T1 compared with R1. This value further decreased significantly during T2 ($p = 0.015$) and increased again significantly during T3 ($p = 0.006$). In the same network, the parameter DC increased significantly during T1 ($p = 0.021$) and remained significantly higher than in R1 during the both consecutive parts of the VOP (T2 ($p = 0.049$) and T3 ($p = 0.019$)). In the further course of the study, it decreased significantly in R2 ($p = 0.027$).

In the CEN, the parameter ReHo increased significantly during the task compared with R1 (T1: $p = 0.002$; T2: $p = 0.007$, T3: $p = 0.002$) and decreased significantly during the R2 ($p = 0.006$). Similar dynamics could be observed for the parameter DC, although the value did not increase significantly during the passive task condition but only in the T2 condition ($p = 0.029$) and then even further in the context of the T3 ($p = 0.034$). The value decreased to a level comparable with R1 in the R2 condition ($p = 0.044$).

Since these post hoc analyses were not confirmatory but rather merely exploratory, no correction for multiple testing was carried out.

Inter-network interaction

The functional connectivity between the DMN and CEN increased significantly following the performance of the task ($p = 0.015$). The connectivity strength between the DMN and the SN remained stable ($p = 0.25$), whereas it increased significantly between the SN and CEN ($p = 0.0004$) (Fig 5).

The investigation of the relationship between the RT in the response condition and the inter-network connectivity revealed only a significant negative correlation between the RT and the inter-network connectivity between DMN and CEN ($r = -0.43$, $p = 0.04$) in the pre-task RS (R1). All other correlations were not significant. Even more, the analysis of the associations between the RT and the inter-network connectivity changes remained also non-

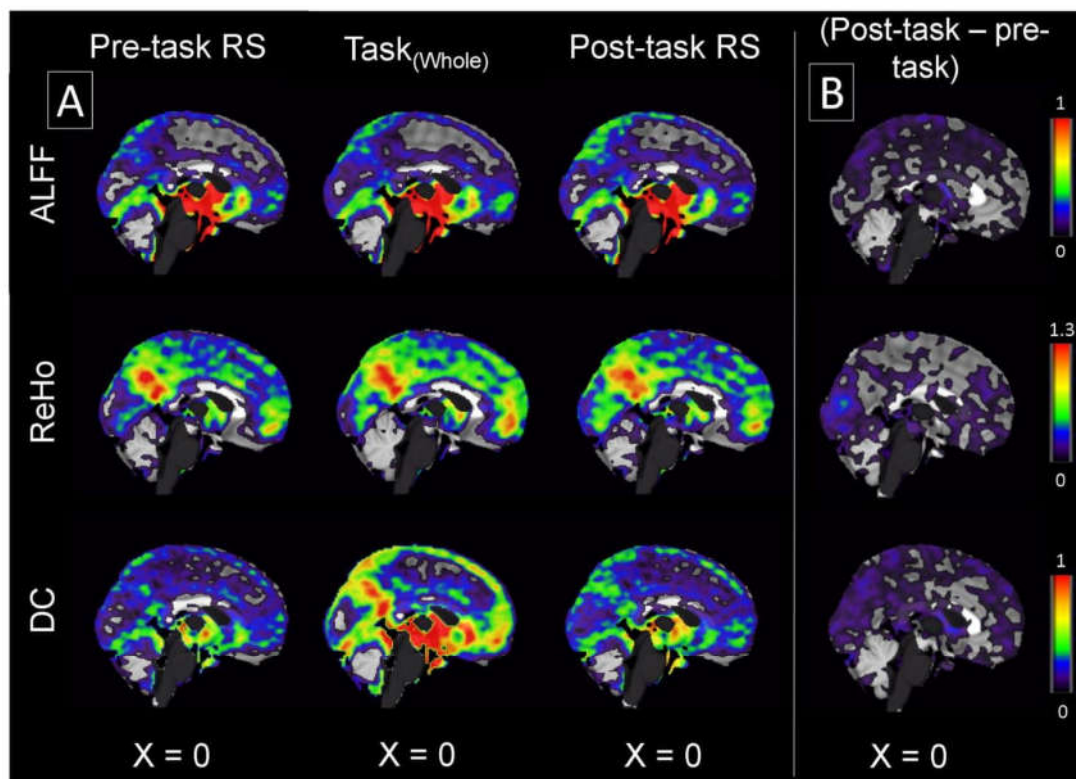


Fig 3. fMRI measures (ALFF, ReHo, and DC) from 21 subjects depicted for the whole brain. The difference between the two resting states (R2-R1) for each three fMRI measures is shown in the right row (B).

<https://doi.org/10.1371/journal.pone.0246709.g003>

significant for all observations (change of DMN-SN inter-network connectivity and RT: $r = -0.203$; $p = 0.377$; change of DMN-CEN inter-network connectivity and RT: $r = 0.252$; $p = 0.270$; change of CEN-SN inter-network connectivity and RT: $r = -0.165$; $p = 0.476$).

Associations between the pre- and post-task resting-state differences and the task

The correlation between the differences between post-task and pre-task RS parameters ($RSD = R2 - R1$) and the fMRI measures resulting from the pure task effects ($task_{(Whole)} - R1$) are depicted in (Fig 6). Significant positive correlations were found in DMN for ALFF ($r = 0.48$, $p = 0.02$; 95% CI [-0.17, 0.84]) and DC ($r = 0.58$, $p = 0.005$; 95% CI [-0.03, 0.87]); in CEN for ALFF ($r = 0.44$, $p = 0.04$; 95% CI [-0.22, 0.82]), ReHo ($r = 0.69$, $p = 0.004$; 95% CI [0.16, 0.91]) and DC ($r = 0.67$, $p = 0.008$; 95% CI [0.12, 0.91]); and in SN for ALFF ($r = 0.69$, $p = 0.004$; 95% CI [0.16, 0.91]), ReHo ($r = 0.58$, $p = 0.004$; 95% CI [-0.03, 0.87]), and DC ($r = 0.49$, $p = 0.02$; 95% CI [-0.15, 0.84]). Taking into account the confidence intervals, only the correlations for ReHo and DC in CEN, and for ALFF in SN can be considered as significant.

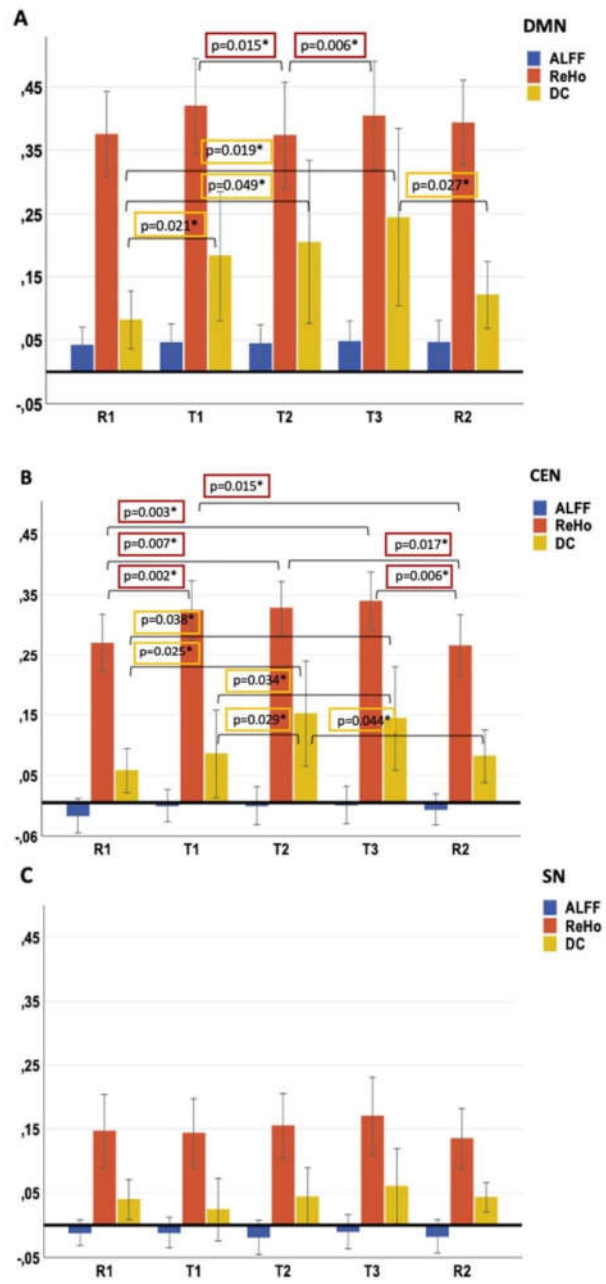


Fig 4. Bar chart representing the mean of the fMRI measures—amplitude of low-frequency fluctuations (ALFF), the regional homogeneity (ReHo), and the degree centrality (DC) in the three resting state networks—default mode network (DMN) (A), central executive network (CEN) (B) and salience network (SN) (C)— across 21 subjects in 5 conditions including resting-state 1 (R1), passive (T1), count (T2), respond (T3), and resting-state 2 (R2).

<https://doi.org/10.1371/journal.pone.0246709.g004>

The investigation of the associations between the RS differences (RSD) and the subjects' RT in the respond condition remained without significant correlations.

Similarity between the first and the second RS and the associations between ReHo and DC

The RSS values calculated separately for the triple networks (DMN, CEN and SN) for each of the fMRI measures (ALFF; ReHo and DC) are shown in Table 3. The RSS values were comparable for all three parameters across all three networks.

The results of the correlations between the two functional connectivity measures—ReHo and DC—remained highly significant in each condition of the investigation, as shown in Table 4. Furthermore, in all three networks we found a significant correlation between the extent of the change in the ReHo parameter (R2-R1) and the DC (R2-R1) parameter: in the DMN: $r = 0.735$, $p < 0.001$, in the CEN: $r = 0.709$, $p < 0.001$, in the SN: $r = 0.586$, $p = 0.005$.

Discussion

In this study, we investigated the effects of a simple visual-oddball paradigm on three basic fMRI measurements of the RS—ALFF (RSA), ReHo, and DC (the local and the global functional connectivity, respectively)—in the three core RS networks—DMN, CEN, and SN. Our analysis revealed different dynamics of changes in brain activity and connectivity in the three networks during the rest-task-rest investigation, the course of which was related to the different requirements of the individual subtasks. The assessment of these properties in the post-task RS phase, on the other hand, showed a high degree of similarity with the pre-task RS. Furthermore, the task performance induced a significant increase in the inter-network correlations between the SN and CEN, as well as between the DMN and CEN, but not between the DMN and SN. Also, the differences between the pre- and the post-task RS (R2—R1) were

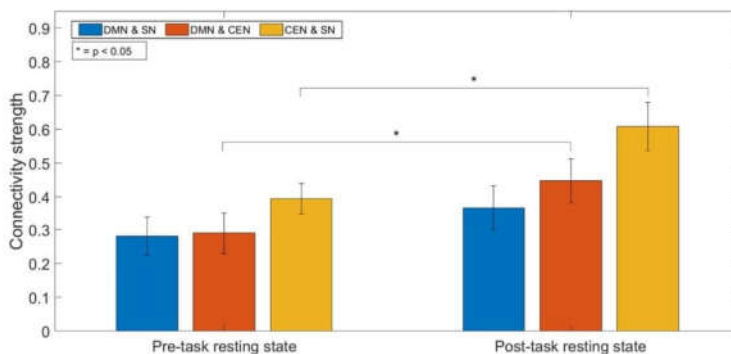


Fig 5. Strength of the FC between each pair of networks in the triple network in the pre- and post-task resting-state. There is a significant increase in FC between the DMN and CEN, and between the CEN and the SN in the post-task resting-state ($p < 0.05$). The bars represent the standard error.

<https://doi.org/10.1371/journal.pone.0246709.g005>

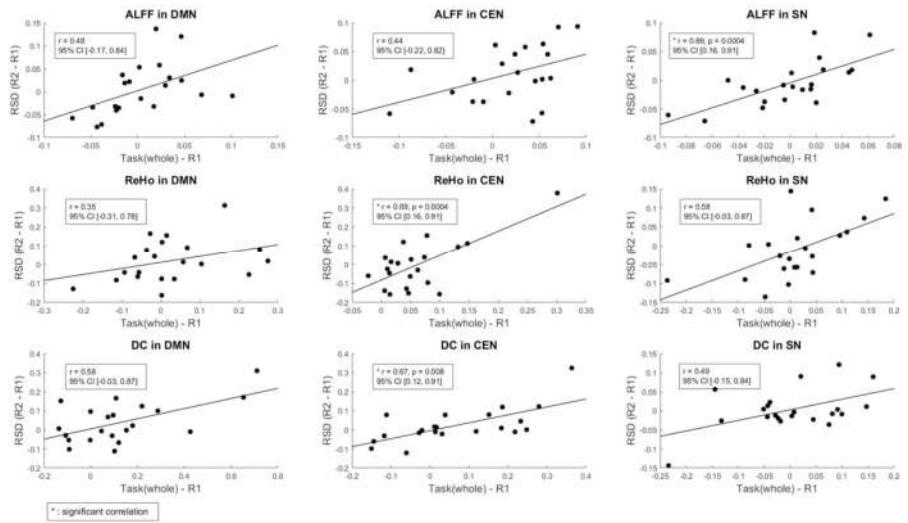


Fig 6. Correlations between the fMRI measures resulting from the pure task_(whole) effects and the RSD in the triple network, including the DMN, CEN, and SN of the fMRI measures.

<https://doi.org/10.1371/journal.pone.0246709.g006>

strongly associated with the main task influence (task_(whole)—R1) in two networks (for ReHo and DC in the CEN and for ALFF in the SN). Finally, at a behavioral level, the task performance (subject’s reaction time in the respond condition) correlated solely with the inter-network connectivity between DMN and CEN in the pre-task RS.

One particularity of our study was the investigation of the properties of the core resting state networks addressing the whole networks, rather the single subregions. In this approach, the temporal dynamic of the intrinsic brain networks is more robust compared to the analysis of single subregions. This is due to a lower susceptibility to noises caused by head motion,

Table 3. Mean values, standard deviation, and the range of the resting-state similarity (RSS) calculated separately for each resting-state fMRI parameter (ALFF, ReHo, and DC) and for each of the triple networks (default mode network (DMN), salience network (SN), and central executive network (CEN)).

| | RSS (Mean) | RSS (SD) | RSS (Range) |
|------|------------|----------|-------------|
| DMN | | | |
| ALFF | 0.882 | 0.029 | 0.824–0.925 |
| ReHo | 0.812 | 0.039 | 0.698–0.876 |
| DC | 0.756 | 0.0657 | 0.575–0.884 |
| CEN | | | |
| ALFF | 0.874 | 0.044 | 0.763–0.946 |
| ReHo | 0.779 | 0.051 | 0.655–0.867 |
| DC | 0.757 | 0.097 | 0.425–0.864 |
| SN | | | |
| ALFF | 0.886 | 0.048 | 0.721–0.934 |
| ReHo | 0.758 | 0.045 | 0.664–0.851 |
| DC | 0.756 | 0.083 | 0.498–0.880 |

<https://doi.org/10.1371/journal.pone.0246709.t003>

Table 4. The relationships between the fMRI measures (ReHo, and DC) across the brain networks (DMN, CEN, and SN). All correlations coefficients were positive and significant at $p < 0.01$.

| Correlations between ReHo and DC | | | | | | | | | |
|----------------------------------|---------|------|---------|------|---------|------|---------|------|---------|
| DMN | | | | | | | | | |
| R1 | | T1 | | T2 | | T3 | | R2 | |
| r | p-value | r | p-value | r | p-value | r | p-value | r | p-value |
| 0.88 | < 0.01 | 0.82 | < 0.01 | 0.84 | < 0.01 | 0.77 | < 0.01 | 0.78 | < 0.01 |
| CEN | | | | | | | | | |
| R1 | | T1 | | T2 | | T3 | | R2 | |
| r | p-value | r | p-value | r | p-value | r | p-value | r | p-value |
| 0.79 | < 0.01 | 0.74 | < 0.01 | 0.66 | < 0.01 | 0.76 | < 0.01 | 0.84 | < 0.01 |
| SN | | | | | | | | | |
| R1 | | T1 | | T2 | | T3 | | R2 | |
| r | p-value | r | p-value | r | p-value | r | p-value | r | p-value |
| 0.76 | < 0.01 | 0.81 | < 0.01 | 0.6 | < 0.01 | 0.73 | < 0.01 | 0.7 | < 0.01 |

<https://doi.org/10.1371/journal.pone.0246709.t004>

respiration, and vascular pulsatility [65,66]. Furthermore, this approach allows a statement to be made about the overall function of the networks, rather than the function of single subregions, which in most cases cannot be assigned exclusively to one network. Therefore, our approach considered for each subject the mean values of the voxel-wise fMRI measurements as representative of the properties of the individual networks. These values were used to capture the dynamics of task-induced changes in the individual networks.

Interestingly, we could not find a significant change in the ALFF values at the network level in none of the three investigated networks. This is a somewhat unexpected result, especially since the DMN deactivation during task performance has been reported in numerous studies using different neuroimaging techniques [67–69]. Thereby, it is hypothesized that the deactivation results from reallocation of attentional resources from internal to external sources of information [69]. However, the deactivation extent appears to be associated with the cognitive demand of the task: persisted activity of the DMN is been reported during not sufficiently challenging tasks [7] as well as a lower extent of DMN deactivation has been shown during decreased task demands [70,71]. Indeed, the VOP, particularly the passive subtask, includes a very low cognitive demand limited on a passive observation of the presented stimuli. In our study, the passive stimuli observation resulted mainly in the activation of the visual cortex for both, the target and the frequent stimuli, which could be observed during all three conditions. Although the general activation was much more extensive in the two other subtasks, we did not observe any significant change in ALFF values in the three target networks in any of these conditions. In one previous investigation, the authors reported a reduction of both, fractional ALFF (fALFF) and FC during sustained working memory task in the posterior areas of DMN, while changes in the ACC were less marked [72]. In contrast to this study, our approach considers the entire network, so that the lack of significant changes in ALFF values could be attributed to a cumulative mutual cancellation of the different changes in different parts of the network.

During the subtask T2, however, in which not only passive observation but also active counting of irregular stimuli was required, we observed a significant reduction in the ReHo value in DMN, which is in concordance with previously reported reduction of ReHo in the DMN during a simple cognitive task [48]. Generally, a reduction in ReHo seems to indicate a decrease in activity in the observed region [73,74]. Interestingly, a renewed increase in ReHo occurred in the DMN during the response task (T3). ReHo, often referred to as the local FC is defined by the temporal coherence or synchronization of the BOLD time series within a set of

a given voxel's nearest neighbors [26]. ReHo represents the most efficient, reliable, and widely used index of local FC [75,76]. An increase in ReHo indicates an increased local synchronization of spontaneous neural activity [72]. This finding may be attributed to the fact, that an important part of the DMN—the posterior cingulate cortex (PCC)—showed a significant activation in the respond condition only.

The described alterations were accompanied by an incremental increase in DC values and their significant reduction after the transition to the second RS. DC represents the overall connectivity between particular brain regions to other brain areas [8,75]. An increase in DC of specific brain hubs indicates a more extensive communication with distinct brain areas. Earlier investigations reveal that the increase of functional connectivity may result in higher global efficiency that facilitates global information transmission [77] that has been required during the tasks performance. Otherwise, a DC decrease after task performance has been previously reported after subjects performed a sustained auditory working memory task [72].

In the CEN, we observed a gradual increase in ReHo in DC during the task and a significant decrease of both values and thus a return to the level observed during R1 after the completion of the task. At a broad level, the CEN is included in higher order executive functioning, including the cognitive control of thought, emotion regulation, and working memory [16,78,79] and is thus activated during efforts to exert self-control, reappraise threatening stimuli, and to suppress intrusive, unpleasant thoughts [80–82]. CEN activity has been shown to be anti-correlated with activity in the DMN in healthy adults [1,18,19], while some investigations indicate that the CEN also exhibits an inhibitory control on the DMN [83]. Thus, the task associated ReHo and DC increase in the CEN express the involvement of this network in responding to the task demands. The decrease following the completion of a cognitive paradigm may be the basis for the restoration of the regular activity of the DMN within the scope of a decline in DMN inhibition which occurred as a result of increased CEN activity during the task performance.

All three investigated fMRI measures remained broadly stable during the rest-task-rest design in the SN. The SN as a network known to demonstrate competitive interactions during cognitive information processing [6,19] and, thus, having a critical role in switching between two other major RS networks (the DMN and the CEN [1]). In particular, the main hubs of the SN, the frontal inferior insula and ACC, are known to share significant topographic reciprocal connectivity and form a tightly coupled network, ideally placed to integrate information from several brain regions [84,85]. Thus, they seem to moderate arousal during cognitively demanding tasks and play a unique function in initiating control signals that activate the CEN and deactivate the DMN [18]. Previous investigations have linked increased ALFF values in some parts of the SN to a hyperarousal state in patients with MDD [86]. The stable levels of RSA and FC before, during and after a low demanding task in healthy controls could reflect a lack of significant change in arousal by a task that neither required significant cognitive effort from participants nor had any affective components.

The connectivity analysis between the three networks revealed an increased synchronization (in terms of a significantly increased connectivity strength) for the SN with the CEN but not with the DMN in the post-task RS compared to the pre-task RS. This may be an after-task effect of the inter-network interactions during the paradigm performance. Indeed, Sridharan and colleagues have shown that the connectivity strength during the visual oddball paradigm particularly increased between the main nodes of the SN (frontal anterior insula and ACC) and all main nodes of the CEN, while the interactions between the SN and DMN were less pronounced [18].

Interestingly, the connectivity between the CEN and DMN also increased in the post-task resting-state. This finding is consistent with the literature on the cooperative activity of the

DMN and the CEN during different mental operations [87]. An increased coupling between some parts of these two networks has been shown in problem-solving tasks [88], social working memory [89], and during creative idea production [90]. Furthermore, a significant interaction between the DMN and the CEN has also been shown during the RS condition [91].

In our study we observed an association between a stronger pre-task interaction between these two networks and better task performance (expressed here through shorter reaction times). Better synchronisation of the two networks at rest therefore seems to form a basis for faster responsiveness. Thereby, this interaction seems to fluctuate dynamically across short time scales [92], indicating that the temporal relationships between the DMN and CEN shifts depending on the change in the attention focus and the immediately preceding activity. Thus, the increased connectivity between the DMN and the CEN in the post-task RS observed in our study may be an expression of the shifting of attention after task completion.

Several subregions of the triple networks are known to be activated during the performance of cognitively demanding tasks [93]. In the case of the VOP performed in our study, the main task specific activation has been reported previously by Warbrick and colleagues [51]. The target detection specifically activated distinct brain regions than the frequent stimuli during the count and response condition in several brain regions including parietal and frontal regions (partly included in the CEN), with more widespread, left hemisphere dominant pre and post central gyri and frontal pole activation for the respond condition [51]. During the last part of the paradigm (T3), the target > frequent stimuli contrast mainly involved, besides the mentioned parts of the CEN, also parts of the DMN (PCC) and the SN (Insula, ACC). The insula activation was common to the count and respond conditions. The intensive involvement of different subregions of the triple networks in the performance of the task may have contributed to the dynamics in the triple network model networks during this rest-task-rest design. Indeed, we observed positive correlations between the extent of the differences between R1 and R2 regarding specific parameters and the actual task effect on the same parameters in the triple networks. These correlations were significant in the CEN for ReHo and DC measures and in the SN for ALFF. A close relationship between the cognitive level of the previous task and the extent of the modulation in the brain networks has been reported previously. Barnes and colleagues observed that the changes in endogenous dynamics in post-task RS is directly related to the difficulty of task performance [94]. In the case of the VOP used here, the levels of cognitive demand for all three subtasks are not widely different and the whole paradigm did not require high cognitive effort. Accordingly, we observed a high level of resting state similarity for all three parameters in all three networks. However, we observed an increased synchronization for the CEN with the SN as well as with the DMN in the post-task RS. This may be an expression of a more intensive involvement of several subregions of the CEN in the last two parts of the paradigm. Even more, the T3 subtask also included a pronounced activation of the insula and the ACC (parts of the SN) as well as the PCC (DMN) during the counting and responding to the target. Thus, the increased synchronization of the CEN with the SN as well as with the DMN in the post-task RS may be a consequence of this immediately preceding joint activity. Indeed, the extent of the changes in the RSA and local as well as global connectivity in the core RS networks in the post-task condition followed the extent of the task-induced changes within those networks.

Conclusion

In conclusion, in this work we report the dynamics of changes in RSA, local and global connectivity within the triple RS networks during a simple cognitive activity. A particularity of this work is the capture of the properties of the networks as a whole. The observed patterns of

change differed noticeably between the networks and were tightly associated with the task-related brain activity and the distinct involvement of the networks in the performance of the different subtasks. In the post-task RS we could find a very high similarity with the pre-task RS in the individual parameters within the individual networks. However, especially the inter-network analysis showed an increased synchronization of CEN with the DMN and the SN after the task. The differences between the pre- and post-task RS correlated largely with the extent of the pure task-effect. Furthermore, we observed that the RT was shorter (and thus the performance better) in the case of a higher pre-task interaction between the DMN and the CEN. In sum, our results show that the behavior/task not only led to dynamic changes in the properties of three core resting state networks, but also to a change in the interactions between the networks, which could be detected at least immediately after the task. This in turn could have an impact on subsequent activities.

Our results provide some additional insight into the task associated dynamics within and between the triple resting state networks. Further investigations are required in order to understand better their functional importance and interplay.

Supporting information

S1 Fig. BOLD activation in response to target and frequent stimuli. Z: Cluster-corrected threshold.
(DOCX)

S2 Fig. BOLD activation of the tripled two-group difference (“tripled t-test”). Z: Cluster-corrected threshold.
(DOCX)

Acknowledgments

This study is considered to be part of the doctoral thesis (Dr. rer. medic.) of Mr. Hasan Sbaihat, Faculty of Medicine, RWTH Aachen University, Germany. The authors would like to thank Dr. Jorge Arrubla and Tracy Warbrick for their help in data acquisition, and Dr. Shivakumar Viswanathan for providing advice on statistics. Finally, authors would like to thank Ms. Claire Rick and Mr. Dennis Thomas for proofreading the manuscript.

Author Contributions

Conceptualization: Irene Neuner.

Data curation: Hasan Sbaihat.

Formal analysis: Hasan Sbaihat.

Funding acquisition: N. Jon Shah, Irene Neuner.

Methodology: Ravichandran Rajkumar, Tanja Veselinović.

Resources: N. Jon Shah.

Software: Ravichandran Rajkumar.

Supervision: Abed Al-Nasser Assi, N. Jon Shah, Tanja Veselinović, Irene Neuner.

Writing – original draft: Hasan Sbaihat.

Writing – review & editing: Hasan Sbaihat, Ravichandran Rajkumar, Shukti Ramkiran, Abed Al-Nasser Assi, N. Jon Shah, Tanja Veselinović, Irene Neuner.

References

1. Menon V, Uddin LQ. Saliency, switching, attention and control: a network model of insula function. *Brain Struct Funct*. 2010 May 29; 214(5–6):655–67. <https://doi.org/10.1007/s00429-010-0262-0> PMID: 20512370
2. Menon V. Large-scale brain networks and psychopathology: a unifying triple network model. *Trends in Cognitive Sciences*. 2011 Oct; 15(10):483–506. <https://doi.org/10.1016/j.tics.2011.08.003> PMID: 21908230
3. Wu X, Li Q, Yu X, Chen K, Fleisher AS, Guo X, et al. A Triple Network Connectivity Study of Large-Scale Brain Systems in Cognitively Normal APOE4 Carriers. *Front Aging Neurosci*. 2016 Sep 28; 8. <https://doi.org/10.3389/fnagi.2016.00231> PMID: 27733827
4. Krishnadas R, Ryali S, Chen T, Uddin L, Supekar K, Palaniyappan L, et al. Resting state functional hyperconnectivity within a triple network model in paranoid schizophrenia. *The Lancet*. 2014 Feb; 383: S65. [https://doi.org/10.1016/S0140-6736\(14\)60328-7](https://doi.org/10.1016/S0140-6736(14)60328-7)
5. Lin P, Yang Y, Gao J, De Pisapia N, Ge S, Wang X, et al. Dynamic Default Mode Network across Different Brain States. *Sci Rep*. 2017 Apr 6; 7(1). <https://doi.org/10.1038/srep46088> PMID: 28382944
6. Greicius MD, Krasnow B, Reiss AL, Menon V. Functional connectivity in the resting brain: A network analysis of the default mode hypothesis. *Proceedings of the National Academy of Sciences*. 2002 Dec 27; 100(1):253–8. <https://doi.org/10.1073/pnas.0135058100> PMID: 12506194
7. Greicius MD, Menon V. Default-Mode Activity during a Passive Sensory Task: Uncoupled from Deactivation but Impacting Activation. *Journal of Cognitive Neuroscience*. 2004 Nov; 16(9):1484–92. <https://doi.org/10.1162/0899929042568532> PMID: 15601513
8. van den Heuvel MP, Sporns O. Network hubs in the human brain. *Trends in Cognitive Sciences*. 2013 Dec; 17(12):683–96. <https://doi.org/10.1016/j.tics.2013.09.012> PMID: 24231140
9. Hagmann P, Cammoun L, Gigandet X, Meuli R, Honey CJ, Wedeen VJ, et al. Mapping the Structural Core of Human Cerebral Cortex. *Friston KJ, editor. PLoS Biol*. 2008 Jul 1; 6(7):e159. <https://doi.org/10.1371/journal.pbio.0060159> PMID: 18597554
10. Elton A, Gao W. Task-positive Functional Connectivity of the Default Mode Network Transcends Task Domain. *Journal of Cognitive Neuroscience*. 2015 Dec; 27(12):2369–81. https://doi.org/10.1162/jocn_a_00859 PMID: 26244722
11. Wang Z, Liu J, Zhong N, Qin Y, Zhou H, Li K. Changes in the brain intrinsic organization in both on-task state and post-task resting state. *NeuroImage*. 2012 Aug; 62(1):394–407. <https://doi.org/10.1016/j.neuroimage.2012.04.051> PMID: 22569542
12. Li B, Wang X, Yao S, Hu D, Friston K. Task-Dependent Modulation of Effective Connectivity within the Default Mode Network. *Front Psychology*. 2012; 3. <https://doi.org/10.3389/fpsyg.2012.00206> PMID: 22737141
13. Müller NG, Knight RT. The functional neuroanatomy of working memory: Contributions of human brain lesion studies. *Neuroscience*. 2006 Apr; 139(1):51–8. <https://doi.org/10.1016/j.neuroscience.2005.09.018> PMID: 16352402
14. Bressler SL, Menon V. Large-scale brain networks in cognition: emerging methods and principles. *Trends in Cognitive Sciences*. 2010 Jun; 14(6):277–90. <https://doi.org/10.1016/j.tics.2010.04.004> PMID: 20493761
15. Li Q, Liu J, Wang W, Wang Y, Li W, Chen J, et al. Disrupted coupling of large-scale networks is associated with relapse behaviour in heroin-dependent men. *jpn*. 2018 Jan 1; 43(1):48–57. <https://doi.org/10.1503/jpn.170011> PMID: 29252165
16. Seeley WW, Menon V, Schatzberg AF, Keller J, Glover GH, Kenna H, et al. Dissociable Intrinsic Connectivity Networks for Salience Processing and Executive Control. *Journal of Neuroscience*. 2007 Feb 28; 27(9):2349–56. <https://doi.org/10.1523/JNEUROSCI.5587-06.2007> PMID: 17329432
17. Goulden N, Khusnulina A, Davis NJ, Bracewell RM, Bokde AL, McNulty JP, et al. The salience network is responsible for switching between the default mode network and the central executive network: Replication from DCM. *NeuroImage*. 2014 Oct; 99:180–90. <https://doi.org/10.1016/j.neuroimage.2014.05.052> PMID: 24862074
18. Sridharan D, Levitin DJ, Menon V. A critical role for the right fronto-insular cortex in switching between central-executive and default-mode networks. *Proceedings of the National Academy of Sciences*. 2008 Aug 22; 105(34):12569–74. <https://doi.org/10.1073/pnas.0800005105> PMID: 18723676
19. Fox MD, Snyder AZ, Vincent JL, Corbetta M, Van Essen DC, Raichle ME. From The Cover: The human brain is intrinsically organized into dynamic, anticorrelated functional networks. *Proceedings of the National Academy of Sciences*. 2005 Jun 23; 102(27):9673–8. <https://doi.org/10.1073/pnas.0504136102> PMID: 15976020

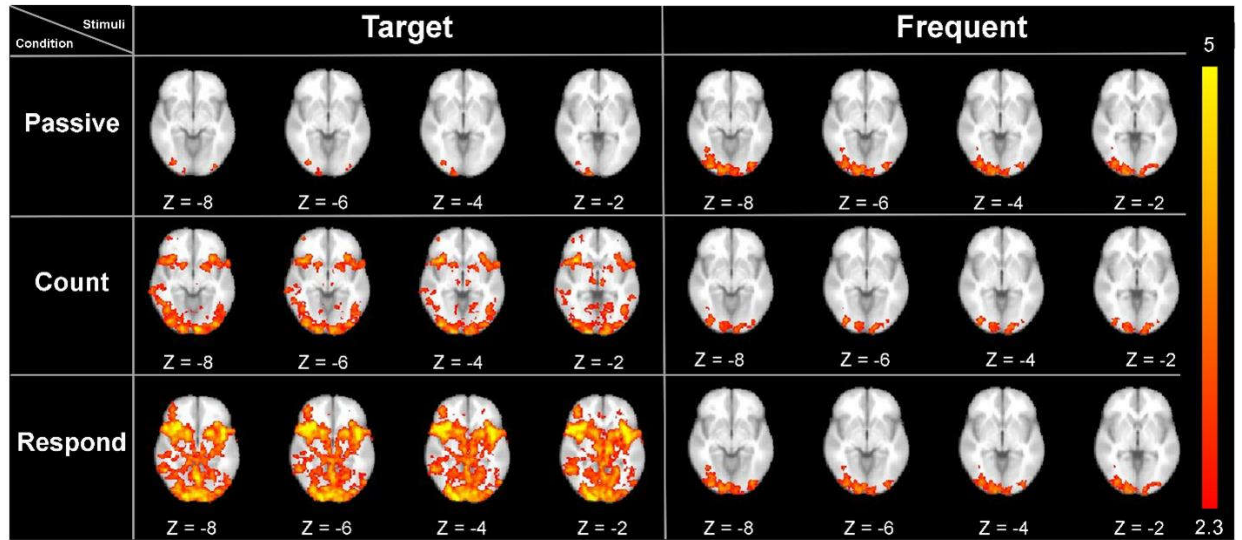
20. Shannon BJ, Raichle ME, Snyder AZ, Fair DA, Mills KL, Zhang D, et al. Premotor functional connectivity predicts impulsivity in juvenile offenders. *Proceedings of the National Academy of Sciences*. 2011 Jun 27; 108(27):11241–5. <https://doi.org/10.1073/pnas.1108241108> PMID: 21709236
21. Chand GB, Dhamala M. Interactions Among the Brain Default-Mode, Salience, and Central-Executive Networks During Perceptual Decision-Making of Moving Dots. *Brain Connectivity*. 2016 Apr; 6(3):249–54. <https://doi.org/10.1089/brain.2015.0379> PMID: 26694702
22. Zheng H, Xu L, Xie F, Guo X, Zhang J, Yao L, et al. The Altered Triple Networks Interaction in Depression under Resting State Based on Graph Theory. *BioMed Research International [Internet]*. 2015; 2015:1–8. <https://doi.org/10.1155/2015/386326> PMID: 26180798
23. Liu Y, Li L, Li B, Feng N, Li L, Zhang X, et al. Decreased Triple Network Connectivity in Patients with Recent Onset Post-Traumatic Stress Disorder after a Single Prolonged Trauma Exposure. *Sci Rep*. 2017 Oct 3; 7(1). <https://doi.org/10.1038/s41598-017-12964-6> PMID: 28974724
24. Fan J, Zhong M, Gan J, Liu W, Niu C, Liao H, et al. Altered connectivity within and between the default mode, central executive, and salience networks in obsessive-compulsive disorder. *Journal of Affective Disorders*. 2017 Dec; 223:106–14. <https://doi.org/10.1016/j.jad.2017.07.041> PMID: 28743059
25. Manoliu A, Riedl V, Zherdin A, Mühlau M, Schwerthöffer D, Scherr M, et al. Aberrant Dependence of Default Mode/Central Executive Network Interactions on Anterior Insular Salience Network Activity in Schizophrenia. *Schizophrenia Bulletin*. 2013 Mar 21; 40(2):428–37. <https://doi.org/10.1093/schbul/sbt037> PMID: 23519021
26. Jiang L, Zuo X-N. Regional Homogeneity. *Neuroscientist*. 2016 Jul 9; 22(5):486–505. <https://doi.org/10.1177/1073858415595004> PMID: 26170004
27. Menon B. Towards a new model of understanding—The triple network, psychopathology and the structure of the mind. *Medical Hypotheses*. 2019 Dec; 133:109385. <https://doi.org/10.1016/j.mehy.2019.109385> PMID: 31494485
28. Imperatori C, Massullo C, Carbone GA, Panno A, Giacchini M, Capriotti C, et al. Increased Resting State Triple Network Functional Connectivity in Undergraduate Problematic Cannabis Users: A Preliminary EEG Coherence Study. *Brain Sciences*. 2020 Feb 28; 10(3):136. <https://doi.org/10.3390/brainsci10030136> PMID: 32121183
29. Sakoğlu Ü, Pearson GD, Kiehl KA, Wang YM, Michael AM, Calhoun VD. A method for evaluating dynamic functional network connectivity and task-modulation: application to schizophrenia. *Magn Reson Mater Phys*. 2010 Feb 17; 23(5–6):351–66. <https://doi.org/10.1007/s10334-010-0197-8> PMID: 20162320
30. Bassett DS, Wymbs NF, Porter MA, Mucha PJ, Carlson JM, Grafton ST. Dynamic reconfiguration of human brain networks during learning. *Proceedings of the National Academy of Sciences [Internet]*. 2011 Apr 18; 108(18):7641–6. <https://doi.org/10.1073/pnas.1018985108> PMID: 21502525
31. Albert NB, Robertson EM, Miall RC. The Resting Human Brain and Motor Learning. *Current Biology*. 2009 Jun; 19(12):1023–7. <https://doi.org/10.1016/j.cub.2009.04.028> PMID: 19427210
32. Lewis CM, Baldassarre A, Committeri G, Romani GL, Corbetta M. Learning sculpts the spontaneous activity of the resting human brain. *Proceedings of the National Academy of Sciences*. 2009 Oct 5; 106(41):17558–63. <https://doi.org/10.1073/pnas.0902455106> PMID: 19805061
33. Stevens WD, Buckner RL, Schacter DL. Correlated Low-Frequency BOLD Fluctuations in the Resting Human Brain Are Modulated by Recent Experience in Category-Preferential Visual Regions. *Cerebral Cortex*. 2009 Dec 21; 20(8):1997–2006. <https://doi.org/10.1093/cercor/bhp270> PMID: 20026486
34. Taubert M, Lohmann G, Margulies DS, Villringer A, Ragert P. Long-term effects of motor training on resting-state networks and underlying brain structure. *NeuroImage*. 2011 Aug; 57(4):1492–8. <https://doi.org/10.1016/j.neuroimage.2011.05.078> PMID: 21672633
35. Sami S, Robertson EM, Miall RC. The Time Course of Task-Specific Memory Consolidation Effects in Resting State Networks. *Journal of Neuroscience*. 2014 Mar 12; 34(11):3982–92. <https://doi.org/10.1523/JNEUROSCI.4341-13.2014> PMID: 24623776
36. Hartzell JF, Tobia MJ, Davis B, Cashdollar NM, Hasson U. Differential lateralization of hippocampal connectivity reflects features of recent context and ongoing demands: An examination of immediate post-task activity. *Hum Brain Mapp*. 2014 Oct 8; 36(2):519–37. <https://doi.org/10.1002/hbm.22644> PMID: 25293364
37. Gregory MD, Agam Y, Selvadurai C, Nagy A, Vangel M, Tucker M, et al. Resting state connectivity immediately following learning correlates with subsequent sleep-dependent enhancement of motor task performance. *NeuroImage [Internet]*. 2014 Nov; 102:666–73. <https://doi.org/10.1016/j.neuroimage.2014.08.044> PMID: 25173415
38. Squires NK, Squires KC, Hillyard SA. Two varieties of long-latency positive waves evoked by unpredictable auditory stimuli in man. *Electroencephalography and Clinical Neurophysiology*. 1975 Apr; 38(4):387–401. [https://doi.org/10.1016/0013-4694\(75\)90263-1](https://doi.org/10.1016/0013-4694(75)90263-1) PMID: 46819

39. Bledowski C. Localizing P300 Generators in Visual Target and Distractor Processing: A Combined Event-Related Potential and Functional Magnetic Resonance Imaging Study. *Journal of Neuroscience*. 2004 Oct 20; 24(42):9353–60. <https://doi.org/10.1523/JNEUROSCI.1897-04.2004> PMID: 15496671
40. Gur RC, Turetsky BI, Loughhead J, Waxman J, Snyder W, Ragland JD, et al. Hemodynamic responses in neural circuitries for detection of visual target and novelty: An event-related fMRI study. *Hum Brain Mapp*. 2007; 28(4):263–74. <https://doi.org/10.1002/hbm.20319> PMID: 17133387
41. Kiehl KA, Stevens MC, Laurens KR, Pearlson G, Calhoun VD, Liddle PF. An adaptive reflexive processing model of neurocognitive function: supporting evidence from a large scale (n = 100) fMRI study of an auditory oddball task. *NeuroImage*. 2005 Apr; 25(3):899–915. <https://doi.org/10.1016/j.neuroimage.2004.12.035> PMID: 15808990
42. Strobel A, Debener S, Sorger B, Peters JC, Kranczioch C, Hoechstetter K, et al. Novelty and target processing during an auditory novelty oddball: A simultaneous event-related potential and functional magnetic resonance imaging study. *NeuroImage*. 2008 Apr; 40(2):869–83. <https://doi.org/10.1016/j.neuroimage.2007.10.065> PMID: 18206391
43. Warbrick T, Mobascher A, Brinkmeyer J, Musso F, Richter N, Stoecker T, et al. Single-trial P3 amplitude and latency informed event-related fMRI models yield different BOLD response patterns to a target detection task. *NeuroImage*. 2009 Oct; 47(4):1532–44. <https://doi.org/10.1016/j.neuroimage.2009.05.082> PMID: 19505583
44. Linden DEJ. The Functional Neuroanatomy of Target Detection: An fMRI Study of Visual and Auditory Oddball Tasks. *Cerebral Cortex*. 1999 Dec 1; 9(8):815–23. <https://doi.org/10.1093/cercor/9.8.815> PMID: 10601000
45. McCarthy G, Luby M, Gore J, Goldman-Rakic P. Infrequent Events Transiently Activate Human Prefrontal and Parietal Cortex as Measured by Functional MRI. *Journal of Neurophysiology*. 1997 Mar 1; 77(3):1630–4. <https://doi.org/10.1152/jn.1997.77.3.1630> PMID: 9084626
46. Yoshiura T, Zhong J, Shibata DK, Kwok WE, Shrier DA, Numaguchi Y. Functional MRI study of auditory and visual oddball tasks. *NeuroReport*. 1999 Jun; 10(8):1683–8. <https://doi.org/10.1097/00001756-199906030-00011> PMID: 10501557
47. Halgren E, Marinkovic K, Chauvel P. Generators of the late cognitive potentials in auditory and visual oddball tasks. *Electroencephalography and Clinical Neurophysiology*. 1998 Feb; 106(2):156–64. [https://doi.org/10.1016/s0013-4694\(97\)00119-3](https://doi.org/10.1016/s0013-4694(97)00119-3) PMID: 9741777
48. Zang Y, Jiang T, Lu Y, He Y, Tian L. Regional homogeneity approach to fMRI data analysis. *NeuroImage*. 2004 May; 22(1):394–400. <https://doi.org/10.1016/j.neuroimage.2003.12.030> PMID: 15110032
49. Zuo X-N, Ehmke R, Menes M, Imperati D, Castellanos FX, Sporns O, et al. Network Centrality in the Human Functional Connectome. *Cerebral Cortex*. 2011 Oct 2; 22(8):1862–75. <https://doi.org/10.1093/cercor/bhr269> PMID: 21968567
50. Yu-Feng Z, Yong H, Chao-Zhe Z, Qing-Jiu C, Man-Qiu S, Meng L, et al. Altered baseline brain activity in children with ADHD revealed by resting-state functional MRI. *Brain and Development*. 2007 Mar; 29(2):83–91. <https://doi.org/10.1016/j.braindev.2006.07.002> PMID: 16919409
51. Warbrick T, Reske M, Shah NJ. Do EEG paradigms work in fMRI? Varying task demands in the visual oddball paradigm: Implications for task design and results interpretation. *NeuroImage*. 2013 Aug; 77:177–85. <https://doi.org/10.1016/j.neuroimage.2013.03.026> PMID: 23537937
52. Smith SM. Fast robust automated brain extraction. *Hum Brain Mapp*. 2002 Nov; 17(3):143–55. <https://doi.org/10.1002/hbm.10062> PMID: 12391568
53. Jenkinson M, Bannister P, Brady M, Smith S. Improved Optimization for the Robust and Accurate Linear Registration and Motion Correction of Brain Images. *NeuroImage*. 2002 Oct; 17(2):825–41. [https://doi.org/10.1016/s1053-8119\(02\)91132-8](https://doi.org/10.1016/s1053-8119(02)91132-8) PMID: 12377157
54. Jenkinson M, Smith S. A global optimisation method for robust affine registration of brain images. *Medical Image Analysis*. 2001 Jun; 5(2):143–56. [https://doi.org/10.1016/s1361-8415\(01\)00036-6](https://doi.org/10.1016/s1361-8415(01)00036-6) PMID: 11516708
55. Shirer WR, Ryali S, Rykhlevskaia E, Menon V, Greicius MD. Decoding Subject-Driven Cognitive States with Whole-Brain Connectivity Patterns. *Cerebral Cortex*. 2011 May 26; 22(1):158–65. <https://doi.org/10.1093/cercor/bhr099> PMID: 21616982
56. Woolrich MW, Ripley BD, Brady M, Smith SM. Temporal Autocorrelation in Univariate Linear Modeling of fMRI Data. *NeuroImage*. 2001 Dec; 14(6):1370–86. <https://doi.org/10.1006/nimg.2001.0931> PMID: 11707093
57. Woolrich MW, Behrens TEJ, Beckmann CF, Jenkinson M, Smith SM. Multilevel linear modelling for fMRI group analysis using Bayesian inference. *NeuroImage*. 2004 Apr; 21(4):1732–47. <https://doi.org/10.1016/j.neuroimage.2003.12.023> PMID: 15050594

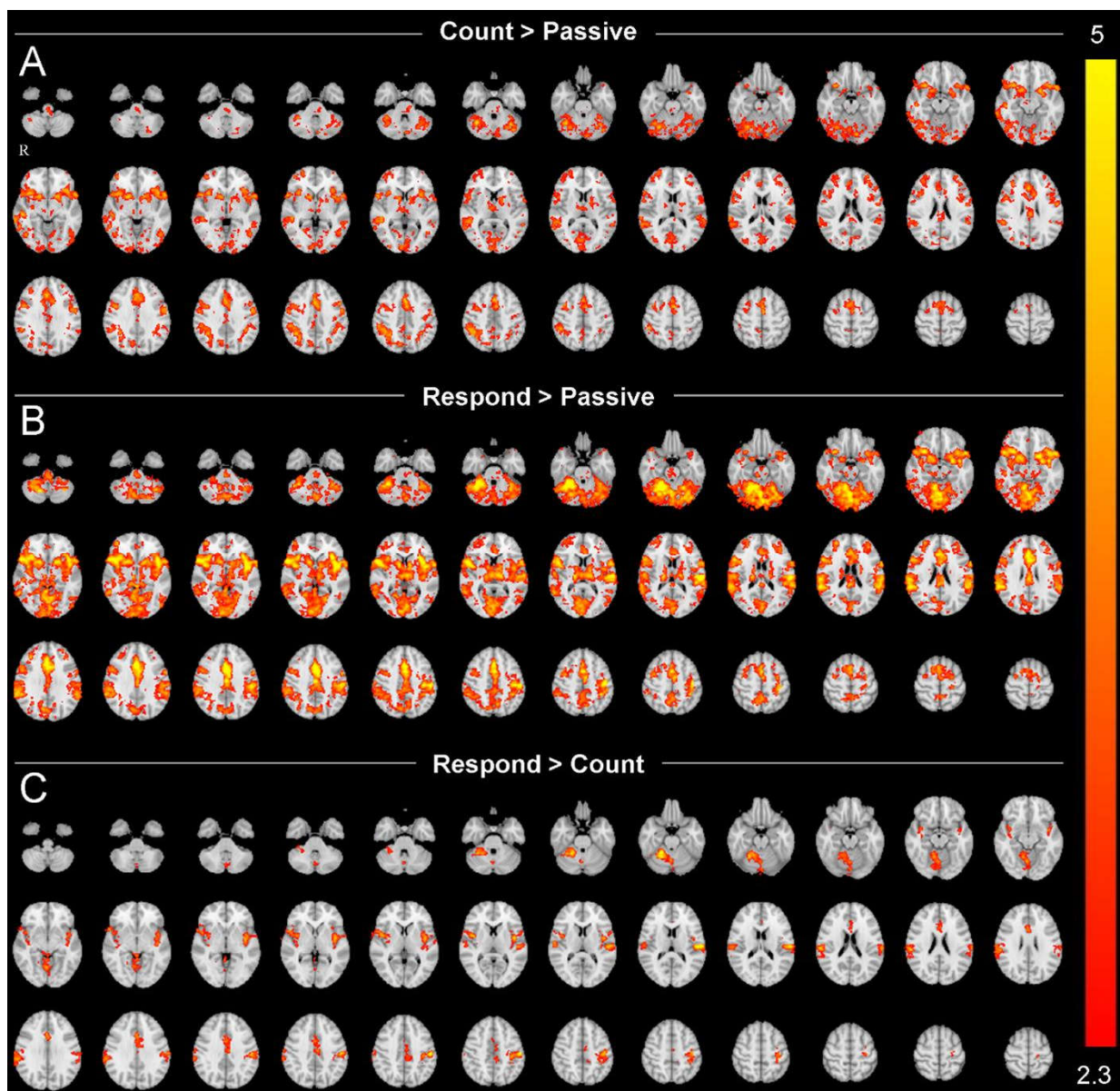
58. Yan C-G, Wang X-D, Zuo X-N, Zang Y-F. DPABI: Data Processing & Analysis for (Resting-State) Brain Imaging. *Neuroinform*. 2016 Apr 13; 14(3):339–51. <https://doi.org/10.1007/s12021-016-9299-4> PMID: 27075850
59. Yan. DPARSF: a MATLAB toolbox for “pipeline” data analysis of resting-state fMRI. *Front Syst Neurosci*. 2010. <https://doi.org/10.3389/fnins.2010.00013> PMID: 20577591
60. Friston K. J., Williams S., Howard R., Frackowiak R. S. J., & Turner R. (1996). Movement-Related effects in fMRI time-series. *Magnetic Resonance in Medicine*, 35(3), 346–355. <https://doi.org/10.1002/mrm.1910350312> PMID: 8699946
61. Takeuchi H, Taki Y, Nouchi R, Sekiguchi A, Hashizume H, Sassa Y, et al. Degree centrality and fractional amplitude of low-frequency oscillations associated with Stroop interference. *NeuroImage*. 2015 Oct; 119:197–209. <https://doi.org/10.1016/j.neuroimage.2015.06.058> PMID: 26123381
62. Gideon RA. The Correlation Coefficients. *J Mod App Stat Meth*. 2007 Nov 1; 6(2):517–29. <https://doi.org/10.22237/jmasm/1193890500>
63. Zou Q-H, Zhu C-Z, Yang Y, Zuo X-N, Long X-Y, Cao Q-J, et al. An improved approach to detection of amplitude of low-frequency fluctuation (ALFF) for resting-state fMRI: Fractional ALFF. *Journal of Neuroscience Methods*. 2008 Jul; 172(1):137–41. <https://doi.org/10.1016/j.jneumeth.2008.04.012> PMID: 18501969
64. Greenhouse S. W., & Geisser S. (1959). On methods in the analysis of profile data. *Psychometrika*, 24(2), 95–112. <https://doi.org/10.1007/bf02289823>.
65. Zuo X.-N., Di Martino A., Kelly C., Shehzad Z. E., Gee D. G., Klein D. F., et al. (2010). The oscillating brain: Complex and reliable. *NeuroImage*, 49(2), 1432–1445. <https://doi.org/10.1016/j.neuroimage.2009.09.037> PMID: 19782143
66. Qi S., Gao Q., Shen J., Teng Y., Xie X., Sun Y., & Wu J. (2018). Multiple Frequency Bands Analysis of Large Scale Intrinsic Brain Networks and Its Application in Schizotypal Personality Disorder. *Frontiers in Computational Neuroscience*, 12. <https://doi.org/10.3389/fncom.2018.00064> PMID: 30123120
67. Mason M. F., Norton M. I., Van Horn J. D., Wegner D. M., Grafton S. T., & Macrae C. N. (2007). Wandering Minds: The Default Network and Stimulus-Independent Thought. *Science*, 315(5810), 393–395. <https://doi.org/10.1126/science.1131295> PMID: 17234951
68. Thomason M. E., Chang C. E., Glover G. H., Gabrieli J. D. E., Greicius M. D., & Gotlib I. H. (2008). Default-mode function and task-induced deactivation have overlapping brain substrates in children. *NeuroImage*, 41(4), 1493–1503. <https://doi.org/10.1016/j.neuroimage.2008.03.029> PMID: 18482851
69. Binder J. R. (2012). Task-induced deactivation and the “resting” state. *NeuroImage*, 62(2), 1086–1091. <https://doi.org/10.1016/j.neuroimage.2011.09.026> PMID: 21979380
70. Leech R., Kamourieh S., Beckmann C. F., & Sharp D. J. (2011). Fractionating the Default Mode Network: Distinct Contributions of the Ventral and Dorsal Posterior Cingulate Cortex to Cognitive Control. *Journal of Neuroscience*, 31(9), 3217–3224. <https://doi.org/10.1523/JNEUROSCI.5626-10.2011> PMID: 21368033
71. McKiernan K. A., Kaufman J. N., Kucera-Thompson J., & Binder J. R. (2003). A Parametric Manipulation of Factors Affecting Task-induced Deactivation in Functional Neuroimaging. *Journal of Cognitive Neuroscience*, 15(3), 394–408. <https://doi.org/10.1162/089892903321593117> PMID: 12729491
72. Tommasin S., Mascali D., Gill T., Eid Assan I., Moraschi M., Fratini M., et al. (2017). Task-Related Modulations of BOLD Low-Frequency Fluctuations within the Default Mode Network. *Frontiers in Physics*, 5. <https://doi.org/10.3389/fphy.2017.00031> PMID: 28845420
73. He Y., Wang L., Zang Y., Tian L., Zhang X., Li K., & Jiang T. (2007). Regional coherence changes in the early stages of Alzheimer’s disease: A combined structural and resting-state functional MRI study. *NeuroImage*, 35(2), 488–500. <https://doi.org/10.1016/j.neuroimage.2006.11.042> PMID: 17254803
74. Shen Z., Jiang L., Yang S., Ye J., Dai N., Liu X., et al. (2017). Identify changes of brain regional homogeneity in early and later adult onset patients with first-episode depression using resting-state fMRI. *PLOS ONE*, 12(9), e0184712. <https://doi.org/10.1371/journal.pone.0184712> PMID: 28910390
75. Zuo X-N, Xu T, Jiang L, Yang Z, Cao X-Y, He Y, et al. Toward reliable characterization of functional homogeneity in the human brain: Preprocessing, scan duration, imaging resolution and computational space. *NeuroImage*. 2013 Jan; 65:374–86. <https://doi.org/10.1016/j.neuroimage.2012.10.017> PMID: 23085497
76. Zuo X-N, Xing X-X. Test-retest reliabilities of resting-state fMRI measurements in human brain functional connectomics: A systems neuroscience perspective. *Neuroscience & Biobehavioral Reviews*. 2014 Sep; 45:100–18. <https://doi.org/10.1016/j.neubiorev.2014.05.009> PMID: 24875392
77. Di X., & Biswal B. B. (2013). Dynamic brain functional connectivity modulated by resting-state networks. *Brain Structure and Function*, 220(1), 37–46. <https://doi.org/https%3A%2F%2Fdoi.org/10.1007/s00429-013-0634-3> PMID: 25713839

78. Barnes A., Bullmore E. T., & Suckling J. (2009). Endogenous Human Brain Dynamics Recover Slowly Following Cognitive Effort. *PLoS ONE*, 4(8), e6626. <https://doi.org/10.1371/journal.pone.0006626> PMID: 19680553
79. Akiki T.J., Averill C.L., Abdallah C.G. A Network-Based Neurobiological Model of PTSD: Evidence From Structural and Functional Neuroimaging Studies. *Curr Psychiatry Rep.* 2017 Sep 19; 19(11). <https://doi.org/10.1007/s11920-017-0840-4> PMID: 28924828
80. Turner B.M., Rodríguez C.A., Liu Q., Molloy M.F., Hoogendijk M., McClure S.M. On the Neural and Mechanistic Bases of Self-Control. *Cerebral Cortex.* 2018 Jan 24; 29(2):732–50. <https://doi.org/10.1093/cercor/bhx355> PMID: 29373633
81. Gagnepain P., Hulbert J., Anderson M.C. Parallel Regulation of Memory and Emotion Supports the Suppression of Intrusive Memories. *J Neurosci.* 2017 May 30; 37(27):6423–41. <https://doi.org/10.1523/JNEUROSCI.2732-16.2017> PMID: 28559378
82. Wessing I., Rehbein M.A., Postert C., FÜRMISS T., Junghöfer M. The neural basis of cognitive change: Reappraisal of emotional faces modulates neural source activity in a frontoparietal attention network. *NeuroImage [Internet].* 2013 Nov; 81:15–25. <https://doi.org/10.1016/j.neuroimage.2013.04.117> PMID: 23664945
83. Chen A. C., Oathes D. J., Chang C., Bradley T., Zhou Z.-W., Williams L. M., et al. (2013). Causal interactions between fronto-parietal central executive and default-mode networks in humans. *Proceedings of the National Academy of Sciences*, 110(49), 19944–19949. <https://doi.org/10.1073/pnas.1311772110> PMID: 24248372
84. Craig A. D. (2002). How do you feel? Interoception: the sense of the physiological condition of the body. *Nature Reviews Neuroscience*, 3(8), 655–666. <https://doi.org/10.1038/nrn894> PMID: 12154366
85. Critchley H. D., Wiens S., Rotshtein P., Öhman A., & Dolan R. J. (2004). Neural systems supporting interoceptive awareness. *Nature Neuroscience*, 7(2), 189–195. <https://doi.org/10.1038/nn1176> PMID: 14730305
86. Liu C.-H., Guo J., Lu S.-L., Tang L.-R., Fan J., Wang C.-Y., et al. (2018). Increased Salience Network Activity in Patients With Insomnia Complaints in Major Depressive Disorder. *Frontiers in Psychiatry*, 9. <https://doi.org/10.3389/fpsy.2018.00093> PMID: 29615938
87. Andrews-Hanna J. R., Smallwood J., & Spreng R. N. (2014). The default network and self-generated thought: component processes, dynamic control, and clinical relevance. *Annals of the New York Academy of Sciences*, 1316(1), 29–52. <https://doi.org/https://doi.org/10.1111/nyas.12360> PMID: 24502540
88. Gerlach K. D., Spreng R. N., Gilmore A. W., & Schacter D. L. (2011). Solving future problems: Default network and executive activity associated with goal-directed mental simulations. *NeuroImage*, 55(4), 1816–1824. <https://doi.org/10.1016/j.neuroimage.2011.01.030> PMID: 21256228
89. Meyer M. L., Spunt R. P., Berkman E. T., Taylor S. E., & Lieberman M. D. (2012). Evidence for social working memory from a parametric functional MRI study. *Proceedings of the National Academy of Sciences*, 109(6), 1883–1888. <https://doi.org/10.1073/pnas.1121077109> PMID: 22308468
90. Beaty R. E., Benedek M., Barry Kaufman S., & Silvia P. J. (2015). Default and Executive Network Coupling Supports Creative Idea Production. *Scientific Reports*, 5(1). <https://doi.org/https://doi.org/10.1038/srep10964> PMID: 26084037
91. Spreng R. N., Sepulcre J., Turner G. R., Stevens W. D., & Schacter D. L. (2013). Intrinsic Architecture Underlying the Relations among the Default, Dorsal Attention, and Frontoparietal Control Networks of the Human Brain. *Journal of Cognitive Neuroscience*, 25(1), 74–86. https://doi.org/10.1162/jocn_a_00281 PMID: 22905821
92. Chang C., & Glover G. H. (2010). Time–frequency dynamics of resting-state brain connectivity measured with fMRI. *NeuroImage*, 50(1), 81–98. <https://doi.org/10.1016/j.neuroimage.2009.12.011> PMID: 20006716
93. Dosenbach N. U. F., Visscher K. M., Palmer E. D., Miezin F. M., Wenger K. K., Kang H. C., et al. (2006). A Core System for the Implementation of Task Sets. *Neuron*, 50(5), 799–812. <https://doi.org/10.1016/j.neuron.2006.04.031> PMID: 16731517
94. Petrides M. Lateral prefrontal cortex: architectonic and functional organization. *Phil Trans R Soc B.* 2005 Apr 29; 360(1456):781–95. <https://doi.org/10.1098/rstb.2005.1631> PMID: 15937012

Supporting information



S1 Fig. BOLD activation in response to target and frequent stimuli in the passive, count and respond condition (group-level mixed-effects FLAME, single group average) for 21 healthy subjects (age: 29 ± 5.6 years), Cluster-corrected threshold ($Z = 2.3$, $p = 0.01$).



S2 Fig. BOLD activation of the tripled two-group difference (“tripled t-test”) for the (target > frequent) first level contrast. The tripled two-group differences are like follows: Count > passive (A), respond > passive (B), and respond > count (C) across 21 healthy subjects (age: 29 ± 5.6 years), Cluster-corrected threshold ($Z = 2.3$, $p = 0.01$).

Test-retest stability of spontaneous brain activity and functional connectivity in the core resting-state networks assessed with ultrahigh field 7-Tesla resting-state functional magnetic resonance imaging

Hasan Sbaihat^{1,2,3} | Ravichandran Rajkumar^{1,3,4} | Shukti Ramkiran^{1,3,4} |
Abed Al-Nasser Assi² | Jörg Felder^{1,2} | Nadim Jon Shah^{1,4,5,6} | Tanja Veselinović³ |
Irene Neuner^{1,3,4}

¹Institute of Neuroscience and Medicine, INM-4, Jülich, Germany

²Department of Medical Imaging, Arab-American University Palestine (AAUP), Jenin, Palestine

³Department of Psychiatry, Psychotherapy, and Psychosomatics, RWTH Aachen University, Aachen, Germany

⁴JARA—BRAIN—Translational Medicine, Aachen, Germany

⁵Department of Neurology, RWTH Aachen University, Aachen, Germany

⁶Institute of Neuroscience and Medicine, INM-11, Forschungszentrum Jülich GmbH, Jülich, Germany

Correspondence

Irene Neuner, Department of Psychiatry, Psychotherapy and Psychosomatics, RWTH Aachen University, Pauwelsstrasse 30, 52074 Aachen, Germany.
Email: i.neuner@fz-juelich.de

Funding information

Bundesministerium für Bildung und Forschung, Grant/Award Number: DBR01436; Federal Ministry of Education and Research

Abstract

The growing demand for precise and reliable biomarkers in psychiatry is fueling research interest in the hope that identifying quantifiable indicators will improve diagnoses and treatment planning across a range of mental health conditions. The individual properties of brain networks at rest have been highlighted as a possible source for such biomarkers, with the added advantage that they are relatively straightforward to obtain. However, an important prerequisite for their consideration is their reproducibility. While the reliability of resting-state (RS) measurements has often been studied at standard field strengths, they have rarely been investigated using ultrahigh-field (UHF) magnetic resonance imaging (MRI) systems. We investigated the intersession stability of four functional MRI RS parameters—amplitude of low-frequency fluctuations (ALFF) and fractional ALFF (fALFF; representing the spontaneous brain activity), regional homogeneity (ReHo; measure of local connectivity), and degree centrality (DC; measure of long-range connectivity)—in three RS networks, previously shown to play an important role in several psychiatric diseases—the default mode network (DMN), the central executive network (CEN), and the salience network (SN). Our investigation at individual subject space revealed a strong stability for ALFF, ReHo, and DC in all three networks, and a moderate level of stability in fALFF. Furthermore, the internetwork connectivity between each network pair was strongly stable between CEN/SN and moderately stable between DMN/SN and DMN/SN. The high degree of reliability and reproducibility in capturing the properties of the three major RS networks by means of UHF-MRI points to its applicability as a potentially useful tool in the search for disease-relevant biomarkers.

Tanja Veselinović and Irene Neuner equally contributed to this study.

This is an open access article under the terms of the Creative Commons Attribution License, which permits use, distribution and reproduction in any medium, provided the original work is properly cited.

© 2022 The Authors. *Human Brain Mapping* published by Wiley Periodicals LLC.

KEYWORDS

7 Tesla, functional connectivity, functional magnetic resonance imaging, high resolution, resting state, test-retest stability, triple-network model

1 | INTRODUCTION

The increasing demand for precision psychiatry during the last decades (Insel & Cuthbert, 2015) has led to an awareness of the need to establish reliable biomarkers for mental health and different psychiatric conditions. According to the National Institutes of Health Biomarkers Definitions Working Group, biomarkers are “a characteristic that is objectively measured and evaluated as an indicator of normal biological processes, pathogenic processes, or pharmacologic responses to a therapeutic intervention.” (Biomarkers Definitions Working Group, 2001). Consequently, valid biomarkers are increasingly seen as essential for both the precise diagnosis of complex mental disorders and for reliable therapy monitoring.

Since the discovery of temporal correlations obtained by blood-oxygen-level-dependent (BOLD) signal fluctuations during rest in the 1990s (Biswal, Zerrin, Haughton, & Hyde, 1995), the resting-state (RS) research approach has been increasingly used to map regional interactions in the brain and has considered to have a promising potential in the search for biomarkers for brain-related disorders (Blautzik et al., 2013; Washington et al., 2013). Indeed, numerous investigations confirm that the human brain is organized into dynamic, intrinsic, resting-state functional networks (rsNW; Cabral, Kringelbach, & Deco, 2017; Fox et al., 2005; Smith et al., 2013), and the link between serious mental illnesses and abnormal brain connectivity is gaining widespread acceptance (Woodward & Cascio, 2015). Thus, features and patterns derived from spontaneous brain activity and functional connectivity (FC) could be considered as potential neurophysiological biomarkers for various psychopathological phenomena across neuropsychiatric disorders (Blatow, Nennig, Durst, Sartor, & Stippich, 2007; Imperatori et al., 2020).

Resting-state functional MRI (rs-fMRI) measures functional connections in the brain via the temporal correlation of low-frequency ($0.01 < f < 0.1$ Hz) fluctuations in the BOLD fMRI signal. These fluctuations reflect synchronized variations in spontaneous neuronal firing and unconstrained mental activity (e.g., mind wandering; Biswal et al., 1995; Fox & Raichle, 2007; Mason et al., 2007). The main advantage of measuring FC using MRI is its noninvasive nature. Furthermore, the participant is not required to complete an instructed task, meaning that the results are not influenced by the task demands or the efforts and motivation of the participants. Consequently, FC examinations can be considered to be objective. Furthermore, rs-fMRI examinations are well tolerated by most subjects including patients with severe symptomatology and require a reasonably short acquisition time. Thereby, some authors state that acquisition times of about 6 min have provided adequate sampling to obtain robust results (Van Dijk et al., 2010), whereas others recommend, when possible, longer acquisitions (about 12 min; Hacker, Roland, Kim, Shimony, &

Leuthardt, 2019). However, despite the broad applicability, it has to be kept in mind that rs-fMRI measurements may be hampered by minimal head motions as well as by several physiological effects (e.g., respiration and cardiac pulsatility) and various imperfections in MRI system hardware (e.g., heating of the imaging gradients during experiments; Maknojia, Churchill, Schweizer, & Graham, 2019), thus the preprocessing requires a high degree of diligence.

So far, the transition toward the use of RS connectivity patterns as a biomarker in clinical practice has not yet occurred. Among other things, this requires a better understanding of the microscale brain organization. The development of ultrahigh-field (UHF) neuroimaging technologies, that is, UHF-MRI, offer the potential to bridge this shortcoming (Bazin et al., 2014; Dinse et al., 2013; Geyer, Weiss, Reimann, Lohmann, & Turner, 2011). One important consideration hereby is the recognition of the good tolerability of the most UHF-MRI systems (Theysohn et al., 2007).

The usage of UHF-MRI entails several advantages. The benefits include increased spatial sampling in the native image, and thus a high spatial resolution (which decreases partial volume effects; Newton, Rogers, Gore, & Morgan, 2012) improved signal-to-noise ratio (Triantafyllou et al., 2005), increased sensitivity (Kraff, Fischer, Nagel, Mönninghoff, & Ladd, 2014), enhanced amplitude, and percent of signal change in BOLD signal (Sladky et al., 2013; van der Zwaag et al., 2009), significantly accentuated microvasculature contributions (Duong et al., 2003), and significantly reduced nonspecific mapping signals from large vessels, which together can lead to a deeper understanding of the intrinsic properties of functional brain networks (De Martino et al., 2011; Gorgolewski et al., 2015; Holiga et al., 2018). Moreover, these factors considerably increase the quantity of data obtained per scan and enable the consideration of the individual examination.

However, besides the clear advantages provided by UHF-MRI, certain drawbacks must also be taken into account. Commonly discussed disadvantages include some physiological considerations (more intensively pronounced unpleasant transient effects such as vertigo and nausea discomfort (Rauschenberg et al., 2014) but also some technical aspects. As field strength increases, field inhomogeneity—both in the local magnetic field (B_0) due to increased magnetic susceptibility effects and in the radiofrequency transmit and receive fields (B_1+ and B_1-) due to dielectric effects—can cause image artifacts such as geometric distortion and image intensity biases over the brain (Polimeni, Renvall, Zaretskaya, & Fischl, 2018). This may particularly affect single-shot echo-planar imaging (EPI), which represents the mainly used application in fMRI imaging (Preibisch, Castrillón, Bührer, & Riedl, 2015). Besides geometrical distortions, the technical challenges further include position-dependent flip angle, poor inversion, unexpected contrast, intravoxel dephasing as well as increased

tissue-specific absorption rates (SAR) and susceptibility-induced magnetic field variations within a region of interest (ROI; Ladd et al., 2018). The search for adequate solutions to the issues mentioned above has progressed but is far from being complete (Düzel, Costagli, Donatelli, Speck, & Cosottini, 2021; Ladd et al., 2018).

One of the most important requirements for valid biomarkers is reproducibility (Strimbu & Tavel, 2010). In this context, numerous studies have investigated the reliability of RS measurements using MRI at 1.5 and 3.0 Tesla (Braun et al., 2012; Klomp et al., 2013; Manoach et al., 2001; Plichta et al., 2012; Q. Zou et al., 2015) and have demonstrated reproducible results. For example, Somandepalli and colleagues examined reliability within and across diagnostic groups of children with attention-deficit/hyperactivity disorder and typically developing children (Somandepalli et al., 2015). They also examined voxel-wise reliability between groups. Their results demonstrated moderate-to-high reliability across all children and within groups and additionally found that the higher-order functional networks showed more than the lower one (Somandepalli et al., 2015). Z. Li, Kadivar, Pluta, Dunlop, and Wang (2012) examined the reproducibility of different fMRI matrices, such as seed region-based FC, regional homogeneity (ReHo), and the amplitude of low-frequency fluctuation (ALFF), in the RS brain and demonstrated the test-retest reproducibility for ReHo and ALFF in the whole gray matter.

Moreover, long-term reproducibility studies have also shown good results. Song, Panych, and Chen (2016) demonstrated that substantial to moderate long-term within-subject reproducibility can be achieved in rs-fMRI by applying data-driven and predefined ROI-based quantification of reproducibility. Chou, Panych, Dickey, Petrella, and Chen (2012) also examined the long-term reproducibility of intrinsic connectivity networks and reported that RS intrinsic connectivity network parameters might be appropriate biomarkers for monitoring disease progression and treatments.

Although studies relating to the stability of FC measurements at standard field strengths are relatively abundant, far fewer have been conducted at UHF. Recently, Geissberger et al. (2020) investigated the reproducibility of amygdala activation in facial emotion processing at 7 Tesla and found fair to good intersession reliability and excellent reliability for averages over runs. In another study, Berboth, Windischberger, Kohn, and Morawetz (2021) investigated the voxel-wise test-retest reliability of brain activity in response to an emotion regulation task for predefined ROIs implicated in four neural networks. Although test-retest reliability varied considerably across the emotion regulation networks and respective ROIs, high reliability was found in core emotion regulation regions, including the ventrolateral and dorsolateral prefrontal cortex (vlPFC and dlPFC) as well as the middle temporal gyrus (MTG).

Finally, Branco, Seixas, and Castro (2018) used a publicly released data set from the consortium for reliability and reproducibility (Zuo & Xing, 2014) to examine the temporal reliability of the sensorimotor and language networks. The authors reported good temporal reliability at short and medium time scales, as demonstrated by high values of overlap in the same session and 1 week after, for both networks. The results were also shown to be stable, irrespective of data quality metrics and physiological variables.

Given the paucity of research into the reliability of the properties of the core RS networks at UHF, this study aims to address this issue with a focus on three established RS networks—the default mode network (DMN), the central executive network (CEN), and the salience network (SN)—often subsumed as the triple-network model (TNM). The networks of the TNM are considered to be the core of neurocognitive networks due to the involvement in a wide range of cognitive tasks (Menon & Uddin, 2010). Moreover, disruption in the synchronized activity of the triple networks has been implicated in various psychiatric diseases (Dong, Wang, Chang, Luo, & Yao, 2017; Jiang et al., 2017; C. Li et al., 2019; Menon, 2011) that often show overlapping dysfunctions particularly in those three networks. In the meantime, it is widely accepted that coordination of these networks plays a key regulatory role in organizing neural responses underlying fundamental brain functions (Nekovarova, Fajnerova, Horacek, & Spaniel, 2014) and it has been proposed that a deepening of the knowledge considering the TMN may be essential to understand pathophysiological dysfunction across several psychiatric disorders, as dysfunction in one network may affect the other two (Menon, 2011).

Thus, we chose to use the publicly available data set obtained from the Gorgolewski project (Gorgolewski et al., 2015) to investigate the stability of these three core RS networks in terms of the intersession stability of the fMRI parameters and the stability of the inter-network correlations between the triple networks. The following four fMRI parameters were used to characterize the different properties of the brain networks: both ALFF (Yu-Feng et al., 2007) and fractional ALFF (fALFF; Q.-H. Zou et al., 2008) were used to evaluate the regional spontaneous activity. Specifically, ALFF indicates the strength of regional spontaneous brain activity, while fALFF represents the relative contribution of specific low-frequency fluctuation to the whole frequency range. The ReHo (Zang, Jiang, Lu, He, & Tian, 2004) was used to investigate local FC; and the degree centrality (DC; Zuo et al., 2012), was used to investigate global FC. Thus, ReHo and DC are considered to be mutually complementary for detecting both local and remote brain activity synchronization (Cui et al., 2016). Together with the ALFF and fALFF parameters, these fMRI metrics enable comprehensive rsNW characterization, displaying a pattern of RS activity, regional temporal integration, and connectivity.

2 | METHODS

2.1 | Subjects

The data used in this study were taken from the open-access data set (Gorgolewski et al., 2015). The original data set consisted of 22 healthy subjects (12 male and 10 female). We excluded six subjects due to head motion and technical issues. The exact reasons for the exclusion are given in Table S1. Therefore, our final data set originated from 16 subjects (9 male and 7 female) age range 22–29 years; mean 25.25 ± 2.01 . According to the original publication, all subjects signed written informed consent. The study was performed in accordance with the declaration of Helsinki and was approved by the Ethical Committee of the Leipzig University.

2.2 | Experimental procedure

The full experimental procedure is described in the original publication of Gorgolewski et al. (2015). All subjects were examined twice using a 7-Tesla whole-body MRI scanner (MAGNETOM 7 Tesla, Siemens Healthcare, Erlangen, Germany). The time between the two sessions was 1 week. Both examinations involved RS fMRI measurements. The focus of our investigation is on the results reported from the 15-min RS sessions.

2.3 | MR data acquisition

During the RS scanning sessions, the subjects were asked to remain awake, keep their eyes open, and focus on a cross. The subjects were also asked to abstain from drinking caffeinated products for at least 2 h before each scan.

All imaging protocols are presented in the original publication of Gorgolewski et al. (2015). MR data were acquired using a 7-Tesla whole-body scanner (MAGNETOM 7 T, Siemens Healthcare, Erlangen, Germany). A combined transmit receive head coil (consisting of a birdcage transmitter and 24 channels phased array receiver; NOVA Medical Inc, Wilmington, MA, USA) was used for imaging. The fMRI data were acquired using an EPI two-dimensional sequence. Data were acquired in the axial orientation. Three hundred volumes were acquired in 15 min for each RS run with the following parameters: repetition time (TR) = 3,000 ms, echo time (TE) = 17 ms, partial Fourier 6/8, GRAPPA acceleration factor iPAT = 3, flip angle (FA) = 70°, field-of-view (FOV) = 192 × 192 mm, imaging matrix 128 × 128 × 70 slices, slice thickness = 1.5 mm, and voxel size 1.5 mm³.

High-resolution T1-weighted images were acquired using a three-dimensional magnetization prepared rapid gradient echo (3D MP-2RAGE) sequence (TR = 5 s, TE = 2.45 ms, T_{1/2} = 0.9/2.75 s, partial Fourier 6/8, GRAPPA acceleration factor iPAT = 2, FA_{1/2} = 5°/3°, FOV = 224 × 224 × 168 mm³, imaging matrix 320 × 320 × 240, and voxel size 0.7 mm³).

2.4 | fMRI data preprocessing and analysis

The fMRI images were preprocessed using data processing and analysis for brain imaging (Yan, Wang, Zuo, & Zang, 2016) and SPM12 (<http://www.fil.ion.ucl.ac.uk/spm/>) toolboxes built on MATLAB software package version 2017b (The Math Works, Inc., Natick, MA, USA). The preprocessing was performed as follows: the first 10 volumes were removed, followed by slice timing correction, realignment of images and field map correction, individual T1 images were co-registered to the functional images. The transformed T1 images were segmented to grey matter, white matter (WM), and cerebrospinal fluid (CSF). Then the Friston 24-parameter model was used to remove the nuisance signals by regressing out the head motion effects from the

realigned data. Also, the signals from WM and CSF were regressed out to reduce the impact of physiological noise. As motion could influence the FC results, the Friston 24-parameter model and framewise displacement were used to estimate any head motion at the subject level. Any subjects who had head motion exceeding 1.5 mm in translation or 1.5° in rotation were excluded (Table S1). Afterward, to keep only the high-quality data, motion scrubbing was applied to remove minimal motion frames (volumes exhibiting framewise displacement >0.2 mm were excluded). After scrubbing, the percentage of volumes left for each subject and session is reported in Table S2. Then the fMRI parameters were computed in the native space. Default masks (whole brain, white matter, gray matter, and CSF) were generated based on the segmented T1 image and then were applied before computing the fMRI parameters. ALFF value was calculated by transforming the BOLD signal time series to the frequency domain using the fast Fourier transformation, then the power spectrum was obtained. Later ALFF is calculated as the sum of amplitudes within a low-frequency band of 0.01–0.1 Hz for each voxel (Yu-Feng et al., 2007). The fALFF value was calculated dividing the power within the low-frequency range (ALFF) by the total power in the entire measurable frequency range (Zuo et al., 2010). Later temporal filtering between 0.01 and 0.1 Hz was applied to all voxels time series on the preprocessed fMRI data to calculate DC and ReHo. The DC was computed by calculating Pearson's correlation coefficient between the time series of a given voxel and all other gray matter voxels in the brain. The correlation vector was binarized by applying a threshold ($r > .25$, $p \leq .001$) and added (Takeuchi et al., 2015). The ReHo was computed by averaging the synchronization or similarity between the time series of a given voxel and its 26 neighboring voxels using Kendall's coefficient of concordance (Zang et al., 2004). The fMRI parameters were normalized using a Z-score standardization procedure (subtracting the mean from each voxel and then dividing the value by the SD of the whole brain). Finally, spatial smoothing with full width at half maximum (FWHM) at 3 mm³ was applied.

2.5 | Triple-network ROIs

The publicly available data set was used to specifically extract and analyze the triple RS networks. The TNM included 15 ROIs, which were selected following the specifications from networks atlas provided by the Conn toolbox (Whitfield-Gabrieli & Nieto-Castanon, 2012). The masks for the DMN and CEN consisted of four ROIs each, and the SN mask included seven ROIs. Concretely, the DMN included the medial prefrontal cortex (MPFC), the left and right lateral parietal cortex and the posterior cingulate cortex (PCC). The CEN included the right and left lateral prefrontal cortex (rPFC, lPFC) and the right and left posterior parietal cortex (PPC). The SN included the anterior cingulate cortex (ACC), the left and right anterior insula, the left and right rostral prefrontal cortex, and the left and right supramarginal gyrus. The masks for the three networks are shown in Figure 1.

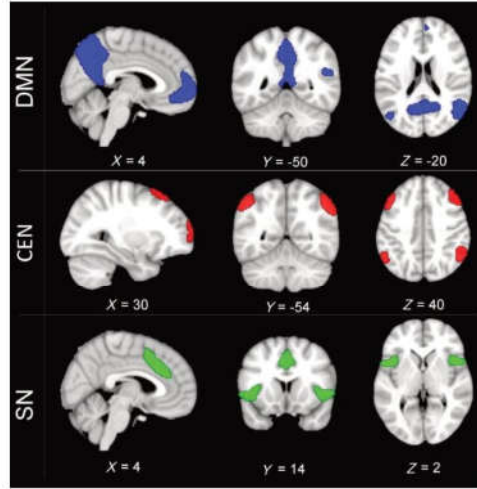


FIGURE 1 Depiction of the masks for the three core resting state networks: the default mode network (DMN, blue color), the central executive network (CEN, red color), and the salience network (SN, green color) overlaid on MNI152 template. CEN, central executive network; DMN, default mode network; SN, salience network

2.6 | ROI-based FC analysis

To keep the original spatial resolution of the functional images, the defined masks were warped into the individual space, and then the connectivity between the ROIs within the triple networks was computed by extracting the mean BOLD signal time series from each of three networks' ROI. Pearson's correlation coefficient was computed between each pair of the ROI's mean BOLD signal time series, resulting in two 15×15 connectivity matrices for each subject. Fisher's r to z transformation was applied for all connectivity matrices to improve the normality.

2.7 | Stability analysis

2.7.1 | Intersession stability of the fMRI parameters in the triple networks

We used Lin's concordance correlation coefficient (CCC) instead of Pearson's correlation because it estimates the variation from the 45° line (L. I. Lin, 1989; McBride, Lin, Bland, & Altman, 2005), thus, the CCC gives more accurate reliability results. Lin's CCC (ρ_c) was calculated using the following formulas (1-8) (L. I. Lin, 1989; L. Lin, Hedayat, Sinha, & Yang, 2002; McBride et al., 2005):

$$\rho_c = \frac{2\sigma_{yx}}{\sigma_y^2 + \sigma_x^2 + (\mu_y - \mu_x)^2}, \quad (1)$$

where the mean (μ_x) of each fMRI parameter in each session was computed as follows:

$$\mu_x = \frac{1}{n} \sum_{n=1}^n x_n. \quad (2)$$

The variance (σ_x^2) within each session for each fMRI parameter was computed as follows:

$$\sigma_x^2 = \frac{1}{n} \sum_{n=1}^n (x_n - \mu_x)^2. \quad (3)$$

The covariance (σ_{yx}) between two sessions for each fMRI parameter was computed as follows:

$$\sigma_{yx} = \frac{1}{n} \sum_{n=1}^n (y_n - \mu_y)(x_n - \mu_x). \quad (4)$$

The CCC can also be written as a product of accuracy and precision $\rho_c = \chi_a \rho$, where precision ρ is Pearson's correlation coefficient and accuracy is the term χ_a given by the equation:

$$\chi_a = \frac{2}{\varpi + \frac{1}{\varpi} + v^2}, \quad (5)$$

where

$$v^2 = \frac{(\mu_y - \mu_x)^2}{\sigma_y \sigma_x}, \quad (6)$$

and

$$\varpi = \frac{\sigma_y}{\sigma_x}. \quad (7)$$

Also, the sample counterpart of CCC is given by

$$r_c = \frac{2rS_yS_x}{S_y^2 + S_x^2 + (\bar{y} - \bar{x})^2}, \quad (8)$$

where the r is sample Pearson's correlation coefficient, \bar{y} and \bar{x} are the sample means, and the S_y^2 and S_x^2 are the sample variances.

The four fMRI parameters (ALFF, fALFF, ReHo, and DC) were extracted from the triple-network voxels for all subjects in both sessions. The extracted values were used to calculate the voxel-based CCC at the subject level. CCC was calculated using MATLAB-based function `f_CCC` available at https://github.com/robertpetermatthew/f_CCC/blob/master/f_CCC.m (Robert Matthew 2020). CCC including the confidence interval for the same was calculated with an adjusted significance threshold (α) of .00026. The significance threshold was precomputed accounting for multiple comparison correction via Bonferroni method (Chen, Feng, & Yi, 2017). Since 16 subjects were

tested for four fMRI parameters in three RS networks, a total of 192 tests were made. This resulted in adjusted significance threshold (α) of $.05/192 = .00026$. The computed CCC value and the confidence intervals with adjusted alpha are reported in Table S3.

The mean of the intermeasurement stability for the fMRI parameters in each network was calculated. Thereby, the Dancey and Reidy scale was applied to interpret Pearson's and Spearman's correlation coefficients (Dancey & Reidy, 2004). Thus, correlation coefficients $<.40$ were considered to be weak, values between $.40$ and $.69$ were considered moderate, values between $.70$ and $.99$ were considered strong, and correlation coefficients of 1.00 were considered perfect. As the CCC should be interpreted close to other correlation coefficients (e.g., Pearson's; Altman & Altman, 1999; Akoglu, 2018), we used the same scale for assessing both the inter-session stability of the fMRI parameters and the stability of the internetwork correlations.

2.7.2 | Stability of the internetwork correlations between the three networks

To calculate the stability of the FC between the three networks, the internetwork connectivity matrices of the triple networks were computed for each session. Subsequently, Spearman's correlation coefficients between the connectivity values in each pair of networks, in each session, at a significance level of $p < .01$ were calculated as shown in Figure 2. False discovery rate (FDR) was used to correct for multiple comparison. The mean value of Spearman's correlation coefficients for each pair of networks was then calculated. Spearman's correlation was used instead of Pearson's correlation owing to the small sample size (4, 4, and 7 ROIs in the DMN, CEN, and SN, respectively).

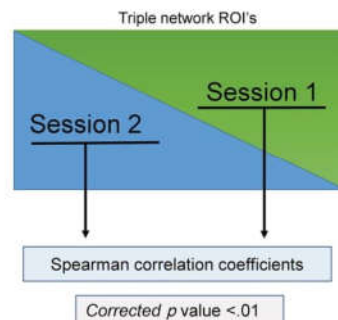


FIGURE 2 Schematic representation of the calculation procedure for assessing internetwork stability. We first calculated the connectivity between each network pair in each session, and Spearman's correlation coefficients were then calculated from those values to determine the inter-session stability of the internetwork connectivity

3 | RESULTS

3.1 | Intersession stability of the fMRI parameters in the triple networks

The mean values of the fMRI parameters (ALFF, f/ALFF, ReHo, and DC) across 16 subjects obtained in each session are visualized in Figure 3. The visual inspection reveals stable levels of ALFF and fALFF as well as DC and ReHo.

The values of the CCCs, representing the intraindividual, intermeasure stability of the fMRI parameters for each participant in each network, are shown in Table 1.

Figure 4 illustrates the mean of the intermeasurement stability for the fMRI parameters in each network

We observed the highest mean stability of ALFF parameter to be in both the DMN (0.90 ± 0.07 ; range from 0.72 to 0.96 ; strong stability) and the SN (0.90 ± 0.06 ; range from 0.74 to 0.95 ; strong stability) closely followed by the CEN (0.87 ± 0.07 ; range from 0.69 to 0.95 ; strong stability).

The mean stability of fALFF parameter was moderate in all three networks: DMN: 0.66 ± 0.16 (range from 0.19 to 0.85); CEN: 0.60 ± 0.19 (range from 0.02 to 0.90); SN: 0.54 ± 0.25 (range from -0.20 to 0.83).

The mean stability of ReHo parameter was found to be strong in all three networks: DMN: 0.86 ± 0.08 (range from 0.64 to 0.93); CEN: 0.84 ± 0.09 (range from 0.56 to 0.94); SN: 0.83 ± 0.07 (range from 0.69 to 0.91).

The mean stability of DC parameter was found to be strong in all three networks: SN: 0.73 ± 0.16 (range from 0.24 to 0.92); CEN: 0.71 ± 0.15 (range from 0.25 to 0.90); DMN: 0.70 ± 0.17 (range from 0.32 to 0.89).

3.2 | Stability of the internetwork correlations between the three networks

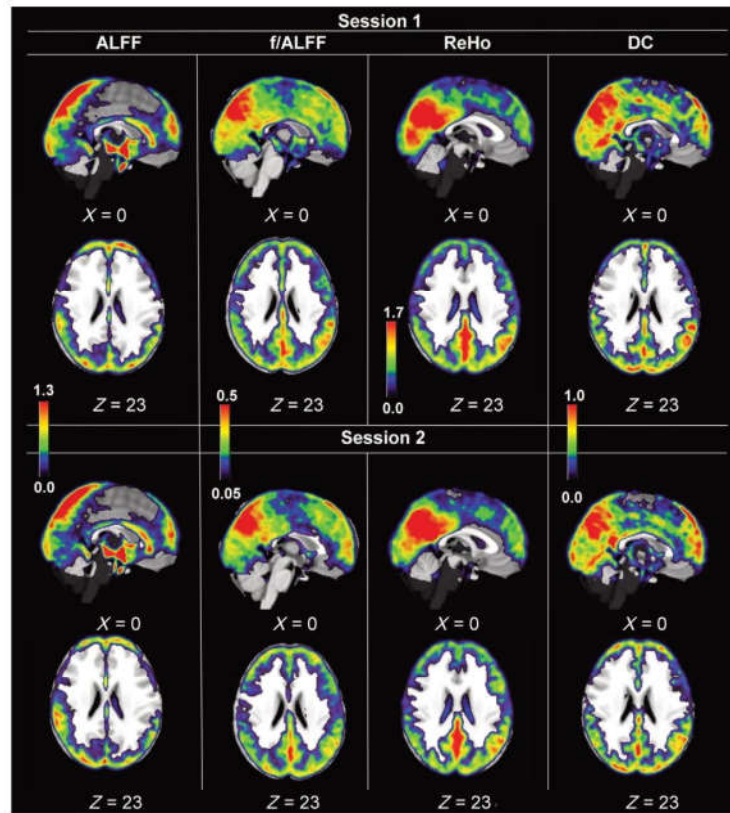
The ROI-based FC correlation matrix obtained during each of the two measurements is shown in Figure 5, and the concrete values are given in the Tables S4 and S5. Spearman's correlation coefficients representing the stability of the internetwork FC between the triple networks at the individual level are shown in Table 2. Also, the mean values of Spearman's correlation coefficients for each pair of networks are shown in Figure 6.

The internetwork connectivity showed a strong to moderate stability between the investigated network pairs: between DMN and SN: 0.69 ± 0.17 (range from 0.36 to 0.94); between DMN and CEN: 0.62 ± 0.20 (range from 0.12 to 0.94); between CEN and SN: 0.77 ± 0.11 (range from 0.60 to 0.91). Bars represent standard deviation.

4 | DISCUSSION

The aim of this study was to investigate the stability of the properties of three core RS networks (DMN, CEN, and SN) and the reliability of

FIGURE 3 Depiction of the average of each functional magnetic resonance imaging (fMRI) parameters (amplitude of low-frequency fluctuations [ALFF], fractional ALFF [fALFF], regional homogeneity [ReHo], and degree centrality [DC]) as computed from 16 subjects in both sessions. All analysis took place in the native space. Only for presentation purposes, the values were transferred to the standard space. The color bar is common for both sessions in ReHo parameter



the connectivity between these networks based on the Conn Atlas (Whitfield-Gabrieli & Nieto-Castanon, 2012). The analysis was performed using a publicly available open-access data set (Gorgolewski et al., 2015) obtained at a 7-Tesla UHF-MRI scanner. The study was motivated by the question of whether RS data from UHF examinations could be used for extraction of biomarkers to potentially support diagnosis as well as therapy planning and monitoring) in psychiatric disorders.

In terms of inter-session stability, our investigation revealed CCCs of a moderate to strong level. Specifically, the strongest stability was observed for the ALFF parameter that showed a strong stability in all three networks. This observation confirms previous reports about the high test-retest reproducibility of different parameters characterizing the spontaneous brain activity obtained at standard field strengths (Jia et al., 2020; Z. Li et al., 2012; Somandepalli et al., 2015; Zuo, Biswal, & Poldrack, 2019; Zuo & Xing, 2014). Generally, the ALFF reflects spontaneous neural activity of the brain (Zuo et al., 2010). In recent years, ALFF has been increasingly applied to characterize neuropsychiatric disorders, such as attention deficit and hyperactivity

disorder (Zang et al. 2007), Alzheimer's disease (He et al., 2007), mild cognitive impairment (Han et al., 2012), bipolar disorder (J. Liu et al., 2012), schizophrenia (Hoptman et al., 2010; Turner, 2013), Tourette's syndrome (Cui et al., 2014) and obsessive-compulsive disorder (Bu et al., 2019).

In parallel to ALFF, we also analyzed the stability of fALFF, which is considered as an improved approach to ALFF detection (Q.-H. Zou et al., 2008), and in particular measures the relative contribution of low-frequency fluctuations within a specific frequency band with respect to the whole detectable frequency range (Zuo et al., 2010). Thus, it enables the amplitude of regional neuronal activity to be studied, potentially identifying brain areas with abnormal local functioning (Chen et al., 2015). In our study, the stability of the fALFF values was moderate in all three networks. This somewhat lower stability of fALFF compared with ALFF is in concordance with some previous reports (Küblböck et al., 2014; Yan, Craddock, Zuo, Zang, & Milham, 2013; Zuo et al., 2010). While ALFF is more receptive for the potential artifact in the neighborhood to blood vessels and the cerebral ventricles, fALFF is a proportional parameter composed of

TABLE 1 The intraindividual intermeasure stability of the spontaneous brain activity and connectivity (short and long) within the triple networks represented by concordance correlation coefficients. The gray highlight indicates the computed CCC value and the confidence intervals with adjusted alpha (0.00026) are reported in Supplementary Material - Table 3 (S-Tab. 3).

| Subjects | DMN | | | | CEN | | | | SN | | | |
|----------|------|-------|------|------|------|-------|------|------|------|--------------------|------|------|
| | ALFF | fALFF | ReHo | DC | ALFF | fALFF | ReHo | DC | ALFF | fALFF | ReHo | DC |
| Sub01 | 0.72 | 0.19 | 0.77 | 0.40 | 0.75 | 0.02 | 0.75 | 0.25 | 0.74 | -0.20 ^a | 0.70 | 0.24 |
| Sub02 | 0.93 | 0.76 | 0.87 | 0.75 | 0.88 | 0.69 | 0.88 | 0.73 | 0.92 | 0.67 | 0.89 | 0.81 |
| Sub03 | 0.84 | 0.44 | 0.64 | 0.47 | 0.69 | 0.44 | 0.56 | 0.62 | 0.87 | 0.35 | 0.76 | 0.78 |
| Sub04 | 0.93 | 0.80 | 0.92 | 0.74 | 0.85 | 0.62 | 0.89 | 0.80 | 0.91 | 0.66 | 0.88 | 0.84 |
| Sub05 | 0.76 | 0.74 | 0.93 | 0.87 | 0.83 | 0.52 | 0.84 | 0.80 | 0.76 | 0.41 | 0.84 | 0.81 |
| Sub06 | 0.96 | 0.70 | 0.90 | 0.61 | 0.90 | 0.51 | 0.84 | 0.65 | 0.93 | 0.37 | 0.85 | 0.67 |
| Sub07 | 0.90 | 0.61 | 0.84 | 0.76 | 0.85 | 0.56 | 0.82 | 0.77 | 0.90 | 0.41 | 0.79 | 0.64 |
| Sub08 | 0.93 | 0.62 | 0.81 | 0.71 | 0.90 | 0.50 | 0.73 | 0.70 | 0.95 | 0.46 | 0.79 | 0.64 |
| Sub09 | 0.96 | 0.85 | 0.91 | 0.89 | 0.94 | 0.90 | 0.94 | 0.90 | 0.92 | 0.75 | 0.84 | 0.90 |
| Sub10 | 0.93 | 0.75 | 0.92 | 0.83 | 0.92 | 0.63 | 0.90 | 0.71 | 0.95 | 0.58 | 0.81 | 0.67 |
| Sub11 | 0.95 | 0.75 | 0.91 | 0.76 | 0.95 | 0.76 | 0.93 | 0.77 | 0.92 | 0.69 | 0.86 | 0.78 |
| Sub12 | 0.89 | 0.59 | 0.89 | 0.75 | 0.87 | 0.61 | 0.91 | 0.67 | 0.90 | 0.59 | 0.87 | 0.78 |
| Sub13 | 0.93 | 0.73 | 0.92 | 0.71 | 0.93 | 0.69 | 0.87 | 0.71 | 0.89 | 0.73 | 0.83 | 0.66 |
| Sub14 | 0.91 | 0.72 | 0.91 | 0.72 | 0.81 | 0.72 | 0.80 | 0.73 | 0.90 | 0.75 | 0.69 | 0.87 |
| Sub15 | 0.91 | 0.60 | 0.74 | 0.32 | 0.92 | 0.73 | 0.83 | 0.63 | 0.95 | 0.83 | 0.91 | 0.72 |
| Sub16 | 0.95 | 0.68 | 0.93 | 0.88 | 0.91 | 0.64 | 0.89 | 0.88 | 0.95 | 0.61 | 0.91 | 0.92 |

Note: All correlation coefficients were significant except the fALFF in CEN for the first subject (potential outlier subject).

Abbreviations: ALFF, amplitude of low-frequency fluctuation; CEN, central executive network; DC, degree centrality; DMN, default mode network; fALFF, fractional amplitude of low-frequency fluctuation; ReHo, regional homogeneity; SN, salience network.

^aThe marked subject is considered as a potential outlier; thus, a cross-check of all the raw data and all technical issues mentioned in the original publication was performed. The cross-check did not reveal any particularities for this subject (partial signal drop out or movement). However, when an additional analysis without this subject was performed, the results from this sample size (15 participants) did not differ noticeably from the findings from the whole sample (16 participants), as shown in Figures S1 and S2.

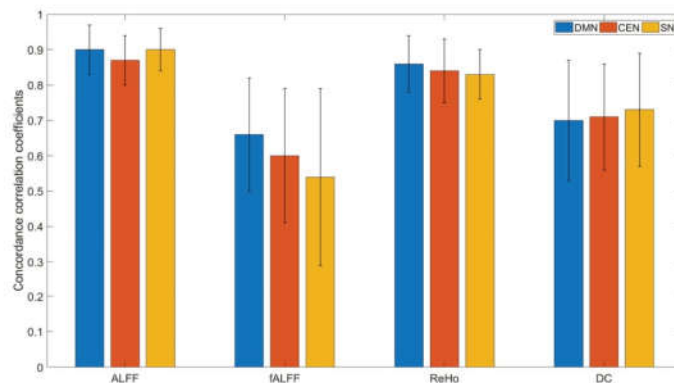


FIGURE 4 Mean of the inter-measurement stability across 16 subjects for the fMRI parameters (amplitude of low-frequency fluctuations (ALFF), fractional ALFF (fALFF), regional homogeneity (ReHo), and degree centrality (DC)) in each core network - the default mode network (DMN), the central executive network (CEN), and the salience network (SN). The error bars represent standard deviation

ALFF in the numerator and the sum of the amplitudes in the whole frequency spectrum in the denominator (Küblböck et al., 2014). Thus, a decrease in reliability of their ratio is to be expected (Arndt, Cohen, Alliger, Swayze II, & Andreasen, 1991).

The SN showed somewhat lower (still moderate) level of fALFF stability compared to the DMN and the CEN. The SN is involved in

detecting, filtering, and integrating relevant internal (e.g., autonomic input) and external (e.g., emotional information) salient stimuli to guide behavior (Bressler & Menon, 2010; Chand & Dhamala, 2016). Furthermore, it has a crucial role in the functional and dynamic switching between the DMN and CEN (i.e., between task-based and task-free states; Y. Liu et al., 2017; Zheng et al., 2015). Thereby, the

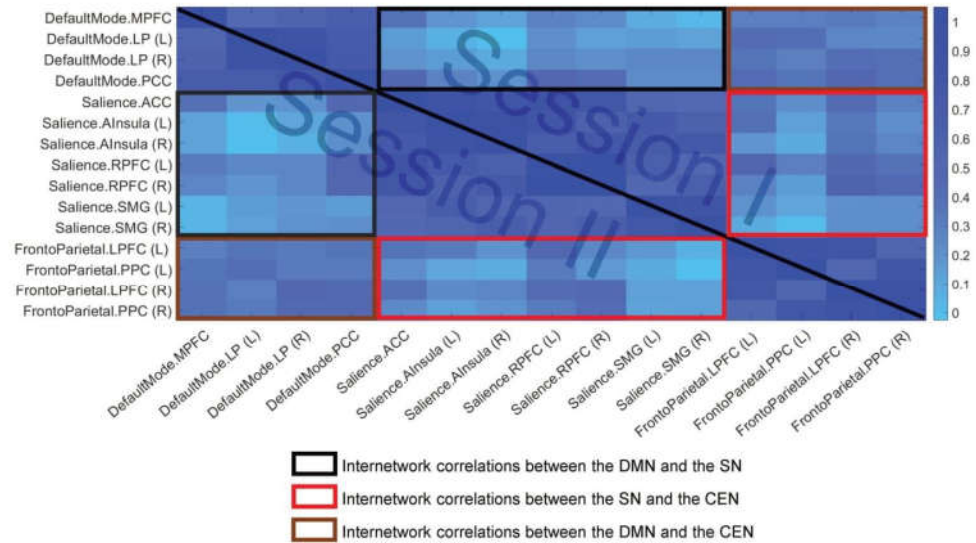


FIGURE 5 The functional connectivity average matrix for 16 subjects between the regions of the three core resting state networks. The default mode network (DMN) includes the following regions: the medial prefrontal cortex (MPFC), the left and right lateral parietal cortex (LP(L), LP(R)), and the posterior cingulate cortex (PCC). The central executive network (CEN) includes the right and left lateral prefrontal cortex (rPFC, lPFC) and the right and left posterior parietal cortex (PPC). The salience network (SN) includes the anterior cingulate cortex (ACC), the left and right anterior insula (Insula), the left and right rostral prefrontal cortex (RPFC), and the left and right supramarginal gyrus (SMG). The upper triangular matrix represents the first session, and the lower triangular matrix represents the second session

TABLE 2 Spearman's correlation coefficients and the corresponding *p* values, which represent the stability of the functional connectivity between each pair of networks (DMN/SN, DMN/CEN, and SN/CEN) when compared between the two sessions for 16 subjects

| Subjects | DMN/SN | | DMN/CEN | | SN/CEN | |
|----------|-------------------------------------|--------------------------|-------------------------------------|--------------------------|-------------------------------------|--------------------------|
| | Spearman's correlation coefficients | Corrected <i>p</i> value | Spearman's correlation coefficients | Corrected <i>p</i> value | Spearman's correlation coefficients | Corrected <i>p</i> value |
| Sub01 | .58 | <.01 | .71 | <.01 | .69 | <.01 |
| Sub02 | .47 | <.01 | .61 | <.01 | .61 | <.01 |
| Sub03 | .59 | <.01 | .53 | <.01 | .60 | <.01 |
| Sub04 | .63 | <.01 | .76 | <.01 | .80 | <.01 |
| Sub05 | .81 | <.01 | .79 | <.01 | .74 | <.01 |
| Sub06 | .56 | <.01 | .12 | <.01 | .80 | <.01 |
| Sub07 | .71 | <.01 | .69 | <.01 | .72 | <.01 |
| Sub08 | .61 | <.01 | .82 | <.01 | .91 | <.01 |
| Sub09 | .80 | <.01 | .60 | <.01 | .68 | <.01 |
| Sub10 | .85 | <.01 | .69 | <.01 | .89 | <.01 |
| Sub11 | .94 | <.01 | .94 | <.01 | .91 | <.01 |
| Sub12 | .61 | <.01 | .59 | <.01 | .90 | <.01 |
| Sub13 | .87 | <.01 | .41 | <.01 | .67 | <.01 |
| Sub14 | .84 | <.01 | .78 | <.01 | .90 | <.01 |
| Sub15 | .36 | <.01 | .34 | <.01 | .71 | <.01 |
| Sub16 | .85 | <.01 | .60 | <.01 | .85 | <.01 |

Abbreviations: CEN, central executive network; DMN, default mode network; SN, salience network.

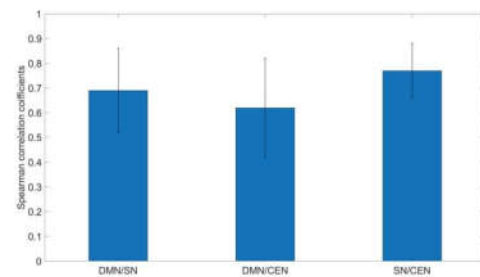


FIGURE 6 Mean of the internetwork correlations stability between the three core resting state networks depicted as the mean correlations between DMN/SN, DMN/CEN, and SN/CEN. CEN, central executive network; DMN, default mode network; SN, salience network

SN responds to the subjective degree of salience (Goulden et al., 2014). It is thought that different regions of the SN could form a sort of information processing loop for representing and responding to homeostatically relevant external and internal stimuli (Seeley, 2019). Indeed, their involvement in emotional functions (Heimer & Van Hoesen, 2006), autonomic functions, and self-awareness (Craig, 2002), as well as in the process of internal (self-)reference that predominate in states of rest and disengagement (Critchley, 2005), is well documented. Since all these internal stimuli can hardly be kept constant at different measurement times (despite the uniform absence of special tasks), it is not surprising that the stability of regional spontaneous activity is somewhat lower in the SN than in the other two networks.

We observed further for all three networks a strong stability for the parameter ReHo. Often designated as a local FC, ReHo defined by the temporal coherence or synchronization of the BOLD time series within a set of a given voxel's nearest neighbors (Jiang & Zuo, 2016) and is becoming increasingly recognized as being a highly sensitive and reliable neuroimaging marker to characterize the human brain (Jiang & Zuo, 2016). The high test-retest reliability of ReHo has been already confirmed in various studies, including a systematic analysis based on previously published papers (Zuo & Xing, 2014). However, the basis for this investigation was data acquired using standard field strength MRI. It has been shown that altered ReHo values may relate to disequilibrium in spontaneous neural activity within and between corresponding brain regions (Chen et al., 2015). Indeed, aberrant ReHo values, indicative of disrupted local functionality, have been linked to several neurological and psychiatric disorders, such as Alzheimer's disease (He et al., 2007), chronic pain attention-deficit hyperactivity disorder (de Celis Alonso et al., 2014), autism spectrum disorders (Paakkki et al., 2010), depression (Guo et al., 2011), bipolar disorder (Shan et al., 2020) and schizophrenia (Ma et al., 2019; Mwansisya et al., 2017); as well as in first-degree relatives of patients with schizophrenia (Liao et al., 2012). In addition, a recent study demonstrated a significant association between ReHo in the DMN and

resilience, as well as with the personality traits extroversion (in the CEN and SN) and conscientiousness (in the SN) (Altinok et al., 2021). Therefore, ReHo appears to be a valuable and powerful tool for detecting aberrant RS brain activity, which can be associated with a wide range of psychopathological abnormalities as well as with different personality traits and varying levels of resilience in healthy individuals.

The long-connectivity parameter (DC) also showed a strong level of stability in all three networks, although the values of inter-measurement stability were somewhat below the values for ALFF and ReHo in all three networks. Divergent from our findings, previous studies reported considerably lower test-retest reliability of the long-range connectivity compared to the short-range connectivity parameters (Braun et al., 2012; Holiga et al., 2018; Telesford et al., 2010). In a comprehensive meta-summary from previously published papers on the test-retest reliability of voxel-wise metrics from non-UHF studies, Zuo and Xing (2014) investigated the long-term (~6 months) test-retest reliabilities measured as intraclass correlation (ICC). In this study, the ICC values for DC ranged from approximately 0.25 in the limbic network (that includes parts of the SN) to 0.5 in the dorsal attentional network (that includes parts of the CEN). In the DMN and the control network, the ICC values reached a value of 0.4. Similarly, in a more recent study performed at a 3-Tesla MRI scanner; the highest part of the observed voxel had a mean ICC value of about 0.35. In opposite to these reports, we obtained reliability for DC which has exceeded the value of 0.7 in all three networks examined. Our results indicate that, especially when investigating long-distance connectivity, the use of 7-Tesla MRI scanners could provide results that are more reliable and thus more reproducible than results from standard field strength MRI. Similar to our findings, one other recent work reports a significant increase of the test-retest reliability at the intranetwork when comparing seed-based connectivity between 7 and 3 Tesla scans (Nemani & Lowe, 2021).

In our final analysis, we investigated the stability of the inter-network connectivity between each pair of the three core RS networks. Earlier investigations indicate that a stabile synchronization of these three networks plays a crucial role in higher cognitive functions. Thereby, the functional connectivity between the DMN and the SN appears to be important for cognitive control (Bonnelle et al., 2012; Menon & Uddin, 2010), and the SN has a central role in switching between the DMN and the CEN (Bonnelle et al., 2012; Liang, Zou, He, & Yang, 2015; Menon & Uddin, 2010; Seeley, 2019). Accordingly, aberrations in these intrinsically well-organized interactions have been linked to pathological states with impaired cognition (Wang et al., 2015), and the observation of altered internetwork interactions generally may be a valuable indicator of psychiatric symptoms.

In our study, the subregions of the DMN and the SN showed predominantly weak positive correlations. Moderate correlations included in both sessions the PCC, showing correlations in the range of .42-.48 with three subregions of the SN (the ACC and the left and right RPPC). Regarding the synchronization between the DMN and the CEN, the correlations between the subregions were also mainly weak. We observed the strongest (moderate) correlations for PCC

(with left and right LPFC in Session 1 and with the left LPFC and right PPC in Session 2), for left LP (with left LPFC in Session 1 and with left PPC in Session 2) as well as for the right LP (with right LPFC in Session 1 and with right LPFC and PPC in Session 2).

In terms of the association between the SN and the CEN, the SN subregions with the strongest positive associations with the CEN were the RPFC, with the moderate correlations observed between the RPFC(R) and the LPFC(R) in both sessions as well as moderate correlations between the left RPFC and left and right LPFC.

The relative strength of the correlations between the specific subregions remained widely constant when comparing the first and the second sessions.

At the whole network level, the internetwork connectivity showed a strong to moderate stability between the investigated network pairs. This high reliability of the between-network connectivity is consistent with the latest report by Nemani and Lowe (2021), who, however, also showed that the high between-network reliability at 7 Tesla was not significantly improved compared to the 3 Tesla results.

5 | CONCLUSION

More than 20 years since the first UHF-MRI scanners were approved for use in human (Robitaille et al., 1999; Yacoub et al., 2001), results from various areas of medicine demonstrate numerous unambiguous advantages of using this technology (Düzel et al., 2021; Platt et al., 2021; Vachha & Huang, 2021). Nevertheless, numerous technical challenges still need to be solved so that the applicability remains limited, especially in the field of clinical research (Düzel et al., 2021; Ladd et al., 2018). In this context, especially considering the growing need for the identification of reliable biomarkers for mental and neurological diseases, the issue of reproducibility of results remains crucial (Griffanti et al., 2016). In a recent work, a significantly increased reliability of RS connectivity at UHF strengths over conventional field strengths has been demonstrated (Nemani & Lowe, 2021). We complement this report with our confirmation of a strong stability of the three RS fMRI metrics (ALFF, ReHo and DC), representing the spontaneous brain activity, local- and long-range connectivity, respectively, in three major RS networks. In opposite to previous investigations at standard field strengths, our results have also revealed a strong reliability for DC in all three networks examined. Thereby, DC could be considered a measure of the long-distance connectivity and even more, it appears to be a very suitable measure to explore RS whole-brain neural network connectivity, due to the reduction of the possible bias caused by selecting brain regions according to the priori assumption (Guo et al., 2020; Buckner et al., 2009; Zuo et al., 2012). Our observation suggests that for rsfMRI measurements at 7 Tesla, long-range connectivity can also be considered a reliable parameter. Taking into account all other advantages of UHF imaging, this technology appears to be well suited for a versatile, reliable, and reproducible characterization of RS networks and their interactions, as shown here with the example of the three RS networks when investigating the regional brain activity, short and long connectivities.

ACKNOWLEDGMENTS

This study is considered to be part of the doctoral thesis (Dr. rer. Medic.) of Hasan Sbaihat, Faculty of Medicine, RWTH Aachen University, Germany. The authors also would like to thank Claire Rick for proofreading the manuscript. Hasan Sbaihat received PhD stipend from the Federal Ministry of Education and Research (BMBF), Germany, under the Palestinian German Science Bridge, project number D.B.R01436. The funders have no role in the study design, data collection, validation, resources, or decision to publish. The study was performed in accordance with the declaration of Helsinki and was approved by the Ethical Committee of the Leipzig University. Open access funding enabled and organized by Projekt DEAL.

CONFLICT OF INTEREST

The authors declare no potential conflict of interest.

AUTHOR CONTRIBUTIONS

Hasan Sbaihat: Data analysis, writing—original draft, methodology; **Ravichandran Rajkumar:** Methodology, software programming, draft review, and editing; **Shukti Ramkiran:** Methodology, draft review, and editing; **Abed Al-Nasser Assi:** Supervision, draft—review and editing; **Jörg Felder:** discussion methodology, review, and editing; **N. Jon Shah:** Supervision, discussion and revision preprocessing, draft review, and editing; **Tanja Veselinović:** Methodology, supervision, draft review and editing; **Irene Neuner:** Conceptualization, supervision, funding, draft review, and editing.

DATA AVAILABILITY STATEMENT

The data used in this study were taken from the open-access data set (Gorgolewski et al., 2015). The data can be accessed using the following link <https://openneuro.org/datasets/ds001168/versions/1.0.1>. Analyzed data are available upon request from the corresponding author.

ORCID

Hasan Sbaihat  <https://orcid.org/0000-0003-4973-3195>

Ravichandran Rajkumar  <https://orcid.org/0000-0001-5875-5316>

Nadim Jon Shah  <https://orcid.org/0000-0002-8151-6169>

REFERENCES

- Akoglu, H. (2018). User's guide to correlation coefficients. *Turkish Journal of Emergency Medicine*, 18(3), 91–93. <https://doi.org/10.1016/j.tjem.2018.08.001>
- Altinok, D. C. A., Rajkumar, R., Nießen, D., Sbaihat, H., Kersey, M., Shah, N. J., ... Neuner, I. (2021). Common neurobiological correlates of resilience and personality traits within the triple resting-state brain networks assessed by 7-Tesla ultra-high field MRI. *Scientific Reports*, 11(1), 11564. <https://doi.org/10.1038/s41598-021-91056-y>
- Altman, D. G., & Altman, E. (1999). *Practical statistics for medical research* (Vol. 2). London, England: Chapman & Hall/CRC.
- Arndt, S., Cohen, G., Alliger, R. J., Swayze, V. W., II, & Andreasen, N. C. (1991). Problems with ratio and proportion measures of imaged cerebral structures. *Psychiatry Research: Neuroimaging*, 40(1), 79–89. [https://doi.org/10.1016/0925-4927\(91\)90031-k](https://doi.org/10.1016/0925-4927(91)90031-k)
- Bazin, P.-L., Weiss, M., Dinse, J., Schäfer, A., Trampel, R., & Turner, R. (2014). A computational framework for ultra-high resolution cortical

- segmentation at 7 Tesla. *NeuroImage*, 93, 201–209. <https://doi.org/10.1016/j.neuroimage.2013.03.077>
- Berboth, S., Windischberger, C., Kohn, N., & Morawetz, C. (2021). Test-retest reliability of emotion regulation networks using fMRI at ultra-high magnetic field. *NeuroImage*, 232, 117917. <https://doi.org/10.1016/j.neuroimage.2021.117917>
- Biomarkers Definitions Working Group. (2001). Biomarkers and surrogate endpoints: Preferred definitions and conceptual framework. *Clinical Pharmacology & Therapeutics*, 69(3), 89–95. <https://doi.org/10.1067/mcp.2001.113989>
- Biswal, B., Zerrin, Y. F., Haughton, V. M., & Hyde, J. S. (1995). Functional connectivity in the motor cortex of resting human brain using echo-planar MRI. *Magnetic Resonance in Medicine*, 34(4), 537–541. <https://doi.org/10.1002/mrm.1910340409>
- Blatow, M., Nennig, E., Durst, A., Sartor, K., & Stippich, C. (2007). fMRI reflects functional connectivity of human somatosensory cortex. *NeuroImage*, 37(3), 927–936. <https://doi.org/10.1016/j.neuroimage.2007.05.038>
- Blautzik, J., Keeser, D., Berman, A., Paolini, M., Kirsch, V., Mueller, S., ... Meindl, T. (2013). Long-term test–retest reliability of resting-state networks in healthy elderly subjects and patients with amnesic mild cognitive impairment. *Journal of Alzheimer's Disease*, 34(3), 741–754. <https://doi.org/10.3233/JAD-111970>
- Bonnelle, V., Ham, T. E., Leech, R., Kinnunen, K. M., Mehta, M. A., Greenwood, R. J., & Sharp, D. J. (2012). Saliency network integrity predicts default mode network function after traumatic brain injury. *Proceedings of the National Academy of Sciences*, 109(12), 4690–4695. <https://doi.org/10.1073/pnas.1113455109>
- Branco, P., Seixas, D., & Castro, S. L. (2018). Temporal reliability of ultra-high field resting-state MRI for single-subject sensorimotor and language mapping. *NeuroImage*, 168, 499–508. <https://doi.org/10.1016/j.neuroimage.2016.11.029>
- Braun, U., Plichta, M. M., Esslinger, C., Sauer, C., Haddad, L., Grimm, O., ... Meyer-Lindenberg, A. (2012). Test–retest reliability of resting-state connectivity network characteristics using fMRI and graph theoretical measures. *NeuroImage*, 59(2), 1404–1412. <https://doi.org/10.1016/j.neuroimage.2011.08.044>
- Bressler, S. L., & Menon, V. (2010). Large-scale brain networks in cognition: Emerging methods and principles. *Trends in Cognitive Sciences*, 14(6), 277–290. <https://doi.org/10.1016/j.tics.2010.04.004>
- Bu, X., Hu, X., Zhang, L., Li, B., Zhou, M., Lu, L., ... Huang, X. (2019). Investigating the predictive value of different resting-state functional MRI parameters in obsessive-compulsive disorder. *Translational Psychiatry*, 9(1), 17. <https://doi.org/10.1038/s41398-018-0362-9>
- Buckner, R. L., Sepulcre, J., Talukdar, T., Krienen, F. M., Liu, H., Hedden, T., Andrews-Hanna, J. R., Sperling, R. A., & Johnson, K. A. (2009). Cortical hubs revealed by intrinsic functional connectivity: mapping, assessment of stability, and relation to alzheimer's disease. *Journal of Neuroscience*, 29(6), 1860–1873. <https://doi.org/10.1523/jneurosci.5062-08.2009>
- Cabral, J., Kringelbach, M. L., & Deco, G. (2017). Functional connectivity dynamically evolves on multiple time-scales over a static structural connectome: Models and mechanisms. *NeuroImage*, 160, 84–96. <https://doi.org/10.1016/j.neuroimage.2017.03.045>
- Chand, G. B., & Dhamala, M. (2016). The saliency network dynamics in perceptual decision-making. *NeuroImage*, 134, 85–93. <https://doi.org/10.1016/j.neuroimage.2016.04.018>
- Chen, H. J., Qi, R., Kong, X., Wen, J., Liang, X., Zhang, Z., ... Zhang, L. J. (2015). The impact of hemodialysis on cognitive dysfunction in patients with end-stage renal disease: A resting-state functional MRI study. *Metabolic Brain Disease*, 30(5), 1247–1256. <https://doi.org/10.1007/s11011-015-9702-0>
- Chen, S.-Y., Feng, Z., & Yi, X. (2017). A general introduction to adjustment for multiple comparisons. *Journal of Thoracic Disease*, 9(6), 1725–1729. <https://doi.org/10.21037/jtd.2017.05.34>
- Chou, Y.-H., Panych, L. P., Dickey, C. C., Petrella, J. R., & Chen, N.-K. (2012). Investigation of long-term reproducibility of intrinsic connectivity network mapping: A resting-state fMRI study. *AJNR. American Journal of Neuroradiology*, 33(5), 833–838. <https://doi.org/10.3174/ajnr.a2894>
- Craig, A. D. (2002). How do you feel? Interoception: The sense of the physiological condition of the body. *Nature Reviews. Neuroscience*, 3(8), 655–666. <https://doi.org/10.1038/nrn894>
- Critchley, H. D. (2005). Neural mechanisms of autonomic, affective, and cognitive integration. *The Journal of Comparative Neurology*, 493(1), 154–166. <https://doi.org/10.1002/cne.20749>
- Cui, L.-B., Liu, K., Li, C., Wang, L.-X., Guo, F., Tian, P., ... Yin, H. (2016). Putamen-related regional and network functional deficits in first-episode schizophrenia with auditory verbal hallucinations. *Schizophrenia Research*, 173(1–2), 13–22. <https://doi.org/10.1016/j.schres.2016.02.039>
- Cui, Y., Jin, Z., Chen, X., He, Y., Liang, X., & Zheng, Y. (2014). Abnormal baseline brain activity in drug-naïve patients with Tourette syndrome: A resting-state fMRI study. *Frontiers in Human Neuroscience*, 7, 913. <https://doi.org/10.3389/fnhum.2013.00913>
- Dancey, C., & Reidy, J. (2004). *Statistics without maths for psychology for windows*. London, England: Pearson Prentice Hall.
- de Celis Alonso, B., Hidalgo, T. S., Dies, S. P., García, F. J., de Celis Carrillo, B., & Barragán, P. E. (2014). A multi-methodological MR resting state network analysis to assess the changes in brain physiology of children with ADHD. *PLoS One*, 9(6), e99119. <https://doi.org/10.1371/journal.pone.0099119>
- de Martino, F., Esposito, F., van de Moortele, P.-F., Harel, N., Formisano, E., Goebel, R., ... Yacoub, E. (2011). Whole brain high-resolution functional imaging at ultra high magnetic fields: An application to the analysis of resting state networks. *NeuroImage*, 57(3), 1031–1044. <https://doi.org/10.1016/j.neuroimage.2011.05.008>
- Dinse, J., Waehnert, M., Tardif, C. L., Schäfer, A., Geyer, S., Turner, R., & Bazin, P.-L. (2013). A histology-based model of quantitative T1 contrast for in-vivo cortical parcellation of high-resolution 7 tesla brain MR images. In *Advanced information systems engineering* (pp. 51–58). Berlin Heidelberg: Springer. https://doi.org/10.1007/978-3-642-40763-5_7
- Dong, D., Wang, Y., Chang, X., Luo, C., & Yao, D. (2017). Dysfunction of large-scale brain networks in schizophrenia: A meta-analysis of resting-state functional connectivity. *Schizophrenia Bulletin*, 44(1), 168–181. <https://doi.org/10.1093/schbul/sbx034>
- Duong, T. Q., Yacoub, E., Adriany, G., Hu, X., Ugurbil, K., & Kim, S.-G. (2003). Microvascular BOLD contribution at 4 and 7 T in the human brain: Gradient-echo and spin-echo fMRI with suppression of blood effects. *Magnetic Resonance in Medicine*, 49, 1019–1027. <https://doi.org/10.1002/mrm.10472>
- Düzel, E., Costagli, M., Donatelli, G., Speck, O., & Cosottini, M. (2021). Studying Alzheimer disease, Parkinson disease, and amyotrophic lateral sclerosis with 7-T magnetic resonance. *European Radiology Experimental*, 5, 36. <https://doi.org/10.1186/s41747-021-00221-5>
- Fox, M. D., & Raichle, M. E. (2007). Spontaneous fluctuations in brain activity observed with functional magnetic resonance imaging. *Nature Reviews. Neuroscience*, 8(9), 700–711. <https://doi.org/10.1038/nrn2201>
- Fox, M. D., Snyder, A. Z., Vincent, J. L., Corbetta, M., Van Essen, D. C., & Raichle, M. E. (2005). From The Cover: The human brain is intrinsically organized into dynamic, anticorrelated functional networks. *Proceedings of the National Academy of Sciences*, 102(27), 9673–9678. <https://doi.org/10.1073/pnas.0504136102>
- Geissberger, N., Tik, M., Sladky, R., Woletz, M., Schuler, A.-L., Willinger, D., & Windischberger, C. (2020). Reproducibility of amygdala activation in facial emotion processing at 7T. *NeuroImage*, 211, 116585. <https://doi.org/10.1016/j.neuroimage.2020.116585>
- Geyer, S., Weiss, M., Reimann, K., Lohmann, G., & Turner, R. (2011). Microstructural parcellation of the human cerebral cortex—from Brodmann's

- post-mortem map to in vivo mapping with high-field magnetic resonance imaging. *Frontiers in Human Neuroscience*, 5, 19. <https://doi.org/10.3389/fnhum.2011.00019>
- Gorgolewski, K. J., Mendes, N., Wiffling, D., Wladimirov, E., Gauthier, C. J., Bonnen, T., ... Margulies, D. S. (2015). A high-resolution 7-Tesla resting-state fMRI test-retest dataset with cognitive and physiological measures. *Scientific Data*, 2(1), 140054. <https://doi.org/10.1038/sdata.2014.54>
- Goulden, N., Khusnulina, A., Davis, N. J., Bracewell, R. M., Bokde, A. L., McNulty, J. P., ... Mullins, P. G. (2014). The salience network is responsible for switching between the default mode network and the central executive network: Replication from DCM. *NeuroImage*, 99, 180–190. <https://doi.org/10.1016/j.neuroimage.2014.05.052>
- Guo, W., Liu, F., Xue, Z., Yu, Y., Ma, C., Tan, C., ... Zhao, J. P. (2011). Abnormal neural activities in first-episode, treatment-naïve, short-illness-duration, and treatment-response patients with major depressive disorder: A resting-state fMRI study. *Journal of Affective Disorders*, 135(1–3), 326–331. <https://doi.org/10.1016/j.jad.2011.06.048>
- Guo, M., Ren, Y., Yu, H., Yang, H., Cao, C., Li, Y., & Fan, G. (2020). Alterations in degree centrality and functional connectivity in Parkinson's disease patients with freezing of gait: A resting-state functional magnetic resonance imaging study. *Frontiers in Neuroscience*, 14, <https://doi.org/10.3389/fnins.2020.582079>
- Griffanti, L., Rolinski, M., Szewczyk-Krolikowski, K., Menke, R. A., Filippini, N., Zamboni, G., ... Mackay, C. E. (2016). Challenges in the reproducibility of clinical studies with resting state fMRI: An example in early Parkinson's disease. *NeuroImage*, 124, 704–713. <https://doi.org/10.1016/j.neuroimage.2015.09.021>
- Hacker, C. D., Roland, J. L., Kim, A. H., Shimony, J. S., & Leuthardt, E. C. (2019). Resting-state network mapping in neurosurgical practice: A review. *Neurosurgical Focus*, 47(6), E15. <https://doi.org/10.3171/2019.9.focus19656>
- Han, J. W., Kim, T. H., Lee, S. B., Park, J. H., Lee, J. J., Huh, Y., ... Kim, K. W. (2012). Predictive validity and diagnostic stability of mild cognitive impairment subtypes. *Alzheimer's & Dementia*, 8(6), 553–559. <https://doi.org/10.1016/j.jalz.2011.08.007>
- He, Y., Wang, L., Zang, Y., Tian, L., Zhang, X., Li, K., & Jiang, T. (2007). Regional coherence changes in the early stages of Alzheimer's disease: A combined structural and resting-state functional MRI study. *NeuroImage*, 35(2), 488–500. <https://doi.org/10.1016/j.neuroimage.2006.11.042>
- Heimer, L., & Van Hoesen, G. W. (2006). The limbic lobe and its output channels: Implications for emotional functions and adaptive behavior. *Neuroscience & Biobehavioral Reviews*, 30(2), 126–147. <https://doi.org/10.1016/j.neubiorev.2005.06.006>
- Holiga, S., Sambataro, F., Luzy, C., Greig, G., Sarkar, N., Renken, R. J., ... Dukart, J. (2018). Test-retest reliability of task-based and resting-state blood oxygen level dependence and cerebral blood flow measures. *PLoS One*, 13(11), e0206583. <https://doi.org/10.1371/journal.pone.0206583>
- Hoptman, M. J., Zuo, X.-N., Butler, P. D., Javitt, D. C., D'Angelo, D., Mauro, C. J., & Milham, M. P. (2010). Amplitude of low-frequency oscillations in schizophrenia: A resting state fMRI study. *Schizophrenia Research*, 117(1), 13–20. <https://doi.org/10.1016/j.schres.2009.09.030>
- Imperator, C., Massullo, C., Carbone, G. A., Panno, A., Giacchini, M., Capriotti, C., ... Farina, B. (2020). Increased resting state triple network functional connectivity in undergraduate problematic cannabis users: A preliminary EEG coherence study. *Brain Sciences*, 10(3), 136. <https://doi.org/10.3390/brainsci10030136>
- Insel, T. R., & Cuthbert, B. N. (2015). Brain disorders? Precisely. *Science*, 348(6234), 499–500. <https://doi.org/10.1126/science.aab2358>
- Jia, X.-Z., Sun, J.-W., Ji, G.-J., Liao, W., Lv, Y.-T., Wang, J., ... Zang, Y. F. (2020). Percent amplitude of fluctuation: A simple measure for resting-state fMRI signal at single voxel level. *PLoS One*, 15(1), e0227021. <https://doi.org/10.1371/journal.pone.0227021>
- Jiang, L., & Zuo, X.-N. (2016). Regional homogeneity. *Neuroscientist*, 22(5), 486–505. <https://doi.org/10.1177/1073858415595004>
- Jiang, Y., Duan, M., Chen, X., Chang, X., He, H., Li, Y., ... Yao, D. (2017). Common and distinct dysfunctional patterns contribute to triple network model in schizophrenia and depression: A preliminary study. *Progress in Neuro-Psychopharmacology and Biological Psychiatry*, 79, 302–310. <https://doi.org/10.1016/j.pnpbp.2017.07.007>
- Klomp, A., van Wingen, G. A., de Ruiter, M. B., Caan, M. W. A., Denys, D., & Reneman, L. (2013). Test-retest reliability of task-related pharmacological MRI with a single-dose oral citalopram challenge. *NeuroImage*, 75, 108–116. <https://doi.org/10.1016/j.neuroimage.2013.03.002>
- Kraff, O., Fischer, A., Nagel, A. M., Mönninghoff, C., & Ladd, M. E. (2014). MRI at 7 tesla and above: Demonstrated and potential capabilities. *Journal of Magnetic Resonance Imaging*, 41(1), 13–33. <https://doi.org/10.1002/jmri.24573>
- Küblböck, M., Woletz, M., Höflich, A., Sladky, R., Kranz, G. S., Hoffmann, A., ... Windischberger, C. (2014). Stability of low-frequency fluctuation amplitudes in prolonged resting-state fMRI. *NeuroImage*, 103, 249–257. <https://doi.org/10.1016/j.neuroimage.2014.09.038>
- Ladd, M. E., Bachert, P., Meyerspeer, M., Moser, E., Nagel, A. M., Norris, D. G., ... Zaiss, M. (2018). Pros and cons of ultra-high-field MRI/MRS for human application. *Progress in Nuclear Magnetic Resonance Spectroscopy*, 109, 1–50. <https://doi.org/10.1016/j.pnmrs.2018.06.001>
- Li, C., Li, Y., Zheng, L., Zhu, X., Shao, B., Fan, G., Liu, T., Wang, J., & Alzheimer's Disease Neuroimaging Initiative. (2019). Abnormal brain network connectivity in a triple-network model of Alzheimer's disease. *Journal of Alzheimer's Disease*, 69(1), 237–252. <https://doi.org/10.3233/JAD-181097>
- Li, Z., Kadivar, A., Pluta, J., Dunlop, J., & Wang, Z. (2012). Test-retest stability analysis of resting brain activity revealed by blood oxygen level-dependent functional MRI. *Journal of Magnetic Resonance Imaging*, 36(2), 344–354. <https://doi.org/10.1002/jmri.23670>
- Liang, X., Zou, Q., He, Y., & Yang, Y. (2015). Topologically reorganized connectivity architecture of default-mode, executive-control, and salience networks across working memory task loads. *Cerebral Cortex*, 26(4), 1501–1511. <https://doi.org/10.1093/cercor/bhu316>
- Liao, H., Wang, L., Zhou, B., Tang, J., Tan, L., Zhu, X., ... Tan, C. (2012). A resting-state functional magnetic resonance imaging study on the first-degree relatives of persons with schizophrenia. *Brain Imaging and Behavior*, 6(3), 397–403. <https://doi.org/10.1007/s11682-012-9154-7>
- Lin, L., Hedayat, A. S., Sinha, B., & Yang, M. (2002). Statistical methods in assessing agreement. *Journal of the American Statistical Association*, 97(457), 257–270. <https://doi.org/10.1198/016214502753479392>
- Lin, L. I. (1989). A concordance correlation coefficient to evaluate reproducibility. *Biometrics*, 45(1), 255. <https://doi.org/10.2307/2532051>
- Liu, J., Blond, B. N., van Dyck, L. I., Spencer, L., Wang, F., & Blumberg, H. P. (2012). Trait and state corticostriatal dysfunction in bipolar disorder during emotional face processing. *Bipolar Disorders*, 14(4), 432–441. <https://doi.org/10.1111/j.1399-5618.2012.01018.x>
- Liu, Y., Li, L., Li, B., Feng, N., Li, L., Zhang, X., ... Yin, H. (2017). Decreased triple network connectivity in patients with recent onset post-traumatic stress disorder after a single prolonged trauma exposure. *Scientific Reports*, 7(1), 12625. <https://doi.org/10.1038/s41598-017-12964-6>
- Ma, X., Zheng, W., Li, C., Li, Z., Tang, J., Yuan, L., ... Chen, X. (2019). Decreased regional homogeneity and increased functional connectivity of default network correlated with neurocognitive deficits in subjects with genetic high-risk for schizophrenia: A resting-state fMRI study. *Psychiatry Research*, 281, 112603. <https://doi.org/10.1016/j.psyres.2019.112603>

- Maknojia, S., Churchill, N. W., Schweizer, T. A., & Graham, S. J. (2019). Resting state fMRI: Going through the motions. *Frontiers in Neuroscience*, 13, 825. <https://doi.org/10.3389/fnins.2019.00825>
- Manoach, D. S., Halpern, E. F., Kramer, T. S., Chang, Y., Goff, D. C., Rauch, S. L., ... Gollub, R. L. (2001). Test-retest reliability of a functional MRI working memory paradigm in normal and schizophrenic subjects. *American Journal of Psychiatry*, 158(6), 955–958. <https://doi.org/10.1176/appi.ajp.158.6.955>
- Mason, M. F., Norton, M. I., Van Horn, J. D., Wegner, D. M., Grafton, S. T., & Macrae, C. N. (2007). Wandering minds: The default network and stimulus-independent thought. *Science*, 315(5810), 393–395. <https://doi.org/10.1126/science.1131295>
- McBride, G., Lin, L. I., Bland, J. M., & Altman, D. G. (2005). A proposal for strength-of-agreement criteria for Lin's concordance correlation coefficient. *National Institute of Water and Atmospheric Research, Client Report*, 45, 307–310. <https://www.medcalc.org/download/pdf/McBride2005.pdf>
- Menon, V. (2011). Large-scale brain networks and psychopathology: A unifying triple network model. *Trends in Cognitive Sciences*, 15(10), 483–506. <https://doi.org/10.1016/j.tics.2011.08.003>
- Menon, V., & Uddin, L. Q. (2010). Saliency, switching, attention and control: A network model of insula function. *Brain Structure & Function*, 214(5–6), 655–667. <https://doi.org/10.1007/s00429-010-0262-0>
- Mwansisya, T. E., Hu, A., Li, Y., Chen, X., Wu, G., Huang, X., ... Liu, Z. (2017). Task and resting-state fMRI studies in first-episode schizophrenia: A systematic review. *Schizophrenia Research*, 189, 9–18. <https://doi.org/10.1016/j.schres.2017.02.026>
- Nekovarova, T., Fajnerova, I., Horacek, J., & Spaniel, F. (2014). Bridging disparate symptoms of schizophrenia: A triple network dysfunction theory. *Frontiers in Behavioral Neuroscience*, 8, 171. <https://doi.org/10.3389/fnbeh.2014.00171>
- Nemani, A., & Lowe, M. J. (2021). Seed-based test-retest reliability of resting state functional magnetic resonance imaging at 3T and 7T. *Medical Physics*, 48(10), 5756–5764. <https://doi.org/10.1002/mp.15210>
- Newton, A. T., Rogers, B. P., Gore, J. C., & Morgan, V. L. (2012). Improving measurement of functional connectivity through decreasing partial volume effects at 7T. *NeuroImage*, 59(3), 2511–2517. <https://doi.org/10.1016/j.neuroimage.2011.08.096>
- Paakkki, J.-J., Rahko, J., Long, X., Moilanen, I., Tervonen, O., Nikkinen, J., ... Kiviniemi, V. (2010). Alterations in regional homogeneity of resting-state brain activity in autism spectrum disorders. *Brain Research*, 1321, 169–179. <https://doi.org/10.1016/j.brainres.2009.12.081>
- Platt, T., Ladd M.E., & Paech D. (2021). 7 Tesla and beyond. *Investigative Radiology*, 56(11), 705–725. <https://doi.org/10.1097/rli.0000000000000820>
- Plichta, M. M., Schwarz, A. J., Grimm, O., Morgen, K., Mier, D., Haddad, L., ... Meyer-Lindenberg, A. (2012). Test-retest reliability of evoked BOLD signals from a cognitive-emotive fMRI test battery. *NeuroImage*, 60(3), 1746–1758. <https://doi.org/10.1016/j.neuroimage.2012.01.129>
- Pollimeni, J. R., Renvall, V., Zaretskaya, N., & Fischl, B. (2018). Analysis strategies for high-resolution UHF-fMRI data. *NeuroImage*, 168, 296–320. <https://doi.org/10.1016/j.neuroimage.2017.04.053>
- Preibisch, C., Castrillón G., J. G., Bührer, M., & Riedl, V. (2015). Evaluation of multiband EPI acquisitions for resting state fMRI. *InPLoS One* (10, 9), e0136961. <https://doi.org/10.1371/journal.pone.0136961>
- Rauschenberg, J., Nagel, A. M., Ladd, S. C., Theysohn, J. M., Ladd, M. E., Möller, H. E., ... Semmler, W. (2014). Multicenter study of subjective acceptance during magnetic resonance imaging at 7 and 9.4 T. *Investigative Radiology*, 49(5), 249–259. <https://doi.org/10.1097/rli.0000000000000035>
- Robert Matthew (2020). f_CCC, GitHub. Retrieved from https://github.com/robertpetermatthew/f_CCC
- Robitaille, P.-M. L., Warner, R., Jagadeesh, J., Abduljalil, A. M., Kangarlu, A., Burgess, R. E., ... Rayner, D. L. (1999). Design and assembly of an 8 Tesla whole-body MR scanner. *Journal of Computer Assisted Tomography*, 23(6), 808–820. <https://doi.org/10.1097/00004728-199911000-00002>
- Seeley, W. W. (2019). The salience network: A neural system for perceiving and responding to homeostatic demands. *The Journal of Neuroscience*, 39(50), 9878–9882. <https://doi.org/10.1523/jneurosci.1138-17.2019>
- Shan, X., Qiu, Y., Pan, P., Teng, Z., Li, S., Tang, H., ... Wu, H. (2020). Disrupted regional homogeneity in drug-naive patients with bipolar disorder. *Frontiers in Psychiatry*, 11, 825. <https://doi.org/10.3389/fpsyt.2020.00825>
- Sladky, R., Baldinger, P., Kranz, G. S., Tröstl, J., Höfllich, A., Lanzenberger, R., ... Windischberger, C. (2013). High-resolution functional MRI of the human amygdala at 7T. *European Journal of Radiology*, 82(5), 728–733. <https://doi.org/10.1016/j.ejrad.2011.09.025>
- Smith, S. M., Vidaurre, D., Beckmann, C. F., Glasser, M. F., Jenkinson, M., Miller, K. L., ... Van Essen, D. C. (2013). Functional connectomics from resting-state fMRI. *Trends in Cognitive Sciences*, 17(12), 666–682. <https://doi.org/10.1016/j.tics.2013.09.016>
- Somandepalli, K., Kelly, C., Reiss, P. T., Zuo, X.-N., Craddock, R. C., Yan, C.-G., ... di Martino, A. (2015). Short-term test-retest reliability of resting state fMRI metrics in children with and without attention-deficit/hyperactivity disorder. *Developmental Cognitive Neuroscience*, 15, 83–93. <https://doi.org/10.1016/j.dcn.2015.08.003>
- Song, X., Panych, L. P., & Chen, N.-K. (2016). Data-driven and predefined ROI-based quantification of long-term resting-state fMRI reproducibility. *Brain Connectivity*, 6(2), 136–151. <https://doi.org/10.1089/brain.2015.0349>
- Strimbu, K., & Tavel, J. A. (2010). What are biomarkers? *Current Opinion in HIV and AIDS*, 5(6), 463–466. <https://doi.org/10.1097/coh.0b013e32833ed177>
- Takeuchi, H., Taki, Y., Nouchi, R., Sekiguchi, A., Hashizume, H., Sassa, Y., ... Kawashima, R. (2015). Degree centrality and fractional amplitude of low-frequency oscillations associated with Stroop interference. *NeuroImage*, 119, 197–209. <https://doi.org/10.1016/j.neuroimage.2015.06.058>
- Telesford, Q. K., Morgan, A. R., Hayasaka, S., Simpson, S. L., Barret, W., Kraft, R. A., ... Laurienti, P. J. (2010). Reproducibility of graph metrics in fMRI networks. *Frontiers in Neuroinformatics*, 4, 117. <https://doi.org/10.3389/fninf.2010.00117>
- Theysohn, J. M., Maderwald, S., Kraff, O., Moeninghoff, C., Ladd, M. E., & Ladd, S. C. (2007). Subjective acceptance of 7 tesla MRI for human imaging. *Magnetic Resonance Materials in Physics*, 21(1–2), 63–72. <https://doi.org/10.1007/s10334-007-0095-x>
- Triantafyllou, C., Hoge, R. D., Krueger, G., Wiggins, C. J., Potthast, A., Wiggins, G. C., & Wald, L. L. (2005). Comparison of physiological noise at 1.5 T, 3 T and 7 T and optimization of fMRI acquisition parameters. *NeuroImage*, 26(1), 243–250. <https://doi.org/10.1016/j.neuroimage.2005.01.007>
- Turner, J. A. (2013). A multi-site resting state fMRI study on the amplitude of low frequency fluctuations in schizophrenia. *Frontiers in Neuroscience*, 7, 137. <https://doi.org/10.3389/fnins.2013.00137>
- van der Zwaag, W., Francis, S., Head, K., Peters, A., Gowland, P., Morris, P., & Bowtell, R. (2009). fMRI at 1.5, 3 and 7 T: Characterising BOLD signal changes. *NeuroImage*, 47(4), 1425–1434. <https://doi.org/10.1016/j.neuroimage.2009.05.015>
- Vachha, B., & Huang, S. Y. (2021). MRI with ultrahigh field strength and high-performance gradients: challenges and opportunities for clinical neuroimaging at 7 T and beyond. *European Radiology Experimental*, 5(1), 35. <https://doi.org/10.1186/s41747-021-00216-2>
- Van Dijk, K. R. A., Hedden, T., Venkataraman, A., Evans, K. C., Lazar, S. W., & Buckner, R. L. (2010). Intrinsic functional connectivity as a tool for human connectomics: Theory, properties, and optimization. *Journal of neurophysiology*, 103(1), 297–321. <https://doi.org/10.1152/jn.00783.2009>

- Wang, P., Zhou, B., Yao, H., Zhan, Y., Zhang, Z., Cui, Y., ... Jiang, T. (2015). Aberrant intra- and inter-network connectivity architectures in Alzheimer's disease and mild cognitive impairment. *Scientific Reports*, 5. <https://doi.org/10.1038/srep14824>
- Washington, S. D., Gordon, E. M., Brar, J., Warburton, S., Sawyer, A. T., Wolfe, A., ... VanMeter, J. (2013). Dysmaturation of the default mode network in autism. *Human Brain Mapping*, 35(4), 1284–1296. <https://doi.org/10.1002/hbm.22252>
- Whitfield-Gabrieli, S., & Nieto-Castanon, A. (2012). Conn: A functional connectivity toolbox for correlated and anticorrelated brain networks. *Brain Connectivity*, 2(3), 125–141. <https://doi.org/10.1089/brain.2012.0073>
- Woodward, N. D., & Cascio, C. J. (2015). Resting-state functional connectivity in psychiatric disorders. *Journal of American Medical Association Psychiatry*, 72(8), 743–744. <https://doi.org/10.1001/jamapsychiatry.2015.0484>
- Yan, C.-G., Craddock, R. C., Zuo, X.-N., Zang, Y.-F., & Milham, M. P. (2013). Standardizing the intrinsic brain: Towards robust measurement of inter-individual variation in 1000 functional connectomes. *NeuroImage*, 80, 246–262. <https://doi.org/10.1016/j.neuroimage.2013.04.081>
- Yan, C.-G., Wang, X.-D., Zuo, X.-N., & Zang, Y.-F. (2016). DPABI: Data processing & analysis for (resting-state) brain imaging. *Neuroinformatics*, 14(3), 339–351. <https://doi.org/10.1007/s12021-016-9299-4>
- Yacoub, E., Shmuel, A., Pfeuffer, J., Van De Moortele, P.-F., Adriany, G., Andersen, P., ... Hu, X. (2001). Imaging brain function in humans at 7 Tesla. *Magnetic Resonance in Medicine*, 45(4), 588–594. <https://doi.org/10.1002/mrm.1080>
- Yu-Feng, Z., Yong, H., Chao-Zhe, Z., Qing-Jiu, C., Man-Qiu, S., Meng, L., ... Yu-Feng, W. (2007). Altered baseline brain activity in children with ADHD revealed by resting-state functional MRI. *Brain Dev*, 29(2), 83–91. <https://doi.org/10.1016/j.braindev.2006.07.002>
- Zang, Y., Jiang, T., Lu, Y., He, Y., & Tian, L. (2004). Regional homogeneity approach to fMRI data analysis. *NeuroImage*, 22(1), 394–400. <https://doi.org/10.1016/j.neuroimage.2003.12.030>
- Zheng, H., Xu, L., Xie, F., Guo, X., Zhang, J., Yao, L., & Wu, X. (2015). The altered triple networks interaction in depression under resting state based on graph theory. *BioMed Research International*, 2015, 1–8. <https://doi.org/10.1155/2015/386326>
- Zou, Q., Miao, X., Liu, D., Wang, D. J. J., Zhuo, Y., & Gao, J.-H. (2015). Reliability comparison of spontaneous brain activities between BOLD and CBF contrasts in eyes-open and eyes-closed resting states. *NeuroImage*, 121, 91–105. <https://doi.org/10.1016/j.neuroimage.2015.07.044>
- Zou, Q.-H., Zhu, C.-Z., Yang, Y., Zuo, X.-N., Long, X.-Y., Cao, Q.-J., ... Zang, Y. F. (2008). An improved approach to detection of amplitude of low-frequency fluctuation (ALFF) for resting-state fMRI: Fractional ALFF. *Journal of Neuroscience Methods*, 172(1), 137–141. <https://doi.org/10.1016/j.jneumeth.2008.04.012>
- Zuo, X.-N., Biswal, B. B., & Poldrack, R. A. (2019). Editorial: Reliability and reproducibility in functional connectomics. *Frontiers in Neuroscience*, 13, 117. <https://doi.org/10.3389/fnins.2019.00117>
- Zuo, X.-N., Di Martino, A., Kelly, C., Shehzad, Z. E., Gee, D. G., Klein, D. F., ... Milham, M. P. (2010). The oscillating brain: Complex and reliable. *NeuroImage*, 49(2), 1432–1445. <https://doi.org/10.1016/j.neuroimage.2009.09.037>
- Zuo, X.-N., & Xing, X.-X. (2014). Test-retest reliabilities of resting-state fMRI measurements in human brain functional connectomics: A systems neuroscience perspective. *Neuroscience & Biobehavioral Reviews*, 45, 100–118. <https://doi.org/10.1016/j.neubiorev.2014.05.009>
- Zuo, X.-N., Ehmke, R., Mennes, M., Imperati, D., Castellanos, F. X., Sporns, O., & Milham, M.P. (2012). Network centrality in the human functional connectome. *Cerebral Cortex*, 22(8), 1862–1875. <https://doi.org/10.1093/cercor/bhr269>

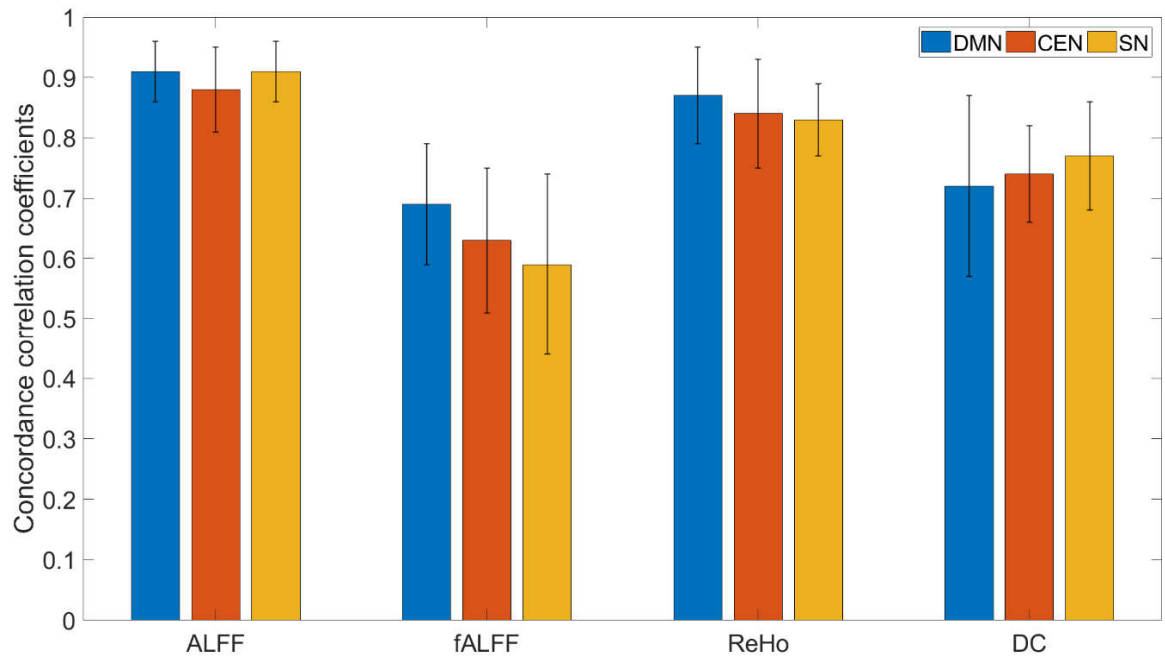
SUPPORTING INFORMATION

Additional supporting information may be found in the online version of the article at the publisher's website.

How to cite this article: Sbaihat, H., Rajkumar, R., Ramkiran, S., Assi, A. A.-N., Felder, J., Shah, N. J., Veselinović, T., & Neuner, I. (2022). Test-retest stability of spontaneous brain activity and functional connectivity in the core resting-state networks assessed with ultrahigh field 7-Tesla resting-state functional magnetic resonance imaging. *Human Brain Mapping*, 1–15. <https://doi.org/10.1002/hbm.25771>

Supporting information

Supplementary Figure 1 (S-Fig. 1)



S-Fig. 1. Mean of the inter-measurement stability across 15 subjects (calculated from the sample excluding one potential outlier subject) for the fMRI parameters (amplitude of low-frequency fluctuations (ALFF), fractional ALFF (fALFF), regional homogeneity (ReHo), and degree centrality (DC)) in each core network, i.e., the default mode network (DMN), the central executive network (CEN), and the salience network (SN). The error bars represent standard deviation.

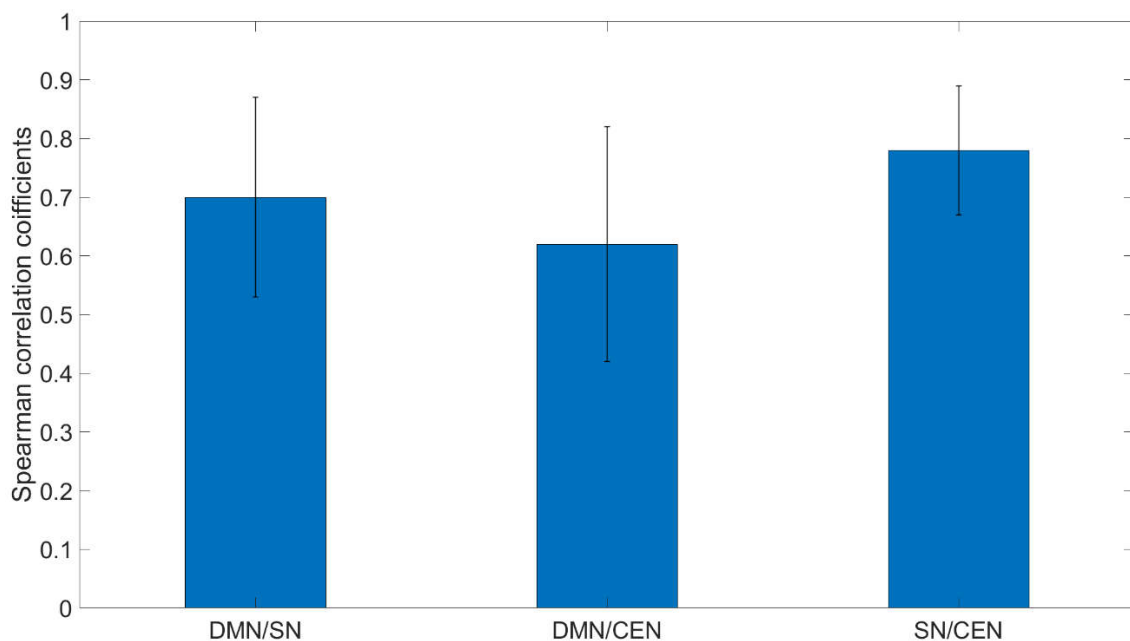
Generally, the results did not differ noticeably from the findings from the whole sample with 16 participants. We observed the mean stability of ALFF parameter to be strong in all three networks with highest in both, the DMN (0.91 ± 0.05 ; range from 0.76 to 0.96), and the SN (0.91 ± 0.05 ; range from 0.76 to 0.95) followed by the CEN (0.88 ± 0.07 ; range from 0.69 to 0.95).

The mean stability of fALFF parameter was found to be moderate in all three networks: DMN: 0.69 ± 0.10 (range from 0.44 to 0.85); CEN: 0.63 ± 0.12 (range from 0.44 to 0.90); SN: 0.59 ± 0.15 (range from 0.35 to 0.83).

The mean stability of ReHo parameter was found to be strong in all three networks: DMN: 0.87 ± 0.08 (range from 0.64 to 0.93); CEN: 0.84 ± 0.09 (range from 0.56 to 0.94); SN: 0.83 ± 0.06 (range from 0.69 to 0.91).

The mean stability of DC parameter was found to be strong in all three networks with highest in the SN: 0.77 ± 0.09 (range from 0.64 to 0.92) followed by the CEN: 0.74 ± 0.08 (range from 0.62 to 0.90); and the DMN: 0.72 ± 0.15 (range from 0.32 to 0.89).

Supplementary Figure 2 (S-Fig. 2)



S-Fig.2. Mean of the inter-network correlations stability between the three core resting state networks depicted as the mean correlations between the DMN/SN, the DMN/CEN, and the SN/CEN. The error bars represent standard deviation. This calculation was performed on the sample of 15 participants, i.e., without the one participant who was considered as a potential outlier.

The inter-network connectivity showed a variant stability between the investigated network-pairs: between DMN and SN: 0.70 ± 0.17 ; (range from 0.36 to 0.94) strong stability; between DMN and CEN: 0.62 ± 0.21 (range from 0.12 to 0.94) moderate stability; between CEN and SN: 0.78 ± 0.11 (range from 0.60 to 0.91) strong stability.

Supplementary Table 1 (S-Tab. 1)

| Subjects number in original data set | Excluding criteria | Subjects number in this study |
|---|--|--------------------------------------|
| 27430 | Included in study | Sub 01 |
| 27431 | Included in study | Sub 02 |
| 27432 | Included in study | Sub 03 |
| 27433 | Included in study | Sub 04 |
| 27434 | Included in study | Sub 05 |
| 27435 | Included in study | Sub 06 |
| 27436 | Included in study | Sub 07 |
| 27437 | Included in study | Sub 08 |
| 27438 | Excluded due to the motion (more than 2.0 mm in session 1) | *** |
| 27439 | Included to study | Sub 09 |
| 27440 | Excluded due to the low-resolution of fMRI images in both sessions | *** |
| 27441 | Included in study | Sub 10 |
| 27442 | Included in study | Sub 11 |
| 27443 | Included in study | Sub 12 |
| 27444 | Excluded due to fMRI data missing in the right frontal region | *** |
| 27445 | Excluded due to the motion (more than 2.5 mm in session 2) | *** |
| 27446 | Included in study | Sub 13 |
| 27447 | Included in study | Sub 14 |
| 27448 | Included in study | Sub 15 |
| 27449 | Included in study | Sub 16 |
| 27450 | Excluded due to motion (more than 3.0 mm in session 1) | *** |
| 27451 | Excluded due to the motion (more than 2.5 mm in session 2) | *** |

S-Tab.1. Showing the included and excluded subjects in our study. Some subjects were excluded due to motion, missing of the data, or low-resolution fMRI images.

Supplementary Table 2 (S-Tab. 2)

| Subject number | Percentage volumes left in Session 1 | Percentage volumes left in Session 2 |
|-----------------------|---|---|
| 1 | 91 | 99 |
| 2 | 100 | 100 |
| 3 | 99 | 95 |
| 4 | 99 | 99 |
| 5 | 93 | 99 |
| 6 | 99 | 99 |
| 7 | 98 | 100 |
| 8 | 100 | 90 |
| 9 | 98 | 87 |
| 10 | 96 | 88 |
| 11 | 100 | 100 |
| 12 | 100 | 100 |
| 13 | 99 | 100 |
| 14 | 99 | 100 |
| 15 | 98 | 100 |
| 16 | 91 | 79 |

S-Tab.2. Showing the percentage of volumes left for each subject and session after scrubbing.

Supplementary Table 3 (S-Tab. 3)

| Subjects | DMN | | | CEN | | | SN | | | | | |
|----------|-----------------------|-----------------------|-----------------------|-----------------------|-----------------------|------------------------|-----------------------|-----------------------|-----------------------|----------------------------|-----------------------|-----------------------|
| | ALFF | fALFF | ReHo | ALFF | fALFF | ReHo | ALFF | fALFF | ReHo | DC | | |
| Sub01 | 0.72, CI [0.71, 0.74] | 0.19, CI [0.15, 0.22] | 0.77, CI [0.75, 0.79] | 0.4, CI [0.37, 0.42] | 0.75, CI [0.73, 0.77] | 0.02, CI [-0.03, 0.07] | 0.75, CI [0.73, 0.77] | 0.25, CI [0.21, 0.29] | 0.74, CI [0.72, 0.76] | (-0.20), CI [-0.24, -0.15] | 0.74, CI [0.68, 0.79] | 0.24, CI [0.21, 0.27] |
| Sub02 | 0.93, CI [0.92, 0.93] | 0.76, CI [0.74, 0.77] | 0.87, CI [0.86, 0.89] | 0.75, CI [0.73, 0.76] | 0.88, CI [0.87, 0.89] | 0.69, CI [0.67, 0.71] | 0.86, CI [0.87, 0.89] | 0.73, CI [0.71, 0.75] | 0.92, CI [0.92, 0.93] | 0.67, CI [0.65, 0.69] | 0.89, CI [0.89, 0.90] | 0.81, CI [0.79, 0.82] |
| Sub03 | 0.84, CI [0.83, 0.85] | 0.44, CI [0.42, 0.47] | 0.64, CI [0.62, 0.66] | 0.47, CI [0.44, 0.49] | 0.69, CI [0.67, 0.71] | 0.44, CI [0.40, 0.48] | 0.56, CI [0.53, 0.59] | 0.62, CI [0.59, 0.65] | 0.87, CI [0.85, 0.89] | 0.35, CI [0.31, 0.40] | 0.75, CI [0.74, 0.77] | 0.78, CI [0.76, 0.80] |
| Sub04 | 0.93, CI [0.92, 0.93] | 0.8, CI [0.79, 0.81] | 0.92, CI [0.92, 0.93] | 0.74, CI [0.72, 0.75] | 0.85, CI [0.84, 0.87] | 0.62, CI [0.59, 0.65] | 0.89, CI [0.88, 0.90] | 0.8, CI [0.78, 0.82] | 0.91, CI [0.91, 0.92] | 0.66, CI [0.64, 0.69] | 0.88, CI [0.87, 0.89] | 0.84, CI [0.83, 0.85] |
| Sub05 | 0.76, CI [0.75, 0.78] | 0.74, CI [0.73, 0.75] | 0.95, CI [0.93, 0.94] | 0.67, CI [0.66, 0.68] | 0.83, CI [0.81, 0.84] | 0.52, CI [0.48, 0.55] | 0.84, CI [0.82, 0.85] | 0.8, CI [0.78, 0.82] | 0.76, CI [0.74, 0.78] | 0.41, CI [0.37, 0.45] | 0.84, CI [0.83, 0.85] | 0.81, CI [0.79, 0.82] |
| Sub06 | 0.86, CI [0.85, 0.89] | 0.7, CI [0.68, 0.72] | 0.91, CI [0.89, 0.91] | 0.61, CI [0.59, 0.63] | 0.9, CI [0.89, 0.91] | 0.51, CI [0.47, 0.54] | 0.84, CI [0.82, 0.85] | 0.65, CI [0.61, 0.69] | 0.93, CI [0.93, 0.94] | 0.37, CI [0.34, 0.41] | 0.85, CI [0.84, 0.86] | 0.67, CI [0.64, 0.69] |
| Sub07 | 0.9, CI [0.89, 0.90] | 0.61, CI [0.60, 0.63] | 0.84, CI [0.83, 0.85] | 0.75, CI [0.75, 0.78] | 0.85, CI [0.84, 0.87] | 0.56, CI [0.52, 0.59] | 0.82, CI [0.80, 0.83] | 0.77, CI [0.75, 0.79] | 0.9, CI [0.89, 0.91] | 0.41, CI [0.37, 0.44] | 0.79, CI [0.77, 0.80] | 0.84, CI [0.81, 0.86] |
| Sub08 | 0.93, CI [0.93, 0.93] | 0.62, CI [0.60, 0.64] | 0.81, CI [0.80, 0.82] | 0.71, CI [0.69, 0.72] | 0.9, CI [0.89, 0.91] | 0.5, CI [0.46, 0.53] | 0.73, CI [0.71, 0.76] | 0.7, CI [0.68, 0.73] | 0.95, CI [0.95, 0.95] | 0.46, CI [0.42, 0.49] | 0.79, CI [0.77, 0.81] | 0.84, CI [0.82, 0.86] |
| Sub09 | 0.86, CI [0.85, 0.89] | 0.85, CI [0.84, 0.89] | 0.91, CI [0.90, 0.91] | 0.89, CI [0.88, 0.90] | 0.94, CI [0.93, 0.94] | 0.9, CI [0.89, 0.91] | 0.94, CI [0.93, 0.95] | 0.9, CI [0.88, 0.90] | 0.92, CI [0.92, 0.93] | 0.75, CI [0.73, 0.77] | 0.84, CI [0.83, 0.86] | 0.9, CI [0.89, 0.91] |
| Sub10 | 0.93, CI [0.92, 0.93] | 0.75, CI [0.74, 0.76] | 0.92, CI [0.91, 0.92] | 0.83, CI [0.82, 0.84] | 0.92, CI [0.91, 0.93] | 0.63, CI [0.60, 0.65] | 0.9, CI [0.89, 0.91] | 0.71, CI [0.69, 0.73] | 0.95, CI [0.95, 0.96] | 0.58, CI [0.55, 0.61] | 0.81, CI [0.79, 0.82] | 0.87, CI [0.85, 0.89] |
| Sub11 | 0.85, CI [0.85, 0.89] | 0.75, CI [0.73, 0.78] | 0.91, CI [0.91, 0.92] | 0.78, CI [0.74, 0.77] | 0.85, CI [0.85, 0.89] | 0.76, CI [0.74, 0.79] | 0.93, CI [0.92, 0.94] | 0.77, CI [0.75, 0.80] | 0.92, CI [0.91, 0.92] | 0.69, CI [0.66, 0.71] | 0.86, CI [0.85, 0.87] | 0.78, CI [0.76, 0.80] |
| Sub12 | 0.89, CI [0.89, 0.90] | 0.59, CI [0.58, 0.61] | 0.88, CI [0.88, 0.89] | 0.75, CI [0.73, 0.76] | 0.87, CI [0.86, 0.88] | 0.61, CI [0.58, 0.63] | 0.91, CI [0.90, 0.92] | 0.67, CI [0.65, 0.70] | 0.9, CI [0.89, 0.91] | 0.59, CI [0.56, 0.61] | 0.87, CI [0.86, 0.89] | 0.78, CI [0.76, 0.79] |
| Sub13 | 0.83, CI [0.83, 0.89] | 0.73, CI [0.72, 0.75] | 0.82, CI [0.82, 0.83] | 0.71, CI [0.69, 0.73] | 0.83, CI [0.82, 0.85] | 0.69, CI [0.66, 0.72] | 0.87, CI [0.86, 0.89] | 0.71, CI [0.69, 0.74] | 0.88, CI [0.88, 0.90] | 0.73, CI [0.71, 0.75] | 0.83, CI [0.82, 0.85] | 0.86, CI [0.84, 0.89] |
| Sub14 | 0.91, CI [0.91, 0.92] | 0.72, CI [0.71, 0.74] | 0.91, CI [0.90, 0.91] | 0.72, CI [0.70, 0.73] | 0.81, CI [0.80, 0.83] | 0.72, CI [0.70, 0.75] | 0.8, CI [0.78, 0.82] | 0.73, CI [0.70, 0.75] | 0.9, CI [0.89, 0.91] | 0.75, CI [0.73, 0.78] | 0.69, CI [0.67, 0.72] | 0.87, CI [0.85, 0.89] |
| Sub15 | 0.91, CI [0.91, 0.92] | 0.60, CI [0.59, 0.62] | 0.74, CI [0.73, 0.75] | 0.32, CI [0.31, 0.34] | 0.92, CI [0.91, 0.93] | 0.73, CI [0.71, 0.75] | 0.83, CI [0.82, 0.85] | 0.63, CI [0.61, 0.65] | 0.95, CI [0.95, 0.96] | 0.83, CI [0.82, 0.84] | 0.91, CI [0.90, 0.91] | 0.72, CI [0.70, 0.74] |
| Sub16 | 0.85, CI [0.85, 0.89] | 0.68, CI [0.66, 0.70] | 0.83, CI [0.82, 0.83] | 0.88, CI [0.87, 0.89] | 0.91, CI [0.90, 0.92] | 0.64, CI [0.61, 0.67] | 0.89, CI [0.88, 0.90] | 0.88, CI [0.87, 0.89] | 0.95, CI [0.94, 0.95] | 0.61, CI [0.58, 0.64] | 0.91, CI [0.90, 0.92] | 0.82, CI [0.81, 0.83] |

3 S-Tab.3. The concordance correlation coefficients and their 95 confidence interval level of significance for the fMRI parameters between the two sessions in the default mode network (DMN), the

4 central executive network (CEN), and the salience network (SN).

Supplementary Table 4 (S-Tab. 4)

S-Tab. 4. The average values of the inter-network interaction of the default mode network (DMN), the central executive network (CEN), and the salience network (SN) in session 1.

| Networks | Sub-regions | DMN | | | | | | SN | | | | | | CEN | | | | | |
|----------|-------------|-------|--------|--------|------|------|-------------|-------------|-----------|-----------|---------|---------|----------|---------|----------|---------|--|--|--|
| | | MPPFC | LP (L) | LP (R) | PCC | ACC | Alnsula (L) | Alnsula (R) | RPPFC (L) | RPPFC (R) | SMG (L) | SMG (R) | LPFC (L) | PPC (L) | LPFC (R) | PPC (R) | | | |
| DMN | MPPFC | Inf | 0.51 | 0.57 | 0.65 | 0.37 | 0.18 | 0.11 | 0.28 | 0.23 | 0.07 | 0.02 | 0.30 | 0.30 | 0.31 | 0.28 | | | |
| | LP (L) | 0.51 | Inf | 0.89 | 0.71 | 0.14 | 0.05 | -0.03 | 0.21 | 0.13 | 0.14 | 0.12 | 0.42 | 0.40 | 0.27 | 0.25 | | | |
| | LP (R) | 0.57 | 0.89 | Inf | 0.73 | 0.21 | 0.15 | 0.08 | 0.25 | 0.21 | 0.25 | 0.24 | 0.35 | 0.30 | 0.41 | 0.39 | | | |
| | PCC | 0.65 | 0.71 | 0.73 | Inf | 0.45 | 0.28 | 0.20 | 0.48 | 0.42 | 0.23 | 0.23 | 0.42 | 0.47 | 0.47 | 0.39 | | | |
| | ACC | 0.37 | 0.14 | 0.21 | 0.45 | Inf | 0.89 | 0.82 | 0.87 | 0.79 | 0.54 | 0.50 | 0.35 | 0.34 | 0.41 | 0.28 | | | |
| SN | Alnsula (L) | 0.18 | 0.05 | 0.15 | 0.28 | 0.89 | Inf | 0.95 | 0.66 | 0.61 | 0.72 | 0.80 | 0.38 | 0.14 | 0.34 | 0.22 | | | |
| | Alnsula (R) | 0.11 | -0.03 | 0.08 | 0.20 | 0.82 | Inf | 0.95 | 0.66 | 0.67 | 0.73 | 0.60 | 0.19 | 0.08 | 0.35 | 0.27 | | | |
| | RPPFC (L) | 0.28 | 0.21 | 0.25 | 0.48 | 0.87 | 0.81 | 0.66 | Inf | 1.02 | 0.62 | 0.52 | 0.49 | 0.15 | 0.56 | 0.43 | | | |
| | RPPFC (R) | 0.23 | 0.13 | 0.21 | 0.42 | 0.79 | 0.61 | 0.73 | 1.02 | Inf | 0.52 | 0.62 | 0.29 | 0.15 | 0.56 | 0.43 | | | |
| | SMG (L) | 0.07 | 0.14 | 0.25 | 0.23 | 0.54 | 0.72 | 0.67 | 0.62 | 0.52 | Inf | 0.86 | 0.20 | 0.09 | 0.22 | 0.21 | | | |
| | SMG (R) | 0.02 | 0.12 | 0.24 | 0.23 | 0.50 | 0.60 | 0.73 | 0.52 | 0.62 | 0.86 | Inf | 0.09 | 0.01 | 0.22 | 0.22 | | | |
| | LPFC (L) | 0.30 | 0.42 | 0.35 | 0.42 | 0.35 | 0.38 | 0.19 | 0.49 | 0.29 | 0.20 | 0.09 | Inf | 0.88 | 0.84 | 0.56 | | | |
| CEN | LPFC (L) | 0.30 | 0.40 | 0.30 | 0.34 | 0.22 | 0.14 | 0.08 | 0.30 | 0.15 | 0.09 | 0.01 | 0.88 | Inf | 0.53 | 0.79 | | | |
| | PPC (L) | 0.31 | 0.27 | 0.41 | 0.47 | 0.41 | 0.34 | 0.35 | 0.45 | 0.56 | 0.22 | 0.22 | 0.84 | Inf | 0.94 | 0.94 | | | |
| | PPC (R) | 0.28 | 0.25 | 0.39 | 0.39 | 0.28 | 0.22 | 0.27 | 0.36 | 0.43 | 0.21 | 0.22 | 0.56 | 0.79 | 0.94 | Inf | | | |

Supplementary Table 5(S-Tab. 5)

| Networks | Sub-regions | DMN | | | | | | SN | | | | | | CEN | | |
|----------|-------------|------|--------|--------|------|------|-------------|-------------|----------|----------|---------|---------|----------|---------|----------|---------|
| | | MPFC | LP (L) | LP (R) | PCC | ACC | AInsula (L) | AInsula (R) | RPFC (L) | RPFC (R) | SMG (L) | SMG (R) | LPFC (L) | PCC (L) | LPFC (R) | PCC (R) |
| DMN | MPFC | Inf | 0.55 | 0.60 | 0.68 | 0.38 | 0.11 | 0.12 | 0.32 | 0.27 | 0.03 | 0.03 | 0.30 | 0.35 | 0.37 | 0.38 |
| | LP (L) | Inf | 0.94 | 0.68 | 0.18 | 0.00 | -0.01 | 0.25 | 0.18 | 0.15 | 0.14 | 0.35 | 0.40 | 0.31 | 0.31 | 0.32 |
| | LP (R) | 0.60 | Inf | 0.75 | 0.21 | 0.09 | 0.05 | 0.27 | 0.25 | 0.18 | 0.20 | 0.32 | 0.31 | 0.47 | 0.50 | 0.38 |
| | PCC | 0.68 | 0.68 | Inf | 0.45 | 0.20 | 0.21 | 0.48 | 0.47 | 0.14 | 0.21 | 0.31 | 0.31 | 0.50 | 0.44 | 0.44 |
| | ACC | 0.38 | 0.18 | 0.21 | Inf | 0.81 | 0.81 | 0.90 | 0.79 | 0.60 | 0.46 | 0.23 | 0.38 | 0.24 | 0.24 | 0.24 |
| | AInsula (L) | 0.11 | 0.00 | 0.09 | 0.20 | 0.81 | Inf | 0.94 | 0.72 | 0.62 | 0.55 | 0.55 | 0.31 | 0.09 | 0.09 | 0.09 |
| SN | AInsula (R) | 0.12 | -0.01 | 0.05 | 0.21 | 0.72 | Inf | 0.62 | 0.72 | 0.55 | 0.63 | 0.19 | 0.07 | 0.28 | 0.28 | 0.21 |
| | RPFC (L) | 0.32 | 0.25 | 0.27 | 0.48 | 0.90 | 0.62 | Inf | 1.05 | 0.72 | 0.49 | 0.45 | 0.45 | 0.31 | 0.41 | 0.32 |
| | RPFC (R) | 0.27 | 0.18 | 0.25 | 0.47 | 0.79 | 1.05 | 0.45 | Inf | 0.45 | 0.61 | 0.16 | 0.17 | 0.50 | 0.43 | 0.43 |
| | SMG (L) | 0.03 | 0.15 | 0.18 | 0.14 | 0.46 | 0.66 | 0.55 | 0.45 | Inf | 0.79 | 0.61 | 0.09 | 0.13 | 0.13 | 0.11 |
| | SMG (R) | 0.03 | 0.14 | 0.20 | 0.21 | 0.45 | 0.55 | 0.49 | 0.61 | 0.45 | 0.79 | 0.16 | -0.01 | 0.14 | 0.14 | 0.14 |
| | LPFC (L) | 0.30 | 0.35 | 0.32 | 0.34 | 0.36 | 0.31 | 0.45 | 0.26 | 0.16 | 0.16 | 0.04 | Inf | 0.83 | 0.77 | 0.45 |
| CEN | PPC (L) | 0.35 | 0.40 | 0.31 | 0.31 | 0.21 | 0.09 | 0.31 | 0.17 | 0.09 | -0.01 | 0.83 | Inf | 0.56 | 0.79 | |
| | LPFC (R) | 0.37 | 0.31 | 0.47 | 0.50 | 0.38 | 0.23 | 0.41 | 0.50 | 0.13 | 0.14 | 0.77 | 0.56 | Inf | 0.93 | |
| | PPC (R) | 0.38 | 0.32 | 0.50 | 0.44 | 0.24 | 0.13 | 0.32 | 0.43 | 0.11 | 0.14 | 0.45 | 0.79 | 0.93 | Inf | |

S-Tab.5. The average values of the inter-network interaction of the default mode network (DMN), the central executive network (CEN), and the salience network (SN) in session 2.

Acknowledgments

At the outset, I would like to thank my parents for their support, and continuous encouragement which is the primary reason behind this achievement.

I am very thankful to my supervisor Prof. Dr. Irene Neuner who has always been supporting and advising, and encouraging me all the time. I also thank Prof. Dr. John Shah for his assistance and support.

I am very grateful to my colleagues in the multimodal MR, PET, and EEG imaging group, for their valuable inputs and support.

I would like to express my special thanks to my lovely sister, Amal, and to my brothers (Zaid, Omar, Mahmoud, Ahmed, and Ibrahim) for their trust in me and their continued lovely support.

Many thanks to Juelich research center (Forschungszentrum Jülich), the Palestinian-German Science Bridge PGSB, Federal Ministry of Education and Research (Bundesministerium für Bildung und Forschung - BMBF), and University Hospital Aachen (Universitätsklinikum Aachen) for funding this research.

Last but not the least, a special thanks to all my friends who enriched my life during my Ph.D. - your support and your words of encouragement always meant a lot to me!

Thanks for all your encouragement!

Affidavit according to § 5 (1) for Data Retention

I hereby declare that the original data forming the basis of this doctoral thesis are stored with my supervisor, Prof. Irene Neuner, Head of the Multimodal Imaging in Clinical Neuroscience, Clinic for Psychiatry, Psychotherapy - Psychosomatics, University Hospital Aachen.

Aachen, 10.02.2022

Hasan M H Sbaihat

Affidavit according to § 5 (1) and (2), and § 11 (3) 12 of the doctoral studies regulations

I hereby declare on oath, Hasan M H Sbaihat, that I have contributed a significant part, and thus majority, of the publication:

Hasan Sbaihat, Ravichandran Rajkumar, Shukti Ramkiran, Abed Al-Nasser Assi, N. Jon Shah, Tanja Veselinović, Irene Neuner. Dynamics of task-induced modulation of spontaneous brain activity and functional connectivity in the triple resting-state networks assessed using the visual oddball paradigm. PLoS One. 2021 Nov 4;16(11):e0246709. doi: 10.1371/journal.pone.0246709. PMID: 34735449; PMCID: PMC8568109.

The contributions to the publication were as follows:

| Names ----> | Candidate (Sbaihat) | Practical supervisor (Rajkumar) | Statistician (Ramkiran) | Collaborative partner (Assi) | Supervision (Veselinović, Shah) | Doctoral supervisor (Neuner) | Sum (%) |
|-----------------------------|---------------------|---------------------------------|-------------------------|------------------------------|---------------------------------|------------------------------|---------|
| Conceptualization | | | | | | 100 | 100 |
| Data curation: | 100 | | | | | | 100 |
| Data preprocessing: | 100 | | | | | | 100 |
| Formal analysis: | 100 | | | | | | 100 |
| Data evaluation | 70 | 20 | | | | 10 | 100 |
| Funding acquisition | | | | | 50 | 50 | 100 |
| Statistical evaluation | 20 | 30 | 50 | | | | 100 |
| Methodology | | 50 | | | 50 | | 100 |
| Resources | | | | | 100 | | 100 |
| Supervision | | | | 10 | 30 | 60 | 100 |
| Raw-data arrangement | 70 | 15 | 15 | | | | 100 |
| Software | | 100 | | | | | 100 |
| Writing – original draft | 100 | | | | | | 100 |
| Writing – review & editing: | | 25 | 15 | 5 | 45 | 10 | 100 |

The position as the first author obviously arises from this significant contribution.

Signature of the doctoral candidate

As supervisor and corresponding author I confirm the statements of Hasan M H Sbaihat and as a representative of the collaborative partners Abed Al-Nasser Assi.

Signature of the doctoral supervisor

Signature of the corresp. author

As co-author I endorse the statement of Irene Neuner

Ravichandran Rajkumar

Shukti Ramkiran

N. Jon Shah

Tanja Veselinović

Affidavit according to § 5 (1) and (2), and § 11 (3) 12 of the doctoral studies regulations

I hereby declare on oath, Hasan M H Sbaihat, that I have contributed a significant part, and thus majority, of the publication:

Hasan Sbaihat, Ravichandran Rajkumar, Shukti Ramkiran, Abed Al-Nasser Assi, Jörg Felder, N. Jon Shah, Tanja Veselinović, Irene Neuner. Test-retest stability of spontaneous brain activity and functional connectivity in the core resting-state networks assessed with ultrahigh field 7-Tesla resting-state functional magnetic resonance imaging. Human brain mapping, 2022 January 1-15. DOI: 10.1002/hbm.25771.

The contributions to the publication were as follows:

| Names ---> | Candidate (Sbaihat) | Statistician /Programmer (Rajkumar, Ramkiran) | Physician (Felder) | Collaborative partner (Assi) | Supervision (Veselinović, Shah) | Doctoral supervisor (Neuner) | Sum (%) |
|-----------------------------|---------------------|---|--------------------|------------------------------|---------------------------------|------------------------------|---------|
| Conceptualization | | | | | | 100 | 100 |
| Formal analysis: | 100 | | | | | | 100 |
| Data evaluation | 70 | 20 | 10 | | | | 100 |
| Funding | | | | | | 100 | 100 |
| Statistical evaluation | 40 | 60 | | | | | 100 |
| Methodology | 35 | 40 | 10 | | 15 | | 100 |
| Supervision | | | | 10 | 25 | 65 | 100 |
| Raw-data arrangement | 100 | | | | | | 100 |
| Software | | 100 | | | | | 100 |
| Writing – original draft | 100 | | | | | | 100 |
| Writing – review & editing: | | 30 | 5 | 10 | 35 | 20 | 100 |

The position as the first author obviously arises from this significant contribution.

Signature of the doctoral candidate

As supervisor and corresponding author I confirm the statements of Hasan M H Sbaihat and as a representative of the collaborative partners Abed Al-Nasser Assi.

Signature of the doctoral supervisor

Signature of the corresp. author

As co-author I endorse the statement of Irene Neuner

Ravichandran Rajkumar

Shukti Ramkiran

Jörg Felder

N. Jon Shah

Tanja Veselinović

CURRICULUM VITAE

Hasan M H Sbaihat

CONTACT INFORMATION

Address: Wiesenstraße 7A, 52428 Jülich, Germany
Cell phone: 00491726310105
Emails: h.sbaihat@fz-juelich.de
hasansbaihat@gmail.com

PERSONAL INFORMATION

First name: Hasan
Middle name: M H
Family name: Sbaihat
Date of birth: 26.02.1992
Nationality: Palestinian
Place of birth: Nazareth
Palestine

EDUCATION

| | |
|--|------------|
| Master of Basic Medical Sciences and Biomedicine, Medical Imaging, Faculty of Medicine, Gadjah Mada University (UGM), Yogyakarta, Indonesia. | July. 2016 |
| Bachelor of Medical Imaging, Faculty of Allied Medical Sciences, Arab American University Palestine (AAUP), Palestine. | July. 2014 |
| Martyr Najib Al-Ahmad School – P2450727, P245 Rommana, Palestine | May. 2010 |

PUBLICATIONS

Sbaihat H, Rajkumar R, Ramkiran S, Assi AA, Shah NJ, Veselinović T, Neuner I. Dynamics of task-induced modulation of spontaneous brain activity and functional connectivity in the triple resting-state networks assessed using the visual oddball paradigm. *PLoS One*. 2021 Nov 4;16(11): e0246709. doi: 10.1371/journal.pone.0246709. PMID: 34735449; PMCID: PMC8568109.

Hasan Sbaihat, Ravichandran Rajkumar, Shukti Ramkiran, Abed Al-Nasser Assi, Jörg Felder, N. Jon Shah, Tanja Veselinović, Irene Neuner. Test-retest stability of spontaneous brain activity and functional connectivity in the core resting-state networks assessed with ultrahigh field 7-Tesla resting-state functional magnetic resonance imaging. *Human brain mapping*, 2022 January 1-15. DOI: 10.1002/hbm.25771.

Altinok DCA, Rajkumar R, Nießen D, **Sbaihat H**, Kersey M, Shah NJ, Veselinović T, Neuner I. Common neurobiological correlates of resilience and personality traits within the triple resting-state brain networks

assessed by 7-Tesla ultra-high field MRI. Sci Rep. 2021 Jun 2;11(1):11564. doi: 10.1038/s41598-021-91056-y. PMID: 34079001; PMCID: PMC8172832.

Cláudia Brambilla, Tanja Veselinovic, Ravichandran Rajkumar, Joerg Mauler, Andreas Matusch, Andrej Ruch, Linda Orth, Shukti Ramkiran, **Hasan Sbaihat**, Nicolas Kaulen, Nibal Khudeish, Christine Wyss, Karsten Heekeren, Wolfram Kawohl, Elena Rota Kops, Lutz Tellmann, Jürgen Scheins, Frank Boers, Bernd Neumaier, Johannes Ermert, Markus Lang, Stefan Stüsgen, Hans Herzog, Karl-Josef Langen, Jon Shah, Christoph Lerche, and Irene Neuner. mGluR5 binding changes during a mismatch negativity task in a multimodal protocol with [11C]ABP688 PET/MR-EEG. Transl Psychiatry 12, 6 (2022). <https://doi.org/10.1038/s41398-021-01763-3>.

Nicolas Kaulen, Ravichandran Rajkumar, Claudia Régio Brambilla, Jörg Mauler, Shukti Ramkiran, Linda Orth, **Hasan Sbaihat**, Markus Lang, Christine Wyss, Elena Rota Kops, Jürgen Scheins, Bernd Neumaier, Johannes Ermert, Hans R. Herzog, Karl-Joseph Langen, Christoph Lerche, N. Jon Shah, Tanja Veselinović, and Irene Neuner. mGluR5 and GABAA Receptor Specific Parametric PET Atlas Construction - PET/MR Data Processing Pipeline, Validation and Application. This work has been accepted for publication in the human brain mapping.

7T Mental health: Functional alterations in resting-state within the executive control network and its association with BDI-II and TMT-B in MDD by Ravichandran Rajkumar, Gereon Johannes Schnellbacher, **Hasan Sbaihat**, N. Jon Shah, Tanja Veselinović, and Irene Neuner. This work has been accepted and published as conference abstract in International Society for Magnetic Resonance in Medicine. <https://www.ismrm.org/21/program-files/TeaserSlides/TeasersPresentations/1664-Teaser.html>.

WORK EXPERIENCE

| | |
|---|-------------------------------|
| Worked at the Arab American University as a teacher and supervisor of practical training students in the medical imaging department, Palestine. | September. 2016 - April. 2018 |
| Worked in the Radiology Department of the Women's Union Hospital, Nablus, Palestine. | August. 2016 |
| Worked as a volunteer in Jenin governmental hospital during the last two years of my bachelor's degree. | 2012-2014 |

CONFERENCES AND WORKSHOPS

| | |
|--|--------------|
| Attending the workshop of emerging technologies in medicine, artificial intelligence and microlearning, virchowstraße 163a, 45147 Essen, Germany | 2020 |
| Attending the third conference of medical imaging which held at the University of Birzeit – Ramallah. | July 2013 |
| Completed training of leaders on project management and writing business plans and Entrepreneurship, at the Arab American University. | 2013 |
| Attending the second conference medical imaging, which was held at Arab American University – Jenin. | 2012 |
| Win of the first place with partners in the PACS-PAI project, which involved archiving radiographs of hospitals in one database through a website in the "New Generation of Technology Pioneers" competition, established by Hassib Sabbagh Information Technology Center of Excellence at the Arab American University. | 2012 |
| Participate of the Technology Week suggesting a new project called PACS-PAI which was held in Ramallah. | October-2012 |
| Worked as a volunteer in the Partners for Sustainable Development (PSD). | March-2011 |

SKILLS

Excellent research skills.

Programming and scripting.

functional magnetic resonance imaging (fMRI) image analysis (FSL, SPM, CONN).

Working with both - task-based and resting state-based paradigms.

Data acquisition (fMRI, EEG, and Functional near-infrared spectroscopy (fNIRS)).

Teaching skills.

LANGUAGES PROFICIENCY

Arabic (Mother-tongue) – English – German – Indonesia.